C.R.T.E.A.N
المركز العربي للاستشعار عن بعد لجوار الصحارى الجنوبية

FASRC

Journal of Science and Space Technologies

N° 11
December 2025

A court Specialized regional scientific journal issued by CRTEAN in collaboration with the FASRC

Elevation map of the Lower Mejerda Valley - Tunisia

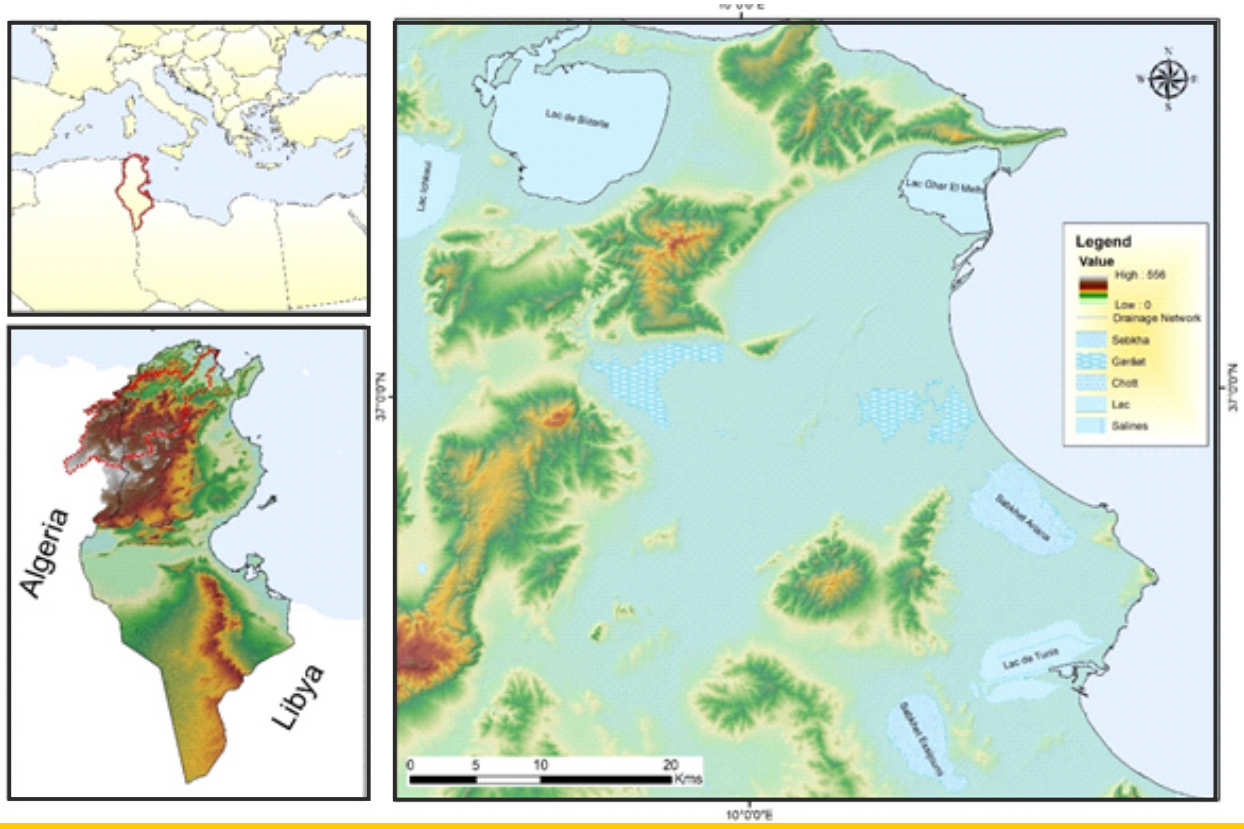

ISSN : 2490 - 4244
www.crtean.org.tn

Contents

6
EDITORIAL

7 - 25
GEOMORPHOLOGICAL AND GEOLOGICAL EVOLUTION OF UTIQUE BASIN (LOWER MEJERDA VALLEY, TUNISIA)

26 - 42
SPATIO-TEMPORAL COMPARISON OF CARBON MONOXIDE EMISSIONS IN KHARTOUM USING SENTINEL-5P & GOOGLE EARTH ENGINE

43 - 50
LAND SURFACE TEMPERATURE (LST) ANOMALIES AS POTENTIAL PRE-SEISMIC INDICATORS: A REMOTE SENSING INVESTIGATION IN SEISMO-TECTONIC REGIONS- SUDAN

51 - 81
CARTOGRAPHIEDES INONDATIONS ET VULNÉRABILITÉS TERRITORIALES DANS LA ZONE MÉRIDIONALE DU LITTORAL NORD-OUEST DU CAP-BON : ANALYSE COMPARATIVE DES ÉVÉNEMENTS DE 2018 ET 2025

82 - 106
AN APPROACH FOR SUDAN'S FLOOD RISK MAPPING

113
كلمة العـــدد

107 - 112
مقاله علمية
" المنتزهات والحدائق الجيولوجية والمستقبل القادم "

JOURNAL OF SCIENCE SPACE TECHNOLOGIES

Journal of Science and Space Technologies (JSST)

The Science and Space Technologies Journal is a peer-reviewed journal publishing basic and applied research articles in the fields of space sciences and technologies. Accepted types of contributions include: original basic and applied research papers, review articles, books and theses reviews and technical notes.

- **General rulesfor publication:**

1. The material sent for publication must be original, not published before or sent to any other destination for publication.
2. The languages of publication are Arabic, English or French.
3. Arabic abstract for text in English or French is needed.
4. The submitted work is confidentially sent to two referees specialized in the subject area. The referee's notes and comments are conveyed to the corresponding chief author so that he/she can revise the text to meet the publication requirements.
5. The journal accepts applied academic studies in the field of geomatics and space technologies.
6. The journal accepts research papers extracted from MSc. or PhD. thesis
7. The journal publishes related technical reports, research papers and studies presented at conferences, symposia and academic activities in special issues.
8. Un-refereed articles published in a special section of the journal.
9. The studies, researches and review articles reflect the views of their author (s), not necessarily the views of the editorial board.
10. Author (s) should not submit their articles to other publishers without notifying the journal.

- **Guidelines for contributors:**

1. The material should be submitted in two copies with Arabic, English or French summary, (8 -12 lines).
2. Illustrative figures should be clearly printed.
3. Abbreviations and terminologies should conform to international standards.
4. The Arabic text font should be Times New Roman (size 14), and 12 for English or French texts.
5. Research title, author name and address should appear in the translated English or French texts.
6. Publication fees for researchers is 100 $ and only 50 $ for students.

- **Manuscript structure and organization**

1. The manuscript should be in the standard scientific paper format with abstract, introduction, materials and methods, results and discussions, summary and references. The abstract should be informative, with emphasis on results and conclusion.
2. Title: the title of the paper should be informative, concise and representing contents of the paper.
3. Author (s) name (s) should include name and last name of every author and their complete addresses. It is necessary for the corresponding author to provide e- mail address.
4. Abstract: preferably less than 300 words and should state concisely the main objectives of the paper, brief description of methods used, main findings and conclusion.
5. Keywords: A list of 3-5 key words from the manuscript must be applied. Key words should include the topic investigated, and special techniques used.
6. Arabic abstract: Authors are requested to prepare an extract Arabic translation of the abstract, which will appear at the top of the article. However, for non-Arabic authors, the translation will be done by the journal editorial board.
7. Introduction: Should emphasize the importance of research, present related literature and give enough information to understand the hypothesis of the author (s); it ends with a paragraph including the objectives of the research.
8. Materials and methods: should be clear and informative, to allow other researchers to repeat the method and obtain the same results.
9. Results and discussion: obtained results and analysis should be in a clear and concise presentation, supported by tables and figures. It should contain corresponding statistical analyses and report from other authors.
10. Conclusion: should be redacted according to the research objectives and results. It should be in clear terms, without abbreviations, acronyms or references.
11. Acknowledgements: if any, this section should be located before references; expressing gratitude to institutions, laboratories and people who supported specially all or part of the research.
12. References: References should be cited chronologically in the text by author (s) and date, e.g. (Ali and Hadi, (2000); Mustafa *et al*., (2005) and Gad (2010), and are not numbered. The total number of references mentioned should not exceed 20 references, at least halve of them should not be more than 10 years date.

●Submission of manuscripts:
Three copies of research articles, as well as a soft copy must be submitted to the Editor-in- Chief, 18, Rue Moussa Ibn Noussair, Elmanzah V, Tunis- Tunisie, or to email: dg.crtean@crtean.int.tn.

●Reprints:
Authors are entitled to 2 reprints free of charge.

●Subscription:
For member States:
20 $ for individuals
40 $ for institutions or organizations
For non-member States:
25 $ for individuals
50 $ for institutions and organizations.

EDITORIAL

The Regional Center for Remote Sensing of North African States (CRTEAN), in partnership with the Union of Arab Scientific Research Councils, is pleased to present to its esteemed readers and researchers the eleventh issue of the Regional Journal of Space Sciences and Technologies, which serves as a rigorous scientific platform dedicated to promoting scientific research and advancing knowledge in the fields of space sciences and their various applications.

This journal is published under the supervision of a peer-reviewed scientific committee comprising a distinguished group of professors and researchers from the member states, thereby ensuring the quality, credibility, and scientific integrity of the published research, in full compliance with international academic standards and research ethics.
This issue features a collection of specialized scientific research articles and studies conducted by researchers and experts from North African countries, addressing contemporary and diverse topics in the fields of remote sensing, geographic information systems (GIS), space sciences and technologies, and their applications in sustainable development, natural resource management, environmental protection, risk reduction, and policy support and decision-making.

The continued publication of this journal reflects the commitment of the Center and its partners to supporting Arab scientific research, strengthening regional cooperation and knowledge exchange, and providing a specialized scientific forum that highlights regional research capacities while linking scientific research to development challenges and scientific and technological progress.

I would like to extend my sincere appreciation and gratitude to the members of the Scientific Advisory and Review Committee, as well as to all the researchers who contributed their valuable scientific work to this issue. I look forward to this publication representing a meaningful addition to the Arab scientific library and contributing to the encouragement of further research and innovation in the fields of space sciences and technologies.

Please accept my highest consideration and respect.

Prof. El hadi Gashut
Dg. CRTEAN
Editor-in-Chief of the Journal

GEOMORPHOLOGICAL AND GEOLOGICAL EVOLUTION OF UTIQUE BASIN (LOWER MEJERDA VALLEY, TUNISIA)

Lamia Khemiri[1],, Seifeddine Gaidi[1,5], Mannoubi Khelil1,[4], Rim Katlane[3] Mohamed Ghanmi[1], Fouad Zargouni[1]*

[1]Faculty of Sciences of Tunis, Tunis El Manar University, Tunis, Tunisia
[3]Laboratory Geomatics of Geosystems, University of Manouba, Manouba, Tunisia
[4]Laboratoire de Géoressources, LGR, Centre de Recherches et des Technologies des Eaux (CERTE), Soliman, Tunisia
[5]Departamento de Geodinámica, Universidad de Granada, Granada, Spain
* *corresponding author: khemiri_lamia@yahoo.com*

ABSTRACT

The Utique Basin, situated in the Lower Mejerda Valley of Tunisia, serves as a dynamic example of ongoing geomorphological and geological evolution influenced by active tectonics. Through a multidisciplinary approach, this study integrates geomorphological observations, morphometric analysis, and structural interpretations to investigate the tectonic activity shaping this region. Using tools like the normalized steepness index (ksn) and hypsometric curves, the research identifies significant tectonic uplift along the northern edges of the basin, contrasting with the relatively stable southern landscapes. Structural analyses of Late Miocene-Quaternary deposits reveal complex thrust faulting and compressional events that have shaped the basin's morphology since the Paleogene. These findings emphasize the basin's position as an active tectonic site with implications for seismic risk management and regional land-use planning. The study highlights the need for advanced seismic mapping and modeling to further understand this geologically complex area.

1. INTRODUCTION

Relief analysis using drainage network metrics (Camafort et al., 2020) and (Gaidi et al., 2020) is an effective tool for detecting and characterizing active tectonic structures in regions with low to moderate tectonic activity. By combining various morphotectonic indices, it is possible to differentiate between uplifting and subsiding regions across different scales. This method, when combined with geomorphological studies, helps to distinguish between the mechanisms influencing topography and the development of associated drainage networks. One of the main objectives of this paper is to investigate and characterize active tectonic processes in this region, in relation with the evolution of the valley of the Mejerda River in its lower part. This paper centers on geomorphological and morphostructural analyses as the initial step in identifying recent and active tectonic structures within the Lower Mejerda Valley, especially the Utique Kechabta Basin and the surrounding reliefs.

2. GEOLOGICAL AND GEOMORPHOLOGICAL SETTING

1.Geographical and climate setting

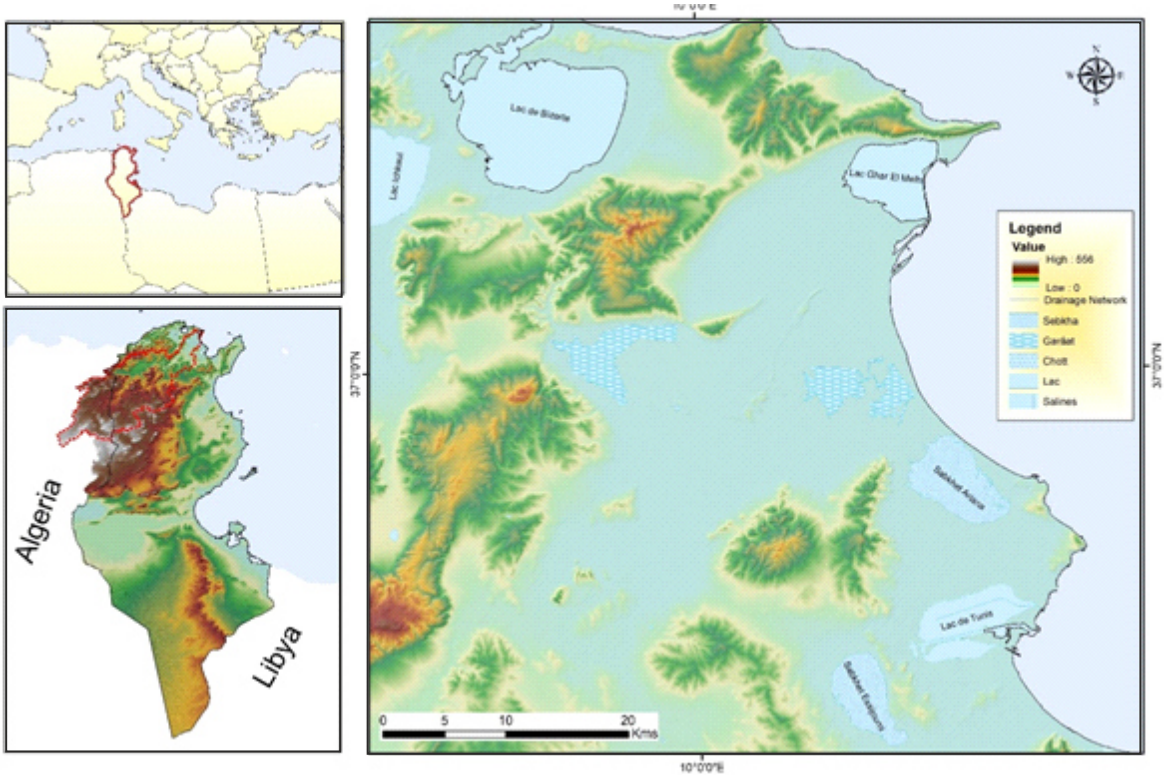

Figure 1: Elevation map of the Lower Mejerda Valley

2. Geological setting

Northern Tunisia features a complex orogenic system, the Tell fold-and-thrust belt (FATB), which is part of the broader Maghrebides range. To the south, this system is connected to the Atlas FATB, an intra-continental chain. The South Tellian Front (STF), which delineates these two FATBs, is flanked by the Upper Miocene to Quaternary deposits of the Mejerda wedge-top basin to the West and the Utique-Kechabta basin to the East. While the Mejerda basin represents an extensional basin that developed during the compressional events from the Late Miocene to the Quaternary (Khelil et al., 2019, 2020, 2021), field mapping and seismic profile interpretations reveal that the Utique-Kechabta basin is characterized by tectonic accretion, where the Tell has been thrust onto its foreland basin (Khelil et al., 2021).

The Utique-Kechabta basin represents the easternmost onshore foreland of the Tell fold-and-thrust belt. This basin appears to be filled with highly subsiding Late Miocene to Quaternary deposits (Rigo L et al., 1996); (Bejaoui et al., 2017); (Booth-Rea et al., 2018a); (Gaidi et al., 2020); (Khelil et al., 2021), which overlay deeper inversional structures at the southern front of the Tunisian Tell. To effectively highlight the structural styles in this foreland domain, we present a structural seismic interpretation within the Utique-Kechabta basin.

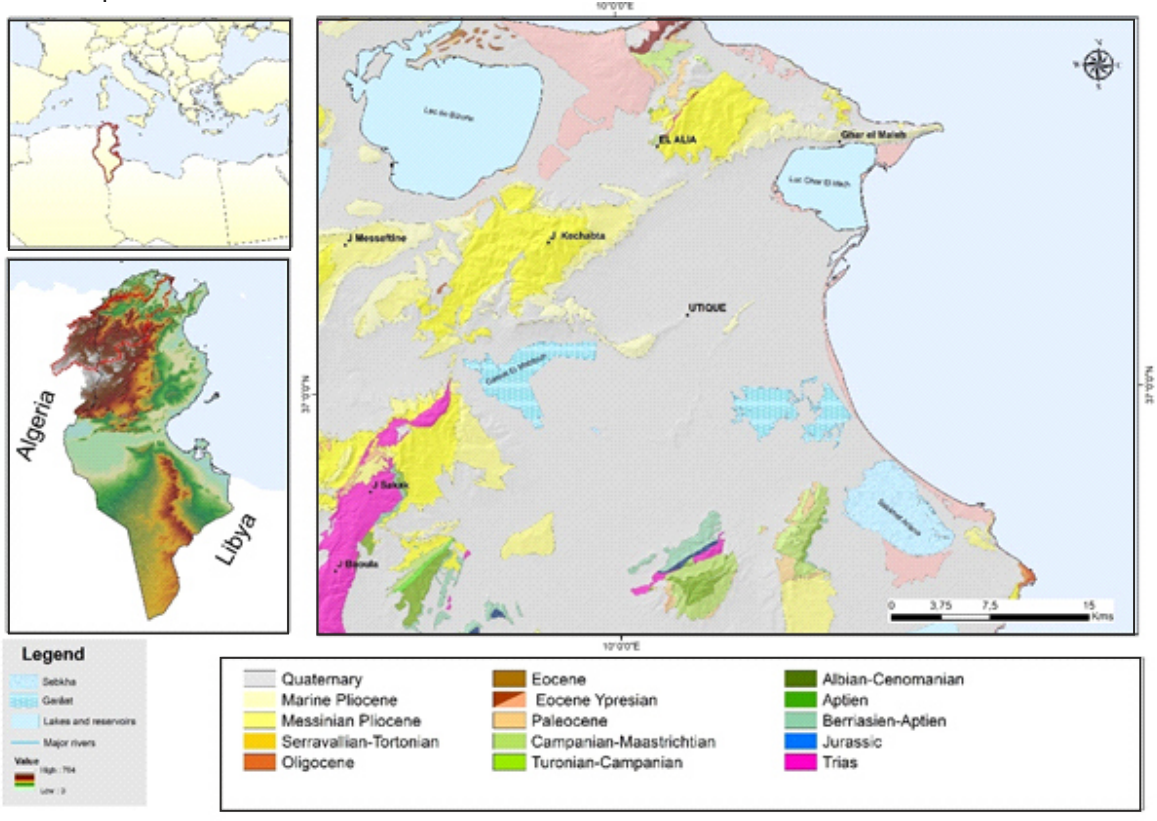

Figure. 2: : Geological map of the Lower Mejerda Valley

The well data from the Utique-Kechabta basin reveal significant variations in litho-facies and thicknesses within the Paleogene and Neogene series, along with an angular unconformity at the base of the Upper Miocene strata overlying various elements of the underlying stratigraphic successions and structures. The syn-folding and synkinematic Upper Miocene sequences reach thicknesses of up to 2,000 meters. Fracture analyses and dipmeter data from the exploration wells have identified horizontal thrust contacts at the base of the Upper Miocene (Khelil et al., 2021).

3. Geomorphological setting

The primary geomorphological features of northern Tunisia are the NE-SW oriented mountain ranges and their associated valleys. In certain areas, the drainage network exhibits rectangular patterns and river deflections, which may indicate significant lithological or tectonic boundaries (Camafort et al., 2020).

The Mejerda River, the largest catchment in Tunisia, drains an area of approximately 23,340 km². It flows along an axial valley for 400 km from eastern Algeria to the Gulf of Tunis in a SW-NE direction, parallel to the region's main faults and folds. The river's source lies in Algeria at an altitude of 1,300 m within the semi-arid Atlas system (Delile et al., 2015). According to Faust et al. (2004), the current climate in this area is Mediterranean subtropical, transitioning from Mediterranean semi-arid conditions in southern Algeria to semi-humid conditions in northern Tunisia. Despite documented morphodynamic changes in the Mejerda's floodplain sediments, linked to North Atlantic Bond events, the river's Quaternary sedimentation appears to have occurred under relatively stable conditions, allowing well-stratified sediment layers to form (Faust et al., 2004); (Zielhofer & Faust, 2008).

The Mejerda's tributaries drain areas ranging from 54 to 2,564 km², with lengths between 8.5 and 163 km. These tributaries predominantly flow in two orthogonal directions, NE-SW and NW-SE.

Tunisia's topography is generally gentle, with an average slope of about 6°. The highest points are found at the Mejerda headwaters in eastern Algeria, reaching up to 1,770 m. The landscape is primarily fluvial, featuring meandering rivers and some locally incised sections (Camafort et al., 2020)

4. Methodology

To achieve this, a multiscale and multidisciplinary approach is employed, integrating geological and geomorphological observations. We applied morphometric tools to analyze the watersheds surrounding the Utique Basin, located in the North-East part of Tunisia. In this region, morphometry and drainage patterns have proven to be reliable indicators of recent tectonic activity (Camafort et al., 2020); (Gaidi et al., 2020). A 10-meter resolution DEM was used to extract the primary drainage system and delineate the basins across the area. We then analyzed the drainage network and topography using quantitative geomorphic parameters, such as Ksn and hypsometry.

4.1. Normalized steepness index

Graded rivers show an exponential relationship between channel slope (S) and up-stream area (A) (Hack, 1957).

This well-known relation is described by the power-law: $S = ks\,A^{-\Theta}$
Where ks is the channel steepness-index and Θ the concavity index (Flint, 1974)
When slope and area data are represented in logarithmic-scale plots, this power relation yields a straight line that can be used to derive ks and Θ parameters by linear regression.

This power-law relation has been used in several tectonic studies, since different area-slope relations can be due to active tectonics, changes in riverbed lithology, and/or climate (e.g. Wobus et al., 2006; Kirby and Whipple, 2012; Whipple et al., 2013; Burbank and Anderson, 2013; (Scotti et al., 2014); (Bellin et al., 2014), (Camafort et al., 2020); (Gaidi et al., 2020).

Some studies have proposed that concavity index (Θ) varies in most natural channels in a narrow range between 0.4 and 0.6, and it is relatively insensitive to differences in uplift rate, lithology and/or climate at steady state (Kirby & Whipple, 2012); (Whipple & Gasparini, 2014). By contrary, steepness index (ksn) is highly sensitive to all the mentioned factors.

In practice, the use of a normalized steepness index (ksn) is extended to avoid the strong correlation of ks and Θ. The ksn index is computed by considering a fixed concavity (Θref) and it is much more robust than fitted ks (Wobus et al., 2006); (Kirby & Whipple, 2012); (Whipple & Gasparini, 2014); (Burbank & Anderson, 2013)). Several studies have proposed a high correlation between ksn index and uplift rate (Kirby & Whipple, 2012); (Bellin et al., 2014).

We derived the ksn index for all the analyzed basins by regression of slope-area plots (Gaidi and al 2020) with the aid of open-source codes available from http://www.geomorphtools.org.

4.2. Hypsometric analysis

The hypsometric curve and the hypsometric integral (HI) are valuable tools for characterizing topography because they are correlated with the stage of geomorphic development of the landscape (STRAHLER, 1952); (Willgoose & Hancock, 1998); (Pérez-Peña et al., 2009). In the present paper, we followed the methodology proposed by (Gaidi et al., 2020).

3. RESULTS

4. Geomorphological data

In the following part, four major watersheds (Fig. 12) delimiting the Utique Basin are identified based on the steepness index map:

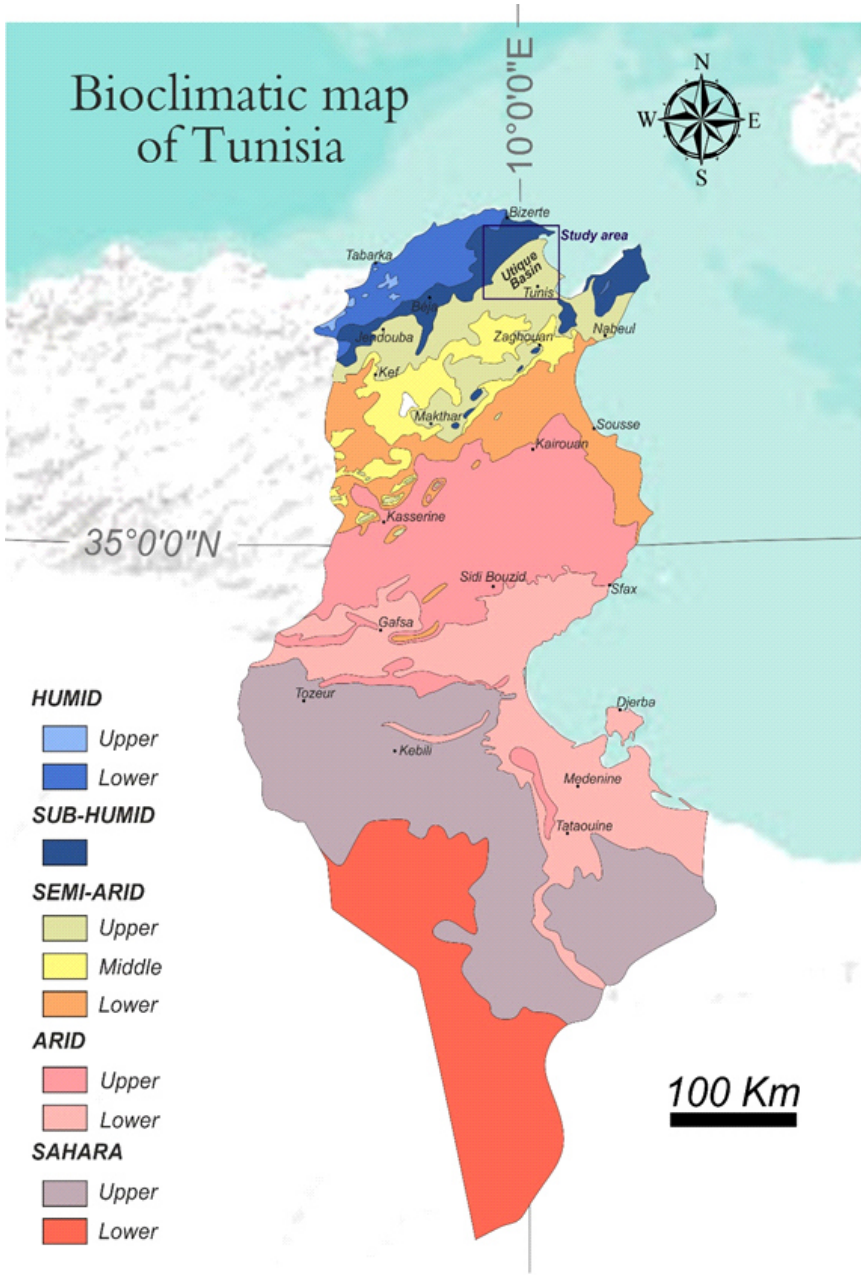

Figure:: Bioclimatic map of Tunisia. Note the location of the study area.

- The Hakima watershed;
- The Messeftine-Kechabta watershed;
- The Sidi Bou Rekouba watershed;
- The Ammar-Nahli watershed.

The Normalized steepness index (ksn) map (Figure.4) shows a difference between the northern and southern edge of Utique Basin. The positive anomalies, with High Ksn values, reflects a recent tectonic activity. It highlights that the Northern reliefs are characterized by a recent landscape evolution, compared to the Southern reliefs. Each major watershed is divided into sub-watersheds (Figure.4), based on the analysis of the rivers network and the relief's. Each sub-watershed is characterized by a hypsometric curve indicating the relief evolution.

Basins in an early stage of development exhibit convex-shaped curves, while mature basins display S-shaped curves. Intensively eroded basins nearing the peneplain stage produce distinctly concave curves (STRAHLER, 1952); (Ohmori, 1993); (Pérez-Peña et al., 2009).

The first watershed "Hakima", located to the North of Utique Basin, is composed of 17 distinguished sub-watersheds (Figure.5). The curves related to the sub-watershed n°17 is concave and shows a low hypsometric index, indicating a peneplain stage (Figure.6). However, the curves related to the sub-watersheds n°11, 12 and 13 for example are convex and shows the highest indexes (Figure.6). It corresponds to young basins, which means that are tectonically active.

The second watershed "Messeftine-Kechabta", to the East of the first one and also located to the North of Utique Basin, is composed of 13 distinguished sub-watersheds (Figure.7). The curves related to the sub-watersheds n°18 and 32 are concave and show low indexes of relief evolution (Figure.8). However, the curves related to the sub-watersheds n°24 and 28 for example are convex and shows high relief evolution (Figure.8). It indicates that this sub-watershed located to the South-East of Messeftine-Kechabta watershed are tectonically active.

The third watershed "Sidi Bou Rekouba", located to the West of Utique Basin, is composed of 13 distinguished sub-watersheds (Figure.9). The curves related to the sub-watersheds n°33 and 36 are concave and show low indexes of relief evolution (Figure.10). However, the curve related to the sub-watershed n°77 for example is S-shaped and indicates that a mature watershed (Figure.10).

The fourth watershed "Ammar-Nahli", located to the South of Utique Basin, is composed of 31distinguished sub-watersheds (Figure.10). The curves related to the sub-watershed 89 is concave and show low indexes of relief evolution (Figure.11). However, the curve related to the sub-watersheds n°72 and 82 for example is S-shaped and indicates that a mature watershed (Figure.12).

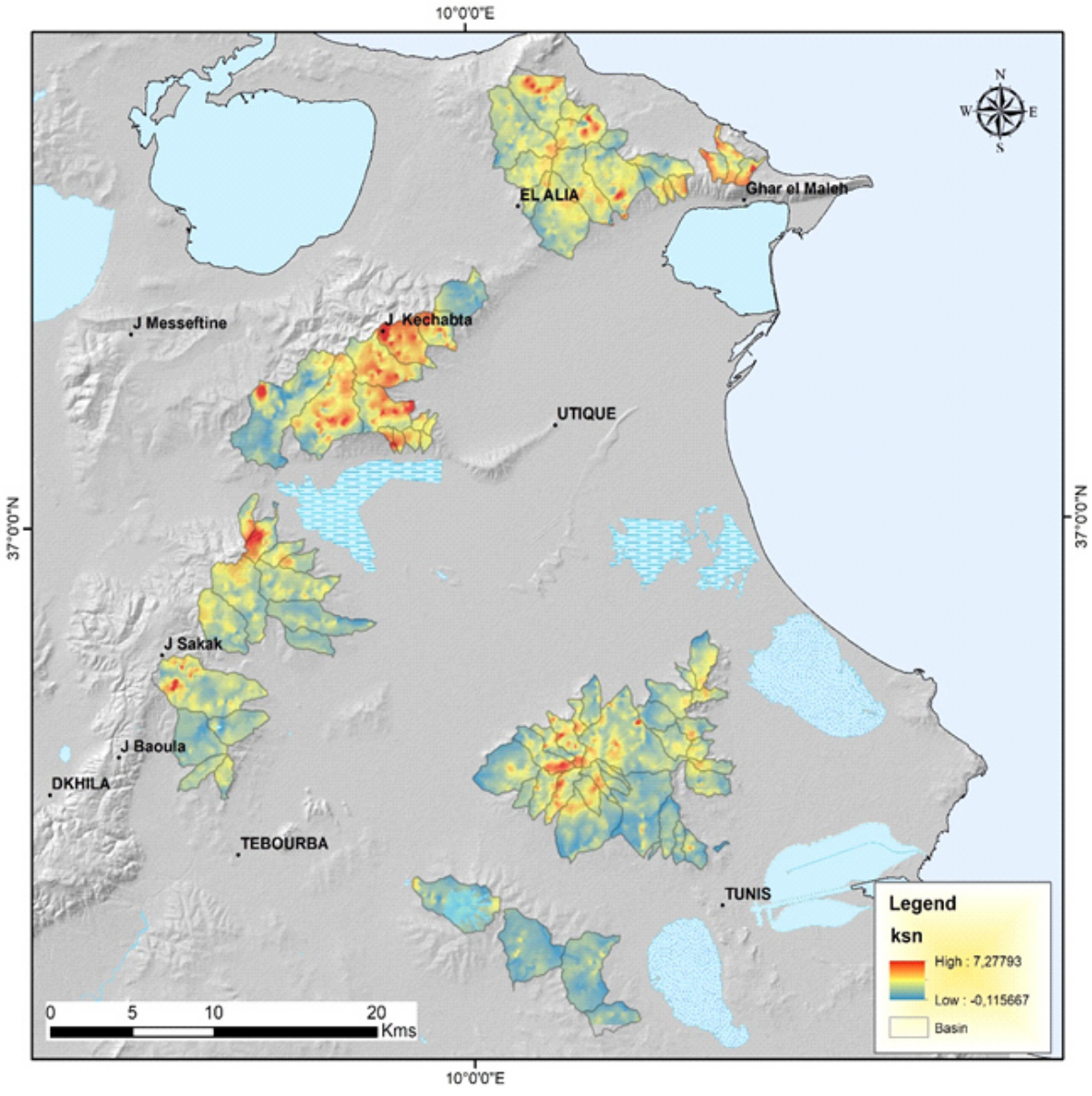

Figure 4: Normalized steepness index (ksn) mapping of the basins surrounding the Lower Mejerda Valley

4. MORPHOSTRUCTURAL DATA

The Utique Basin represents a highly subsiding Upper Miocene-Quaternary foredeep basin, which lies between the Tellian belt to the north and the North Atlas belt to the south. This foredeep basin experienced tectonic inversion during the Upper Miocene-Quaternary period and is now characterized by thrust tectonics, which affect the synkinematic Upper Miocene-Quaternary sequences (Khelil et al., 2021).

This basin is characterized by a low topography and corresponds to the plain of the Lower Valley of Mejerda. It is bordered to the North by some reliefs, such as Jebel Nadour, Jebel Hakima, Jebel Kechabta and Jebel Messeftine, and to the South by Jebel Nahli and Jebel Ammar.

The Late Miocene-Quaternary foredeep deposits (Figure.13) represent the synkinematic layers of the Tell FATB (Khelil et al., 2021) and were formed during the Late Miocene-Quaternary in a continental to lagoonal environment (Harrab, 2013). These deposits exhibit significant facies and thickness variations (Figure.14) and rest unconformably on the underlying folded structures. They fill synclines and depocenters and are affected by faulting and thrusting, having been deposited along the footwall blocks of the thrust units.

The structural map (Figure.15) highlights the structures forming the previously mentioned reliefs which are delimiting the Lower Mejerda Valley, mainly:

The complex Kechabta-Messeftine structure is characterized by a succession of East-North-East – West-South-West folds; the two main folds are Messeftine and Kechabta anticlines (Figure.15) which are separated by a North-East – South-West thrust (East Jebel Sfaia and AGL-1 well in cross-section AB of Figure.16), with a sinistral strike slip component.

The folded Mesozoic to Cenozoic formations are the result of a succession of compressional events:

(1) The Paleogene period aligns with the initial significant compressional forces associated with the Eocene Atlas phase (Khomsi et al., 2019a). On the cross-sections of Figures 16 and 17, this is primarily evidenced by the thinning and absence of parts of the Paleogene sequence.

(2) The Upper Miocene-Quaternary period marks the second major phase compressions (Khomsi et al., 2019b); (Bejaoui et al., 2017); (Gaidi et al., 2020); (Khelil et al., 2021). During this time, the region experienced widespread uplift and significant thrusting. This period also saw a shift in sedimentation from marine to continental and lagoonal environments, characterized by the deposition of large volumes of molasse deposits, sebkha evaporites, and fluvial meandering sequences within a sub-continental setting.

Jebel Hakima Basin is characterized by a complex structure; the North-East – South-West El Alia thrust which overhang tectonically a well-developed Neogene foreland basin (Figure.16). The Mio-Pliocene series are thick, reaching 2000 m. The subsidence of this flexural basin is enhanced by a system of normal faults.

5. DISCUSSION

The geomorphological and geological analysis of the Utique Basin has provided significant insights into the tectonic activity shaping the Lower Mejerda Valley. By applying morphometric tools such as the normalized steepness index (ksn) and hypsometric analysis, we distinguished active tectonic zones, particularly in the northern edge of the basin. High ksn values in these northern watersheds indicate recent tectonic uplift, aligning with prior studies suggesting the presence of tectonic accretion in the Utique-Kechabta basin (Khelil et al., 2021). Conversely, the southern regions demonstrate a more stable, mature landscape, consistent with their lower ksn values and S-shaped hypsometric curves.

The lithological analysis further supports these findings, as the structural complexities observed in the cross-sections of Jebel Hakima and Kechabta highlight the impact of compressional forces that have influenced the region's morphology since the Paleogene. These compressional events, especially during the Upper Miocene-Quaternary period, appear to have been crucial in shaping the geomorphology of the basin. These findings underscore the basin's position as an active tectonic site influenced by thrust faulting and subsidence due to significant fault systems, which have redefined the basin's geomorphology over time.

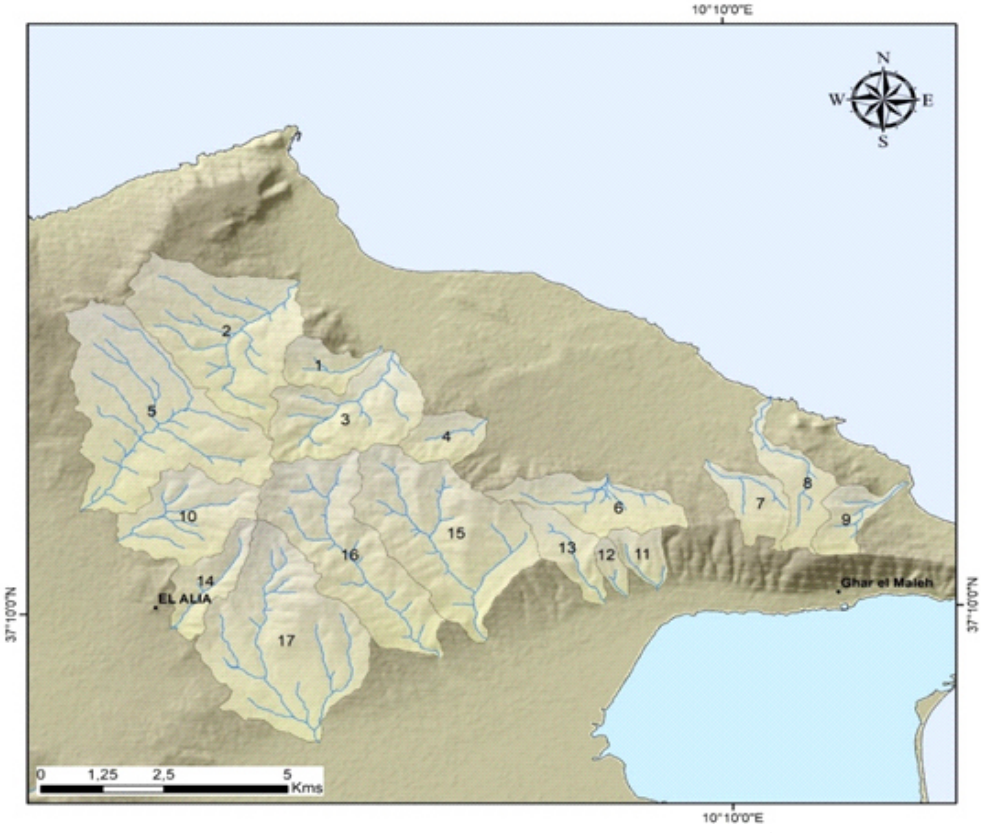

Figure 5: Watersheds within the Hakima basin, which is located to the North of the Lower Mejerda Valley

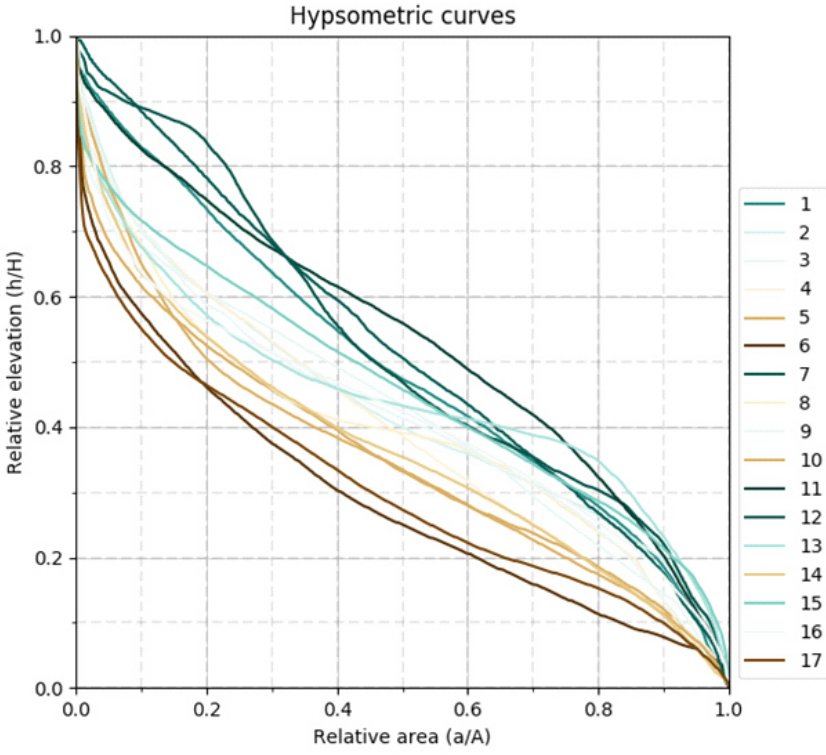

Figure 6: Hypsometric curves relative to watersheds within Hakima basin.

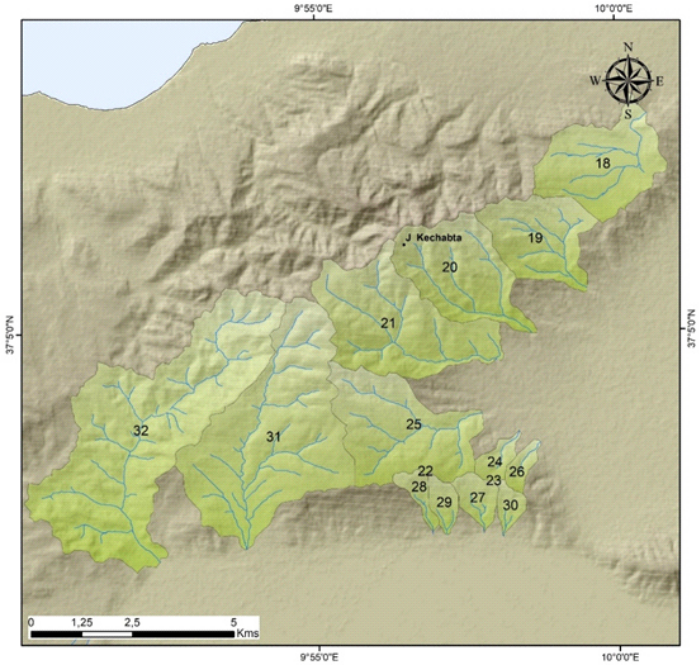

Figure 7: Watersheds within the Messeftine-Kechabta basin, which is located to the North of the Lower Mejerda Valley

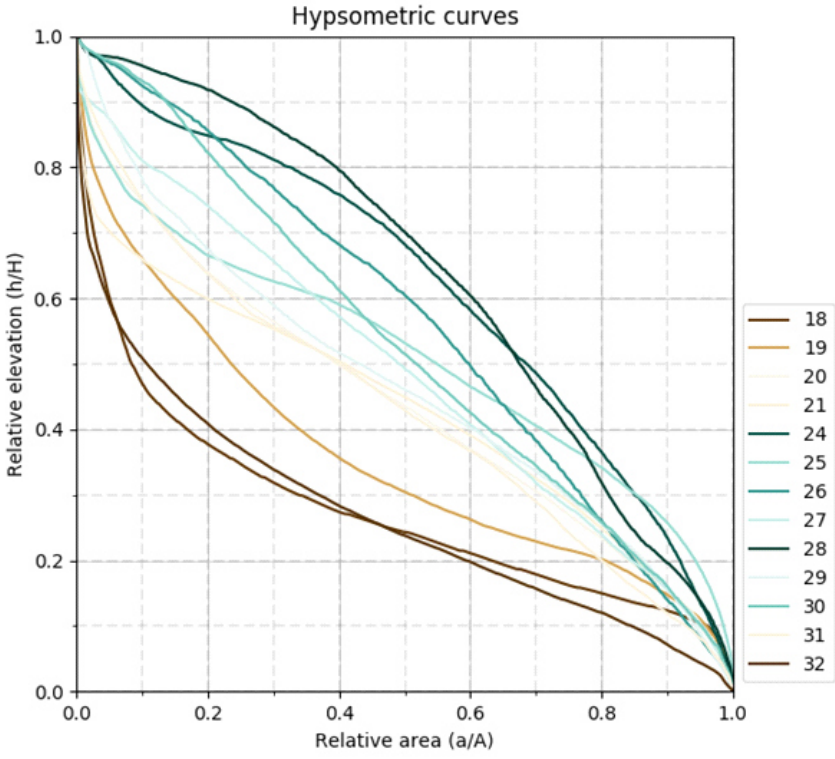

Figure 8: Hypsometric curves relative to watersheds within the Messeftine-Kechabta basin

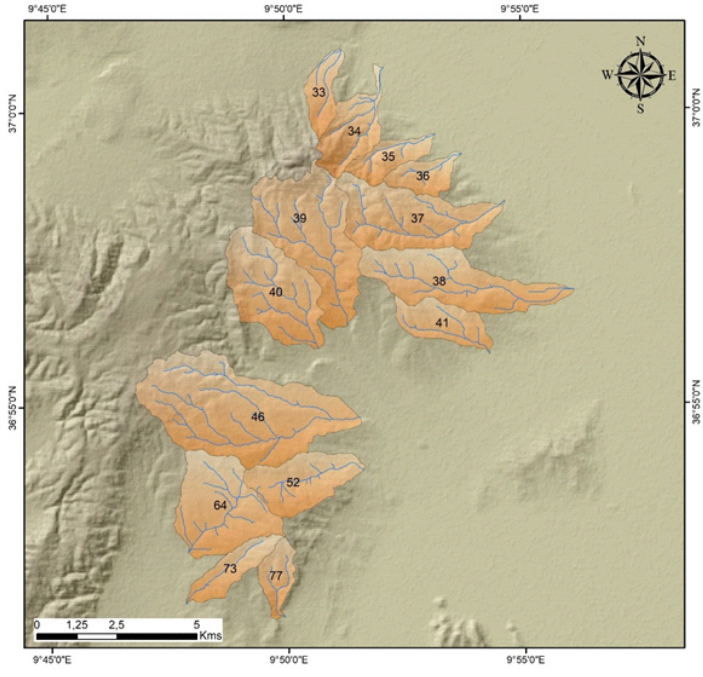

Figure 9: Watersheds within the Sidi Bou Rekouba basin, which is located to the North of the Lower Mejerda Valley

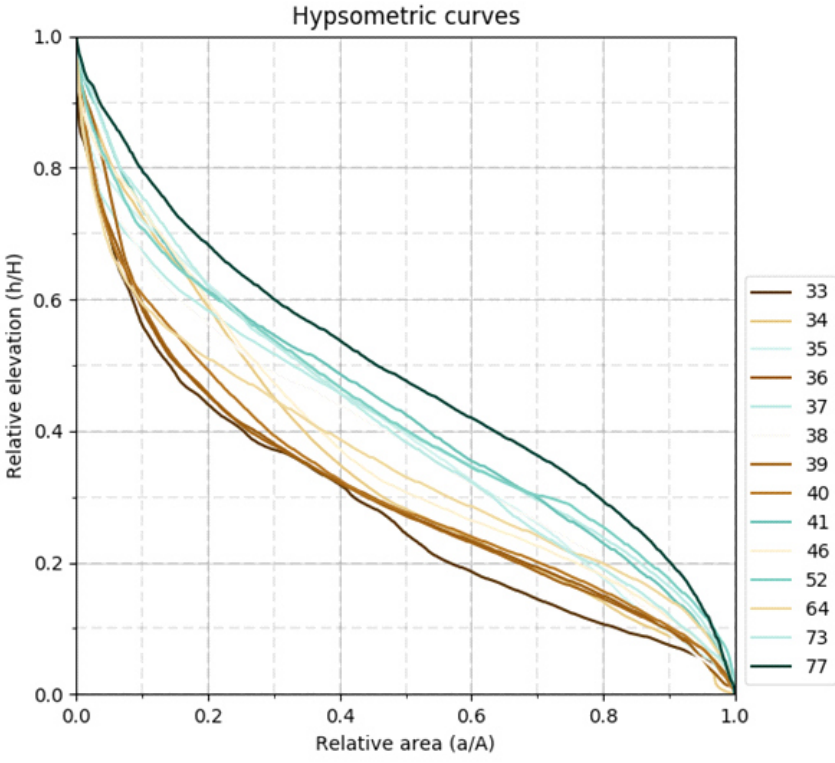

Figure 10: Hypsometric curves relative to watersheds within the Sidi Bou Rekouba basin

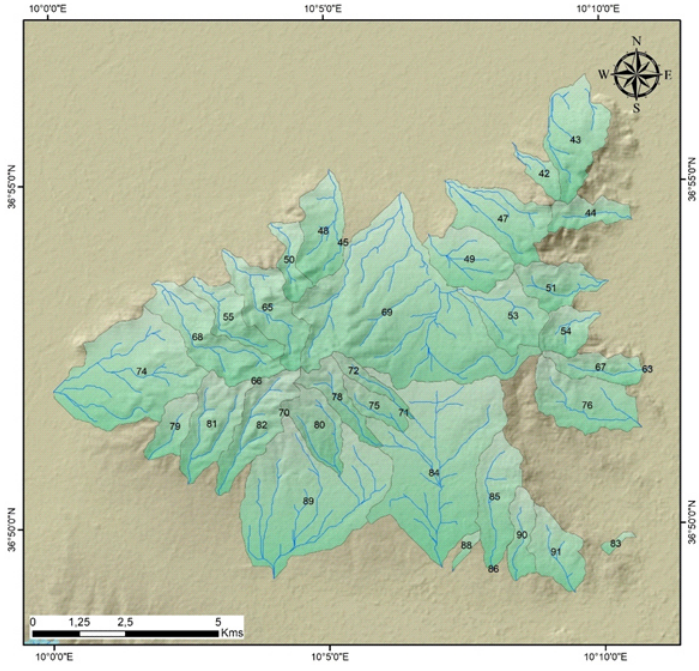

Figure 11: Watersheds within the Ammar-Nahli basin, which is located to the North of the Lower Mejerda Valley

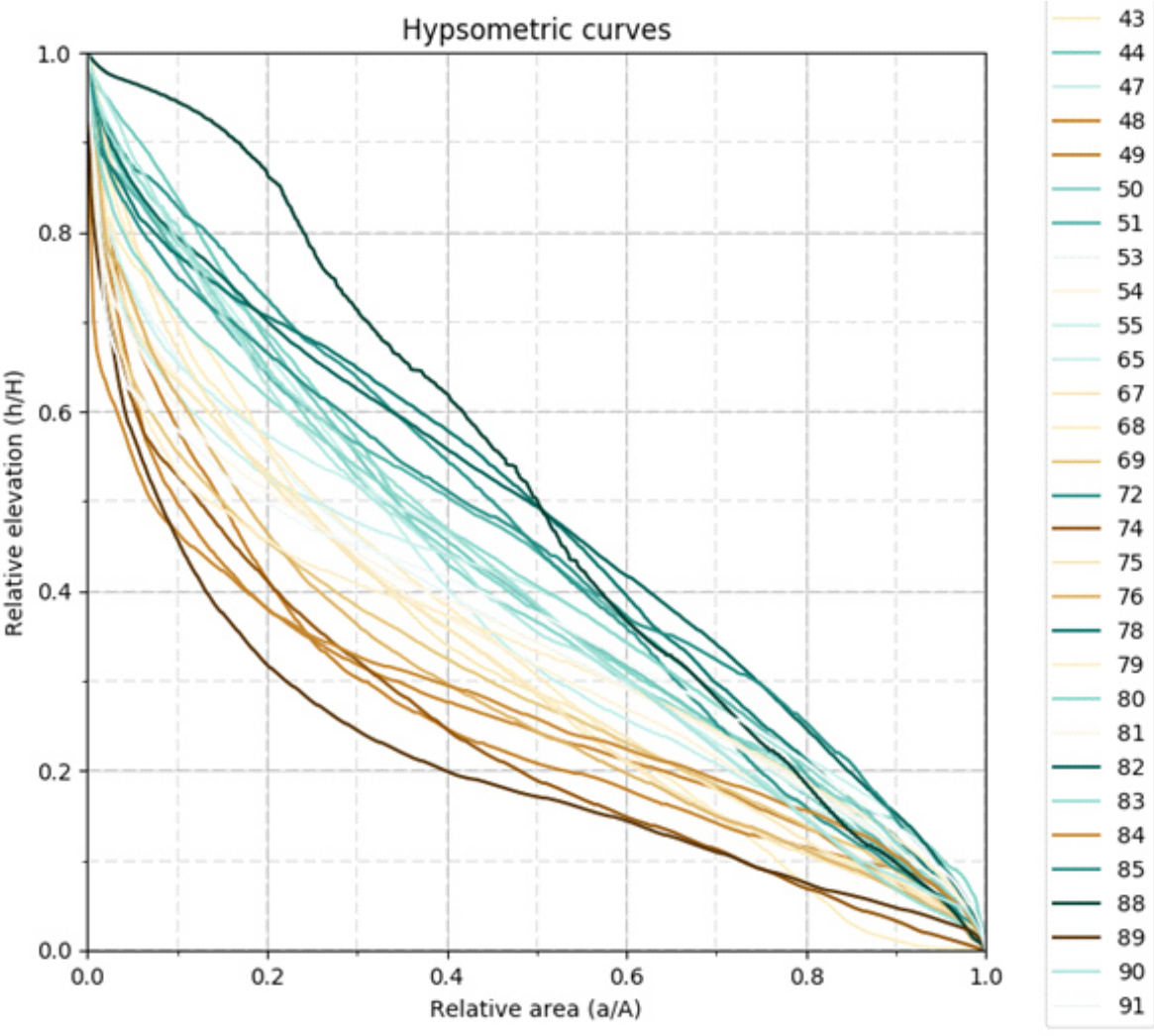

Figure 12.: Hypsometric curves relative to watersheds within the Ammar-Nahli basin

Figure 13: Lithostratigraphic log of the Late Miocene-Quaternary foredeep deposits (modified after (Harrab, 2013)

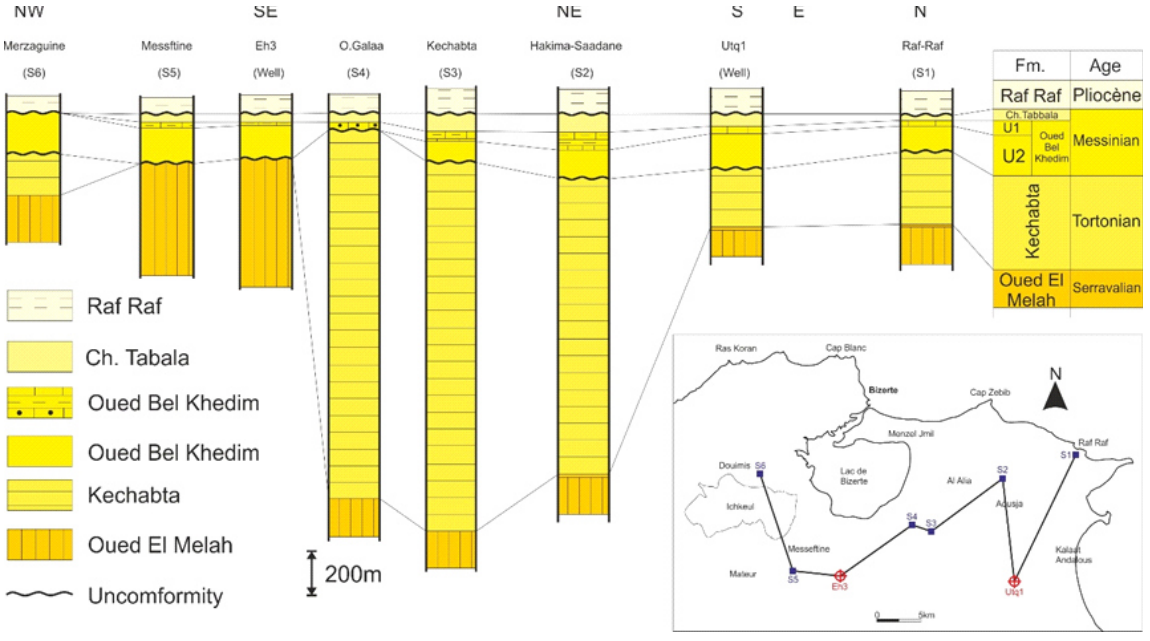

Figure 14: Correlation of the Late Neogene series of the Bizerte basin (Harrab, 2013)

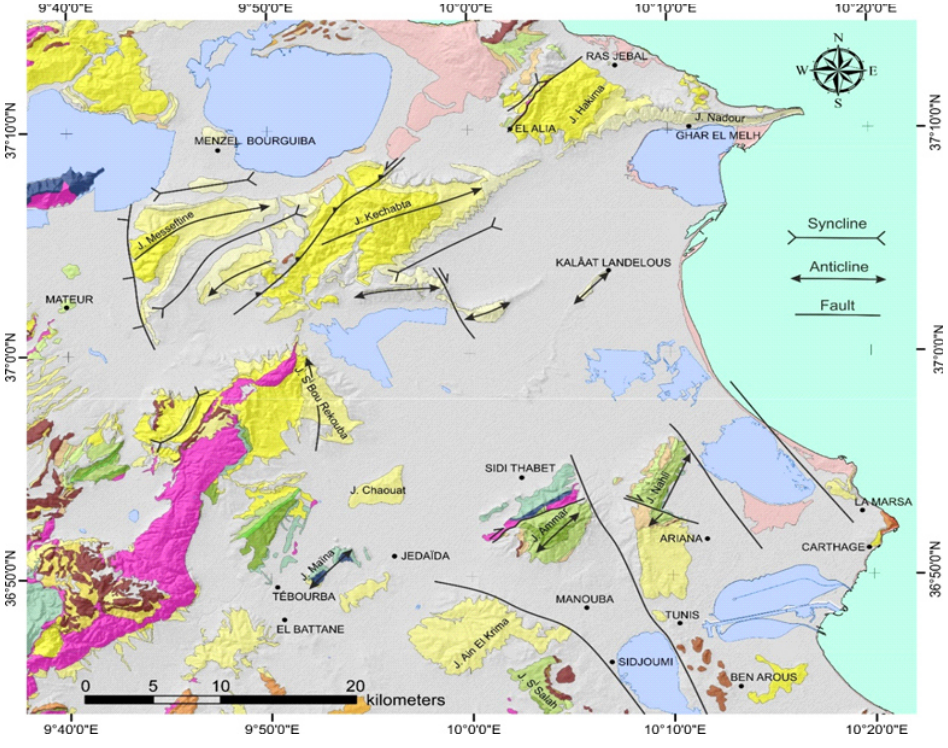

Figure 15: Structural map of the Lower Mejerda Valley

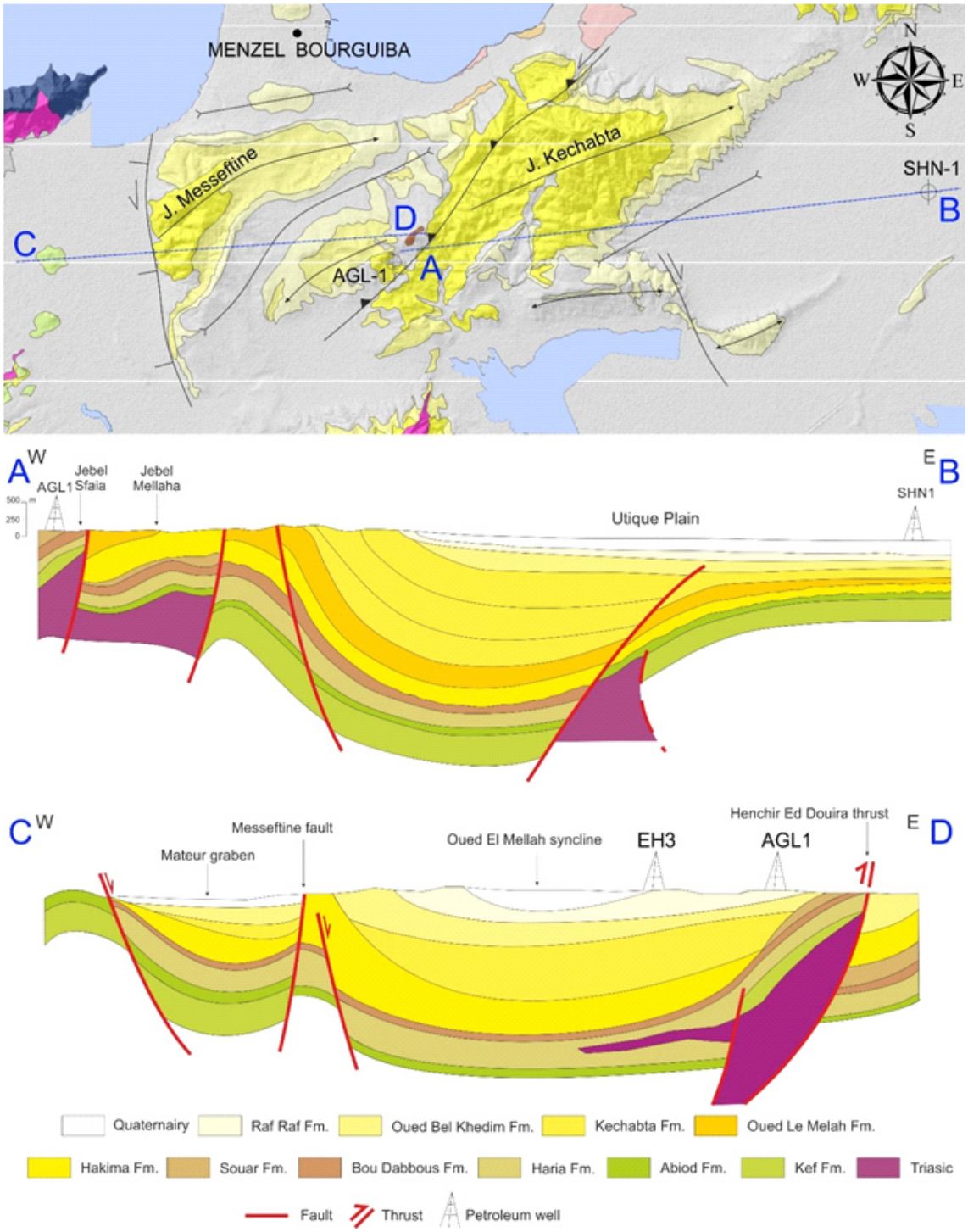

Figure 16: Cross-sections highlighting the main structures of Messeftine and Kechbta basins.

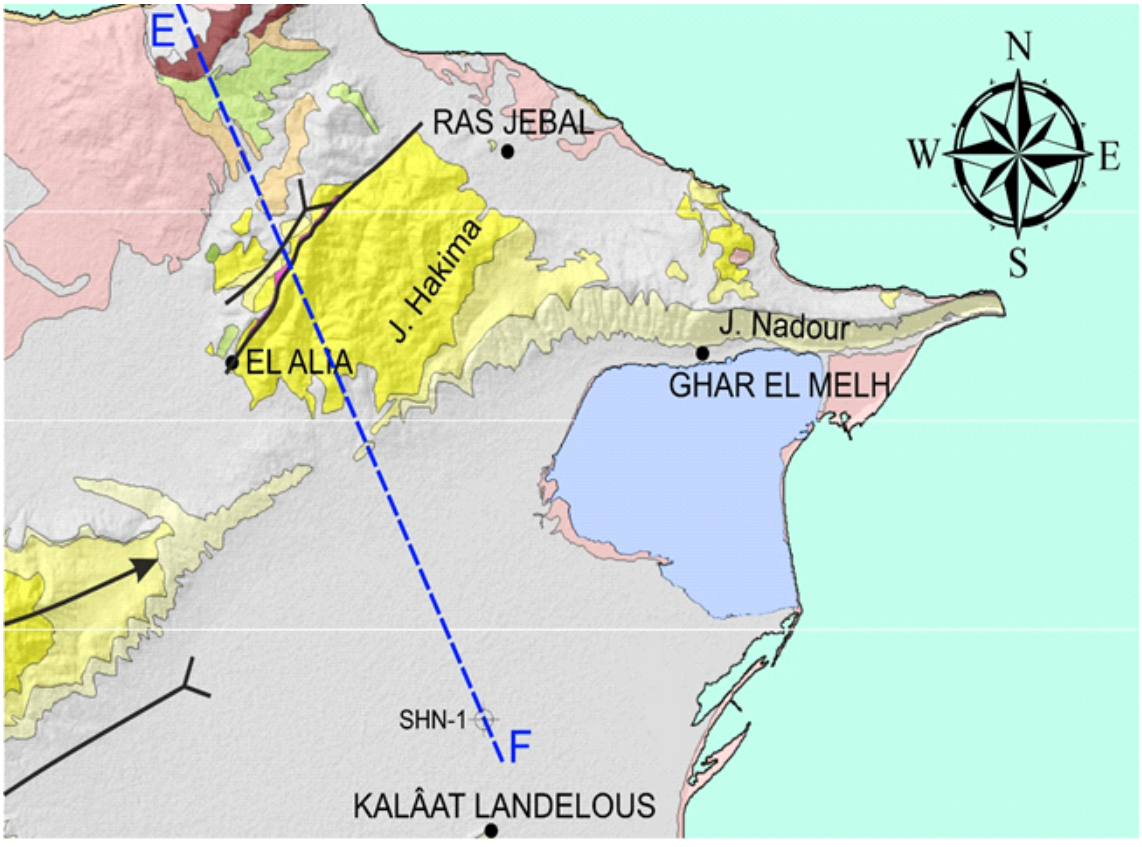

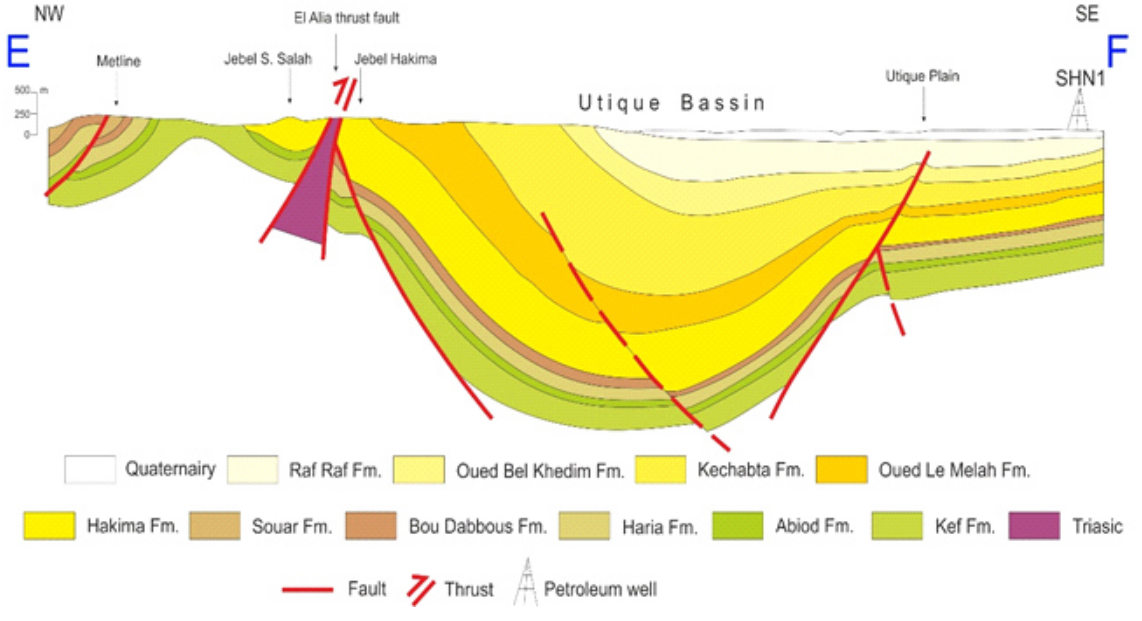

Figure 17: Cross-section highlighting the main structures of Hakima basin

6. CONCLUSIONS

This study has established the Utique Basin as an area of ongoing tectonic and geomorphological evolution within the Lower Mejerda Valley. By integrating geomorphological and morphostructural analyses, we identified contrasting tectonic influences across the basin. Specifically, the northern regions exhibit clear signs of tectonic activity, as reflected in their high ksn values and youthful landscape features, while the southern areas present more stable geomorphic profiles.

These insights have important implications for understanding the active tectonic processes in low to moderate tectonic regions, as well as for regional land use and risk management, given the potential for seismic activity. Future research could focus on high-resolution seismic mapping and advanced morphotectonic modeling to further delineate the structural intricacies of this geologically complex area.

7. REFERENCES

Bejaoui, H., Aïfa, T., Melki, F., & Zargouni, F. (2017). Structural evolution of Cenozoic basins in northeastern Tunisia, in response to sinistral strike-slip movement on the El Alia-Teboursouk Fault. Journal of African Earth Sciences, 134, 174–197. https://doi.org/10.1016/j.jafrearsci.2017.06.021

Booth-Rea, G., Gaidi, S., Melki, F., Marzougui, W., Azañón, J. M., Zargouni, F., Galvé, J. P., & Pérez-Peña, J. V. (2018). Late Miocene Extensional Collapse of Northern Tunisia. Tectonics, 37(6), 1626–1647. https://doi.org/10.1029/2017TC004846

Camafort, M., Pérez-Peña, J. V., Booth-Rea, G., Melki, F., Gràcia, E., Azañón, J. M., Galve, J. P., Marzougui, W., Gaidi, S., & Ranero, C. R. (2020). Active tectonics and drainage evolution in the Tunisian Atlas driven by interaction between crustal shortening and mantle dynamics. Geomorphology, 351. https://doi.org/10.1016/j.geomorph.2019.106954

Delile, H., Abichou, A., Gadhoum, A., Goiran, J. P., Pleuger, E., Monchambert, J. Y., Wilson, A., Fentress, E., Quinn, J., Ben Jerbania, I., & Ghozzi, F. (2015). The Geoarchaeology of Utica, Tunisia: The Paleogeography of the Mejerda Delta and Hypotheses Concerning the Location of the Ancient Harbor. Geoarchaeology, 30(4), 291–306. https://doi.org/10.1002/gea.21514

Gaidi, S., Booth-Rea, G., Melki, F., Marzougui, W., Ruano, P., Pérez-Peña, J. V., Azañón, J. M., Zargouni, F., Chouaieb, H., & Galve, J. P. (2020). Active fault segmentation in Northern Tunisia. Journal of Structural Geology, 139. https://doi.org/10.1016/j.jsg.2020.104146

Khelil, M., Khomsi, S., Roure, F., Vergés, J., & Zargouni, F. (2021). Structural styles of the Tellian fold-and-thrust belt of Tunisia based on structural transects: Insights on the subsurface oil and gas pre-salt plays. Arabian Journal of Geosciences, 14(19). https://doi.org/10.1007/s12517-021-08308-4

A court Specialized regional scientific journal issued by CRTEAN in collaboration with the FASRC

SPATIO-TEMPORAL COMPARISON OF CARBON MONOXIDE EMISSIONS IN KHARTOUM USING SENTINEL-5P & GOOGLE EARTH ENGINE

Marwa A. AlAmin[1], Mahgoub S. Mohamedain[1], Eltaib S.M. Ganawa[2], Eithar Salah[3]

1 Faculty of Geographical and Environmental Science, University of Khartoum, Sudan-< mrwalgabri@gmail.com>(Corresponding Author)
1 College of Forestry and Range Science, Sudan University of Science and Technology- < hajabo69@gmail.com> - Co-Corresponding). P.O. Box: 6146- Pot Code: 11113 Khartoum, Sudan.
2 Faculty of Geographical and Environmental Science, University of Khartoum, Sudan- < ganawagis@gmail.com >.
3 Faculty of Geographical and Environmental Science, University of Khartoum, Sudan - < eitharsalah7@gmail.com> (Co-Corresponding Author)

ABSTRACT

Air pollution is a major risk factor for public health and its impact in developing nations especially under rapid urbanization and ongoing conflict. This study is a synergy of the Google Earth Engine (GEE) platform with remote sensing data to examine spatiotemporal changes in carbon monoxide (CO) concentrations in Khartoum State (Sudan) and their correlation with the Normalized Difference Vegetation Index (NDVI) and Temperature Condition Index (TCI) comparing years 2019 and 2024.The research used three step processes; first sampled monthly CO tropospheric column densities from Sentinel-5P TROPOMI for 2019 and 2024, then calculated NDVI from Sentinel-2 imagery and TCI from GLDAS surface temperature and soil moisture, then conducted statistical analysis for CO - NDVI and CO–TCI relationship analysis, and then mapped the outputs in ArcGIS Pro spatial interpretation.The study revealed that CO levels slightly increased in 2024 duringdry period(February-March)with 0.040 ppm, higher than 0.038 ppm in 2019. This increase could be attributed to conflict-related activities and infrastructure damage. Mid-year CO levels drop by seasonal rainfall effects. 2019 showed greener conditions than 2024, with higher NDVI peaks (~0.12 vs. 0.09) and dry-season minima (~0.08 vs. 0.06).The TCI values in 2024 compared to 2019 were lower in some months, for instant June 60.9 vs. 61.7 and September 55.9 vs. 57.6, indicate thermal stress, and weak CO–NDVI/TCI correlations (R2 0.01–0.04) which could be attributed to conflicts related activities.The findings highlight that higher levels of CO coupled with depletion of vegetation and heat stress, reflect worsening environmental conditions in Khartoum state and emphasize the need to make conflict-based policies that prevent pollution, encourage urban greening, and protect ecosystems and public health.

Keywords: Carbon Monoxide, Google Earth Engine ; NDVI; TCI; Sentinel-5P.

1. INTRODUCTION

Carbon monoxide (CO) is a common air pollutant and is an efficient indicator of traffic- and combustion-related emissions, especially in populated cities; Hwang et al., 2023. The rapid urban growth, industrial emissions, heavy vehicular traffic, and ongoing conflict such as that in Khartoum State, Sudan thatemerged an urgent environmental and public health threat to air pollution. CO emissions occur primarily due to incomplete combustion on vehicles, residential heating, coal power stations, and biomass burning, which poses health risk and environmental degradation (Hwang et al., 2023). While ground-based measures can be very good for assessing pollutant concentrations (Kazami et al., 2023), spatial coverage is limited and frequently fails to capture city-wide patterns of pollution. The increasing availability of earth observation and remote sensing capabilities allows the observation of air quality in greater spatial and temporal scales (Maurya et al., 2022). In particular, the Sentinel-5P, a satellite mission in atmospheric monitoring, which provides high-resolution CO measurements at high sensitivity and has become one of the essential monitoring tools for the regulation of pollutant dynamics in urban environments (Lorente et al., 2019; Enkhjargal et al., 2024; Uyar, 2024) .

In addition, remote sensing combined with cloud-based platforms like Google Earth Engine allows the combination of multiple datasets to provide a comprehensive spatial and temporal assessment of air pollution. This study utilizes Sentinel-5P TROPOMI data to quantify CO concentrations for Khartoum State for 2019 and 2024 with NDVI collected from the Sentinel-2 images, and TCI obtained from GLDAS surface temperature and soil moisture datasets from GLDAS surface temperature and soil moisture datasets (Liu et al., 2023). The NDVI provides insights into the dynamics of vegetation cover and TCI reflects thermal stress, both of which influence CO dispersion and accumulation in urban landscapes. Together, using these environmental indices and GIS-based visualization, we can measure spatial and temporal patterns in CO and explore interactions between those

1.1. Problem Statement

At Khartoum State, air pollution and CO are growing health- and environmental challenges; rapid urbanization, industrial emissions, traffic, and conflict have contributed to increasing air quality challenges. Since ground observation allows only limited snapshots, it has become possible to capture larger-scale patterns of pollution, but technologies developed in remote sensing have expanded the range of better monitoring capabilities. This study lays out an alternative approach using Sentinel-5P satellite data as part of the Google Earth Engine platform to monitor and evaluate spatio-temporal changes in CO concentrations through 2019 and 2024. Using the TCI of CO levels alongside vegetation NDVI values, the study does not only track pollution trends but also explores ways in which environmental stress and human behavior contribute to air quality. These results are intended to provide policymakers with accessible, evidence-based information that can help guide policy actions in combating air pollution and in protecting Khartoum's nearly 10 million residents during dry periods, especially during extremely dry, rainy seasons.

1.2. Objectives

This study aims to usesatellite and cloud data and GEE to map and quantifyCO pollution in Khartoum state for 2019 and 2024 and evaluate the relationship between CO concentrations and environmental factors (NDVI and TCI).To achieve this goal the specific objectives are:

- To generate high-resolution CO concentration maps and changein Khartoum State using Sentinel-5P for 2019 vs. 2024.
- To assess the changes in vegetation cover (NDVI) and temperature conditions (TCI) in Khartoum State between 2019 and 2024.
- To evaluate the relationship between CO concentrations and environmental factors (NDVI and TCI) to understand how vegetation cover and temperature condition influence CO levels.
- To capture those findings from a clear mind that will aid in the prevention of public health and the guidance of better policies.

2. MATERIALS AND METHODS

2.1. Study Area

Khartoum is the capital city of Sudan as well as State, located in central Sudanwith an area of 22,122 km^2 and population of 9.4 million people (OCHA, 2023). It lies between 15° 35' 17" North and 32° 32' 3" East at the intersection of the Blue and White Nile rivers, which forms the River Nile (Figure, 1). The three major cities in Khartoum state are Khartoum, Omdurman and Khartoum North (BahriKhartoum is relatively flat, at elevation 385 m (1,263 ft) and has a hot desert climate typical of the Saharo-Sahelian zone, marking the transition between the Sahara's arid areas and the Sahel's semi-arid lands (Köppen climate classification BWh(Peel et. al., 2007).Figure, 2, shows that Khartoum State has a typical hot, arid climate with high temperatures, During the colder winter months (December,January and February) the monthly mean air temperature ranges from 22–25 °C. It then gradually rises to peak values of 35–36 °C in May–June before slightly declining during the rainy season. For the majority of the year, Khartoum State experiences low precipitation; from November to April in both 2019 and 2024, monthly rainfall was close to 0 mm as shown in Figure, 3. Rainfallstarts to increase in May, reaching 2–3 mm,and rises more noticeably in June, reaching roughly 14 mm in 2019 and 11 mm in 2024. The rainy season peaks in July and August. In 2019, rainfall was approximately 34 mm in July and 68 mm in August; in 2024, it was much higher at roughly 60 mm in July and 88 mm in August. Then, in September, precipitation decreases sharply to about 22 mm in both years, and in October, it drops even more to about 15 mm in 2019 and 7.8mm in 2024. The strong climatic seasonality influencing atmospheric and environmental processes is reflected in the seasonal coincidence of high temperatures and summer rainfall in. The main environmental challenge facing the state is the ongoing war, urbanization, industrial emissions and vehicular pollution and wastes.All factors contributing to air quality problems and greatest pollutant, such as Carbone Monoxide (CO) that particularly sensitive as it has harmful effects on human and natural health.

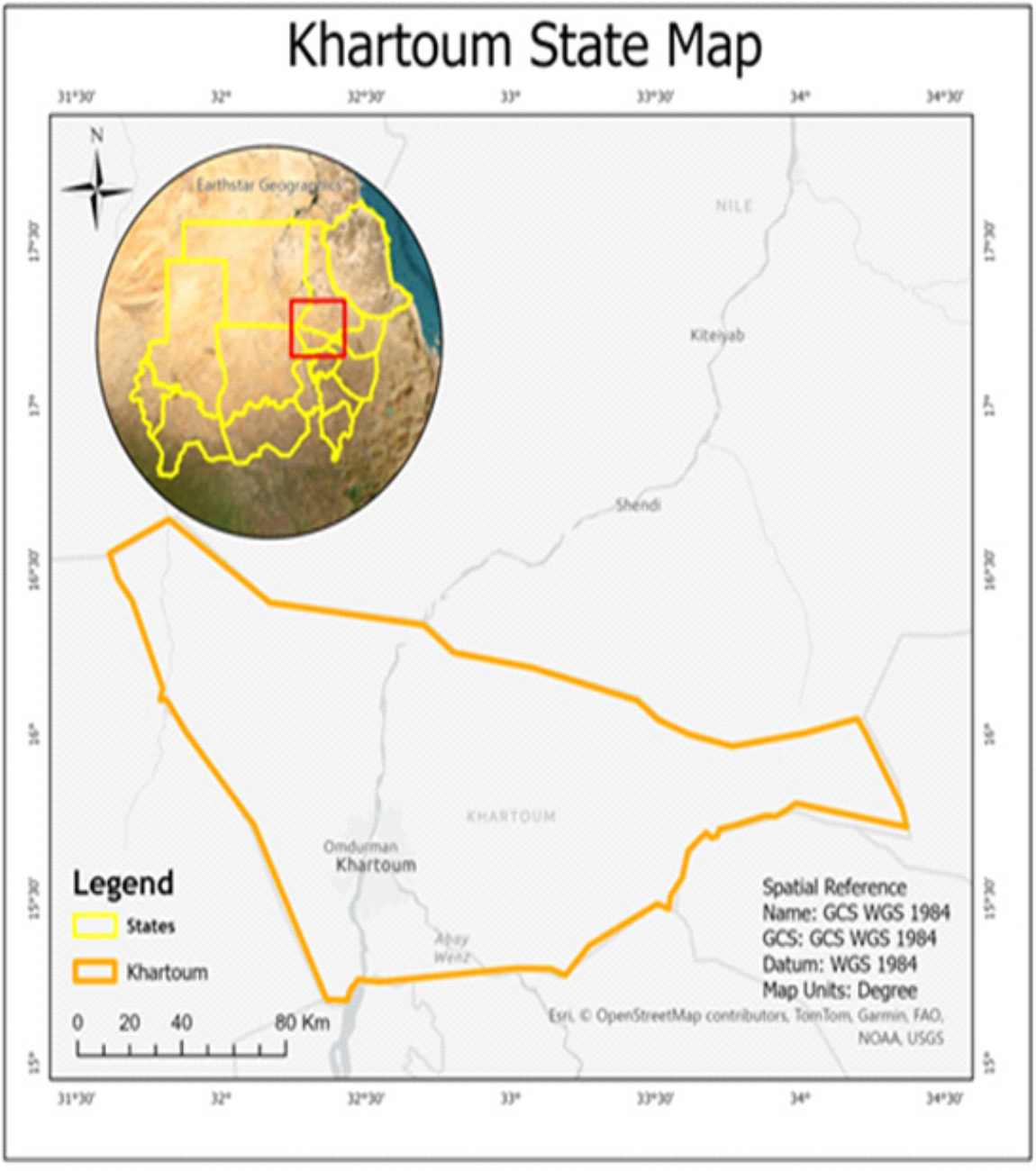

Figure 1: The Study Area, Khartoum State.

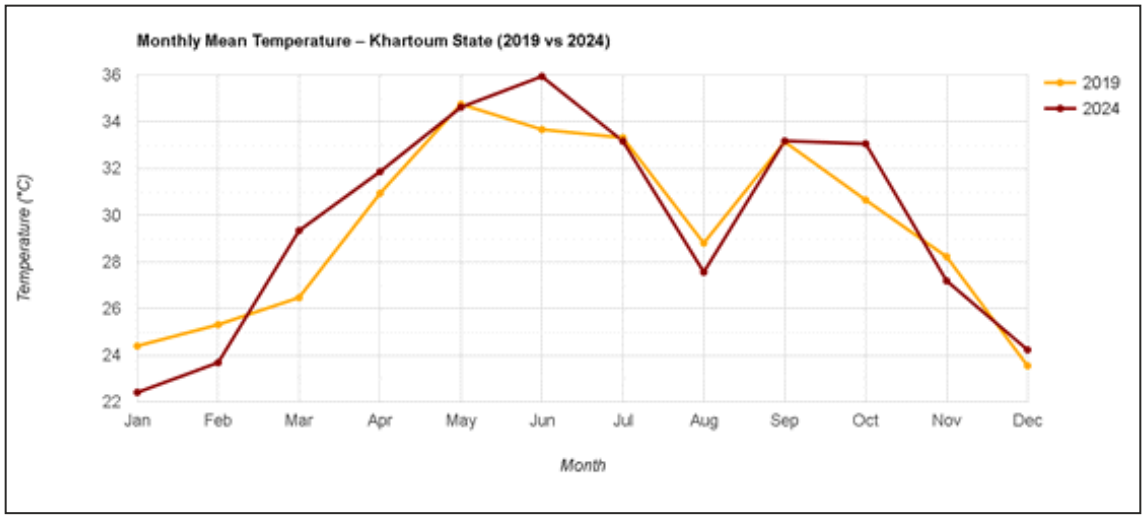

Figure 2: Monthly mean air temperature in Khartoum State for 2019 and 2024

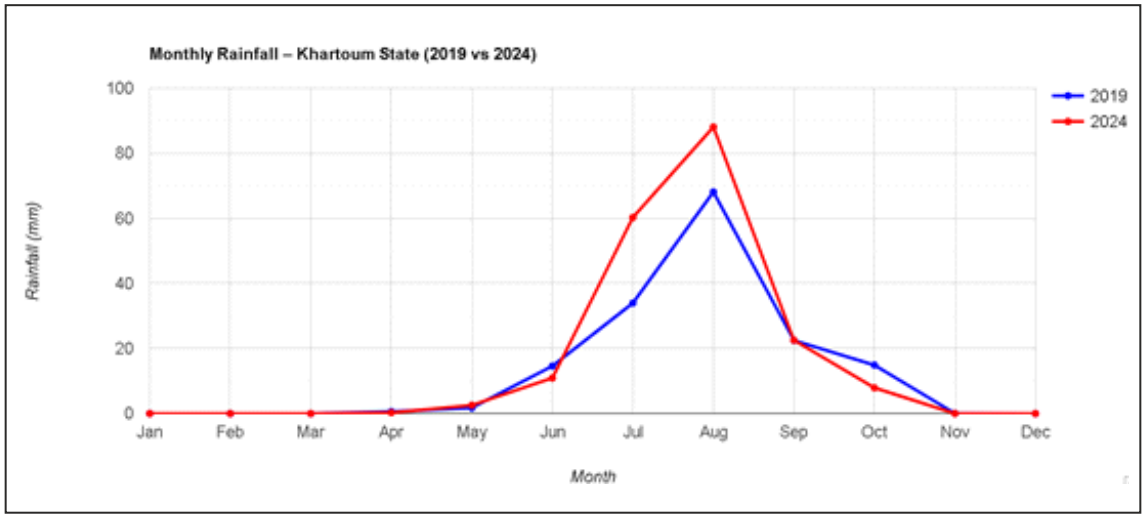

Figure 3:Monthly rainfall distribution in Khartoum State for 2019 and 2024.

2.2. Data Sources and Collection

This study employed Sentinel-5P TROPOMI data to retrieve CO concentrations. TROPOMI (Tropospheric Monitoring Instrument) is a cutting-edge satellite instrument aboard the European Copernicus Sentinel-5 Precursor (S5P) satellite, launched in October 2017. It plays an essential role in gathering data that helps scientists to better understand atmospheric processes and environmental changes (https://www.tropomi.eu/). For the NDVI the ESA Sentinel-2 imagery has been used.The Global Land Data Assimilation System(GLDAS)products were used for theTemperature Condition Index (TCI). All datasets were accessed and processed on Google Earth Engine (GEE), which enabled cloud-based filtering, quality control, and spatial/temporal sub setting for Khartoum State (2019 vs. 2024) (Table, 1).

Table 1: Data Sources

Dataset	Resolution	Data Type	Date Range/ Monthly	Data Source / Platform
Sentinel-5P (TROPOMI)	7 × 3.5 km² (across/along track)	CO Column Density (atmospheric pollutant)	2019&2024	ESA / Google Earth Engine https://developers.google.com/earth-engine/datasets/catalog/COPERNICUS_S5P_OFFL_L3_CO
Sentinel-2	10 m (bands used for NDVI)	Multispectral Reflectance (NDVI)	2019&2024	ESA / Google Earth Engine (GEE) https://developers.google.com/earth-engine/datasets/catalog/COPERNICUS_S2_SR
GLDAS	0.25° (~25 km) grid, 3-hourly	Surface Temperature & Soil Moisture (for TCI)	2019&2024	NASA / Google Earth Engine (GEE) https://developers.google.com/earth-engine/datasets/catalog/NASA_GLDAS_V021_NOAH_G025_T3H
CHIRPS	0.05° (~5 km), daily	Rainfall / Precipitation	2019 & 2024	Climate Hazards Group / Google Earth Engine (GEE) https://developers.google.com/earth-engine/datasets/catalog/UCSB-CHG_CHIRPS_DAILY
ERA5-Land	0.1° (~9 km), monthly	2-m mean air temperature	2019 & 2024	ECMWF / Copernicus / Google Earth Engine (GEE) https://developers.google.com/earth-engine/datasets/catalog/ECMWF_ERA5_LAND_MONTHLY

2.3. Research Design

The research method designed in three stages manner to identify systematic analysis of CO pollution and associated environmental effects within Khartoum State (Figure 4).

Phase 1*: Carbon Monoxide Mapping*: This phase involved retrieving and counting the concentration of carbon monoxide in Khartoum State using Sentinel-5P TROPOMI data for the years 2019 - 2024. The Tropospheric vertical column density of CO was extracted and processed on the GEE platform, which allows cloud-based filtering, quality control and temporal aggregation. This technique allowed obtaining high-resolution spatially continuous CO concentration maps that reflect seasonal changes as well as hotspots of pollution in the study area.

Phase 2: *Vegetation and Surface Condition Analysis (NDVI & TCI):* Phase 2 was conducted to measure changes in vegetation cover and surface conditions using NDVI and TCI values obtained from Sentinel-2 imagery and GLDAS surfacetemperature to assess vegetative health and thermal stress and drought based on and soil moisture datasets. These measures provide information on how vegetation density and surface thermal conditions influence CO dispersal and accumulation in urban landscapes.

Phase 3: *Statistical and Spatial Analysis*: Phase 3 focused on the interaction between CO concentrations and environmental parameters. Analysis of the association between CO, NDVI, and TCI using statistics has been done to assess their relationship to possible causality and provides looking closely at of the relationship between vegetation health and thermal stress in urban air quality. The images from the processed datasets were imported into ArcGIS Pro for spatial visualization, providing detailed maps to show spatial temporal patterns of CO, vegetation, and temperature. This multiphase design builds on an integrated strategy that combines satellite remote sensing, cloud-based data processing, and GIS visualization, with satellite remote sensing to produce meaningful policy-relevant insights on air quality in Khartoum State.

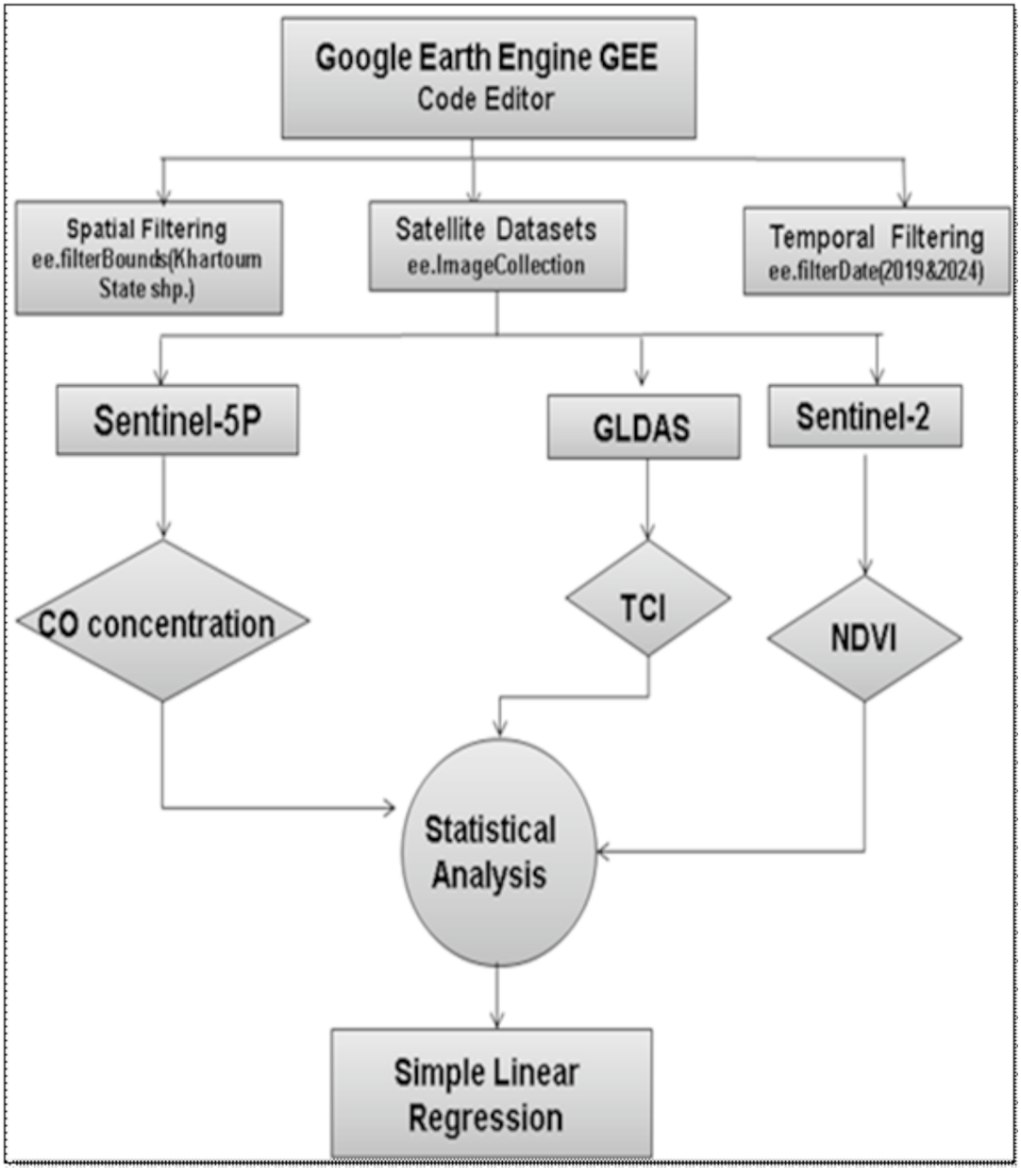

Figure 4: Research Design Methodological Framework

3. RESULTS AND DISCUSSION

This section provides a spatial and temporal snapshot of CO concentration, vegetative health and TCI in Khartoum State for 2019 and 2024. Results identify CO levels, plant cover changes and surface temperature, and correlations between CO and environmental variables. Each map, trend, and regression are illustrated and presented by describing how those occur and specific factors in the impact of air quality in the study area.

3.1. Carbon Monoxide

Figures, 5&6, present the results of concentrations of CO in Khartoum in 2019 and 2024. The average CO concentrations in 2024 were slightly higher than they were in 2019 and the highest was 0.04 ppm in March, 0.06 ppm in February and 0.036 ppm in November. In 2019, the peak CO concentration was recorded in March (0.038 ppm), followed by February (0.037 ppm) and April (0.037 ppm).The higher concentration in March 2024 implies higher emissions, potentially related to conflicts such as displacement, fires or infrastructure damage. In July, the lowest concentrations were (0.028 ppm) and November (0.029 ppm) and September and October (0.030 ppm) in 2024, when seasonal influence was exerted on the dispersion of pollutant.

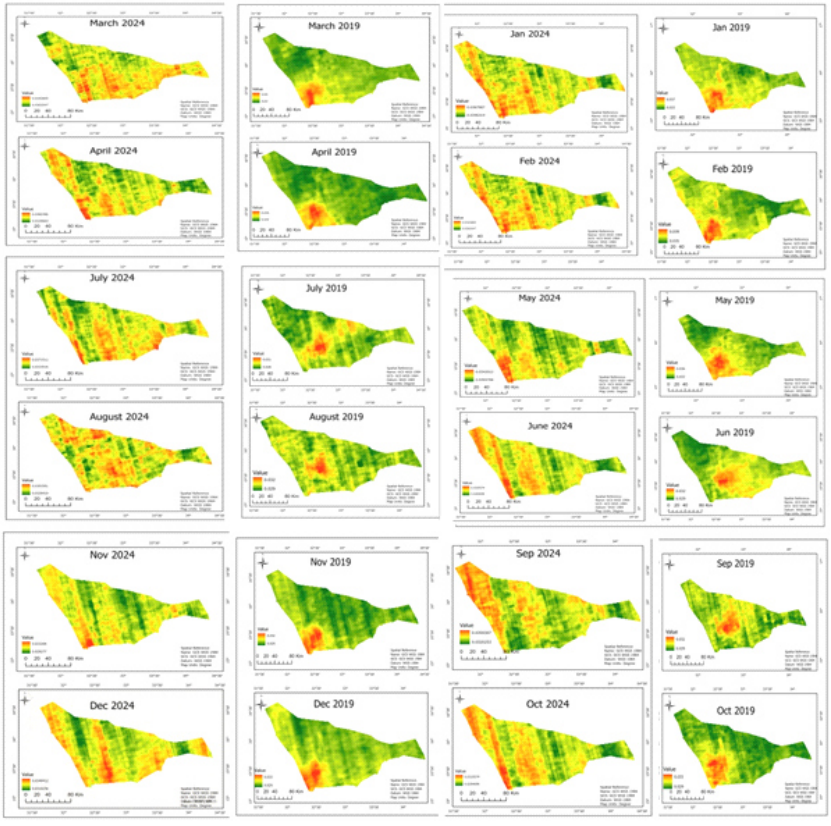

Figure 5: Carbon Monoxide concentration in Khartoum State in 2019 vs. 2024

We conclude that from 2019 to 2024 CO concentrations were slightly higher in Khartoum and highest during dry season. The patterns suggest seasonal factors and conflicts-related emissions are the key drivers of these changes (Figure5).

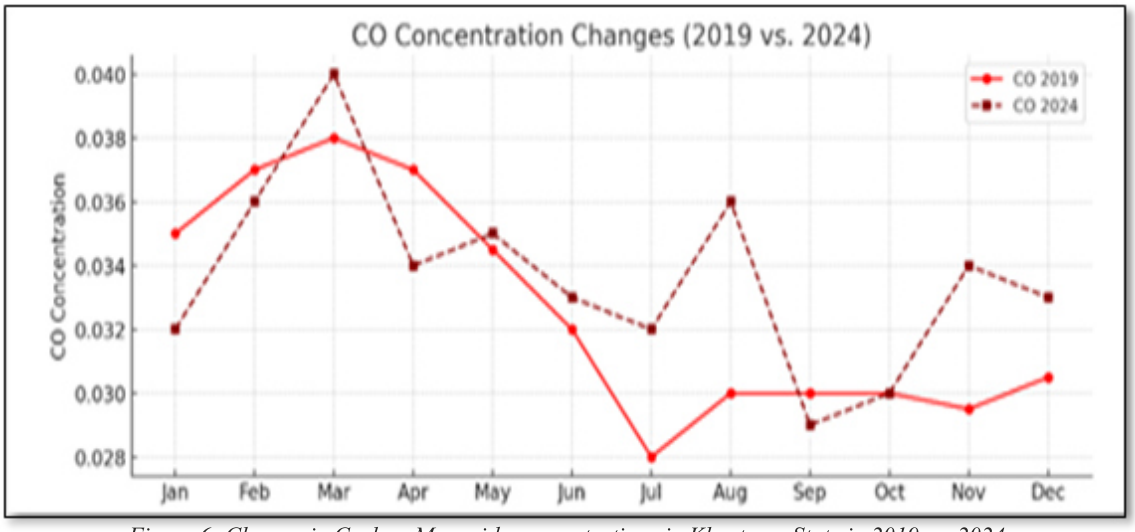

Figure 6: Changesin Carbon Monoxide concentrations in Khartoum State in 2019 vs. 2024

3.2. Normalized Difference Vegetation Index (NDVI)

According to (Figures,7&8), NDVI results indicate better vegetation in 2019 than 2024. In 2019, the highest was in September,October and November with about (0.12) because they represent the peak growing season. while in 2024, NDVI peak was in September (0.12), October (0.09) and December (0.87) but overall values were less than in 2024 falling in the aggregate, suggesting that vegetation was declining due to land degradation, drought and less agricultural activities. During the dry season, the lowest NDVI values were in June and July with average of 0.08 compared to 0.06 in 2024.

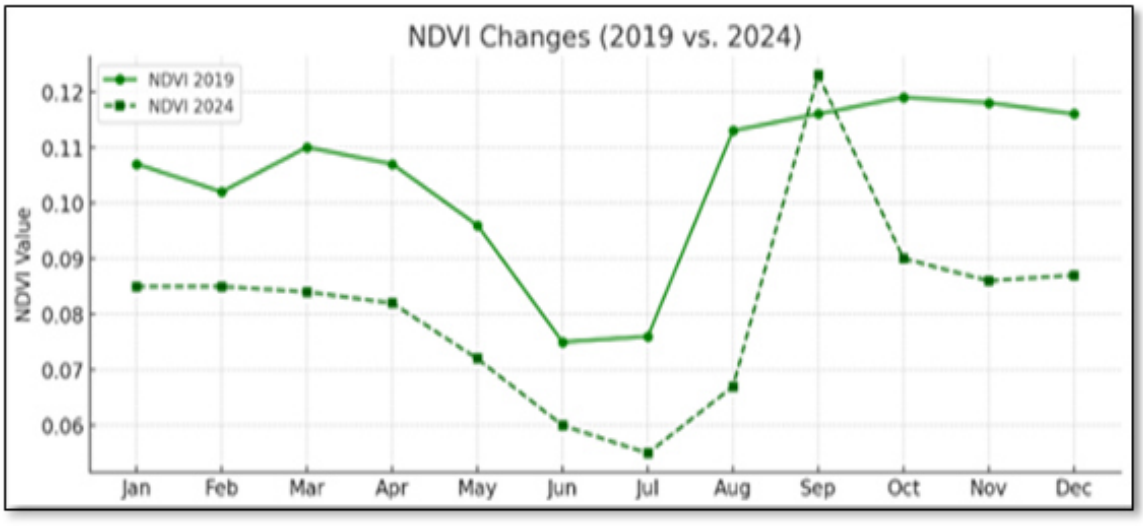

Figure 7:Changes in NDVI values in Khartoum State in 2019 vs. 2024.

These NDVIresults clearly indicate a decline in vegetation health between 2019 and 2024, higher peak and dry season values in 2024. This increases because the natural disaster, drought, and rural development in Khartoum State are related to increased land degradation, drought, and depletion of agriculture.

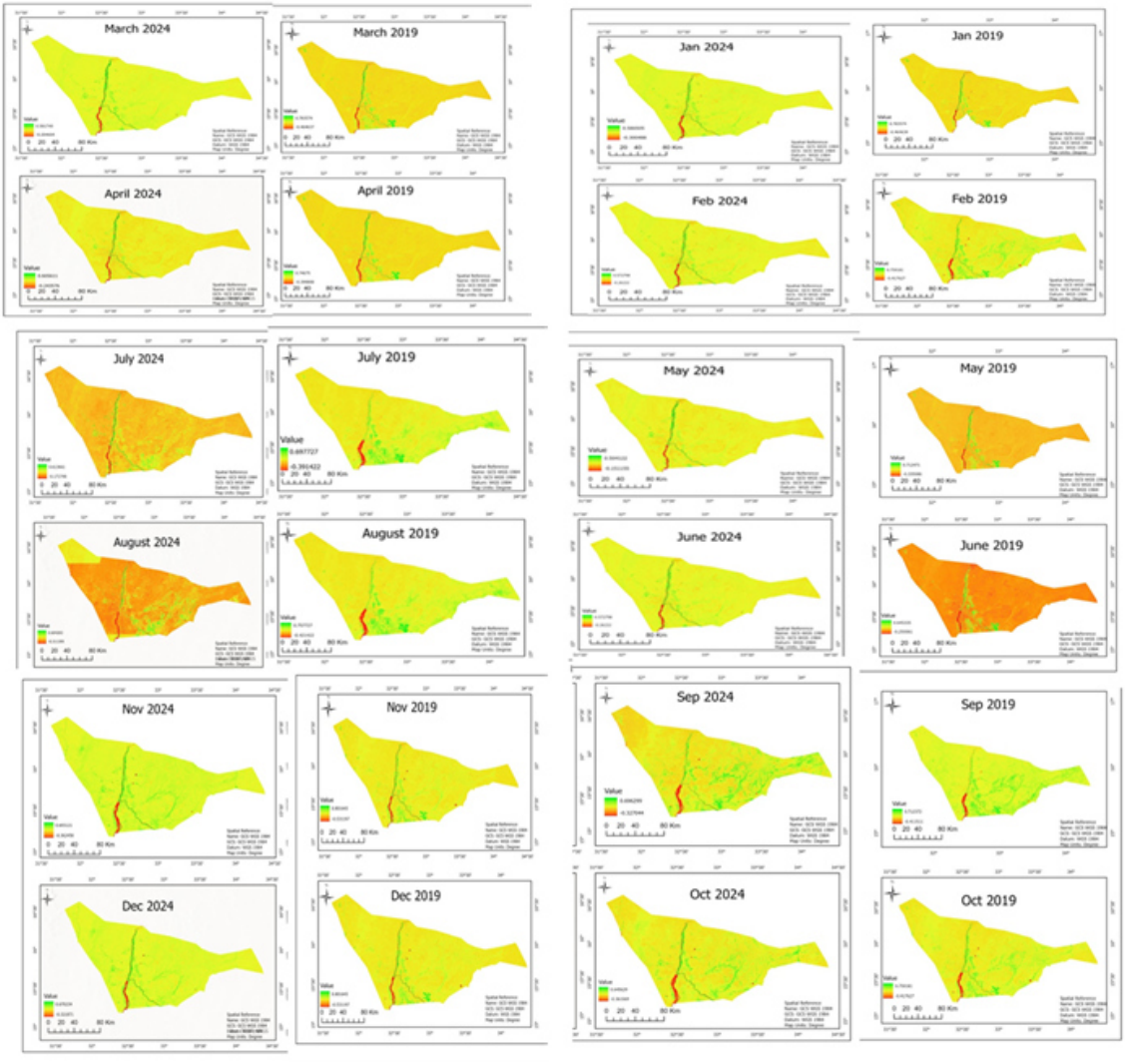

Figure 8: NDVIvalues in Khartoum State in 2019 vs. 2024

3.3. Temperature Condition Index (TCI)

TCI results (Figures,9&10) showed that Khartoum state faced more heat stress in 2024 compared to 2019. In 2019, May and June saw the best days at 61.7, while September reached 57.6. The year 2024 saw lower scores: June hit 60.9, September fell to 55.95, and October dropped to 55.1. December 2019 scored 36.3, January hit 40.5, and November reached 46.05. These numbers were lower than December 2024 at 37.95, November at 43.6, and February at 37.65. These trends could be attributed to changing weather patterns in the land surface, which act as a buffer and increase heat stress. Also changes might link to the loss of plants and the wearing down of soil.

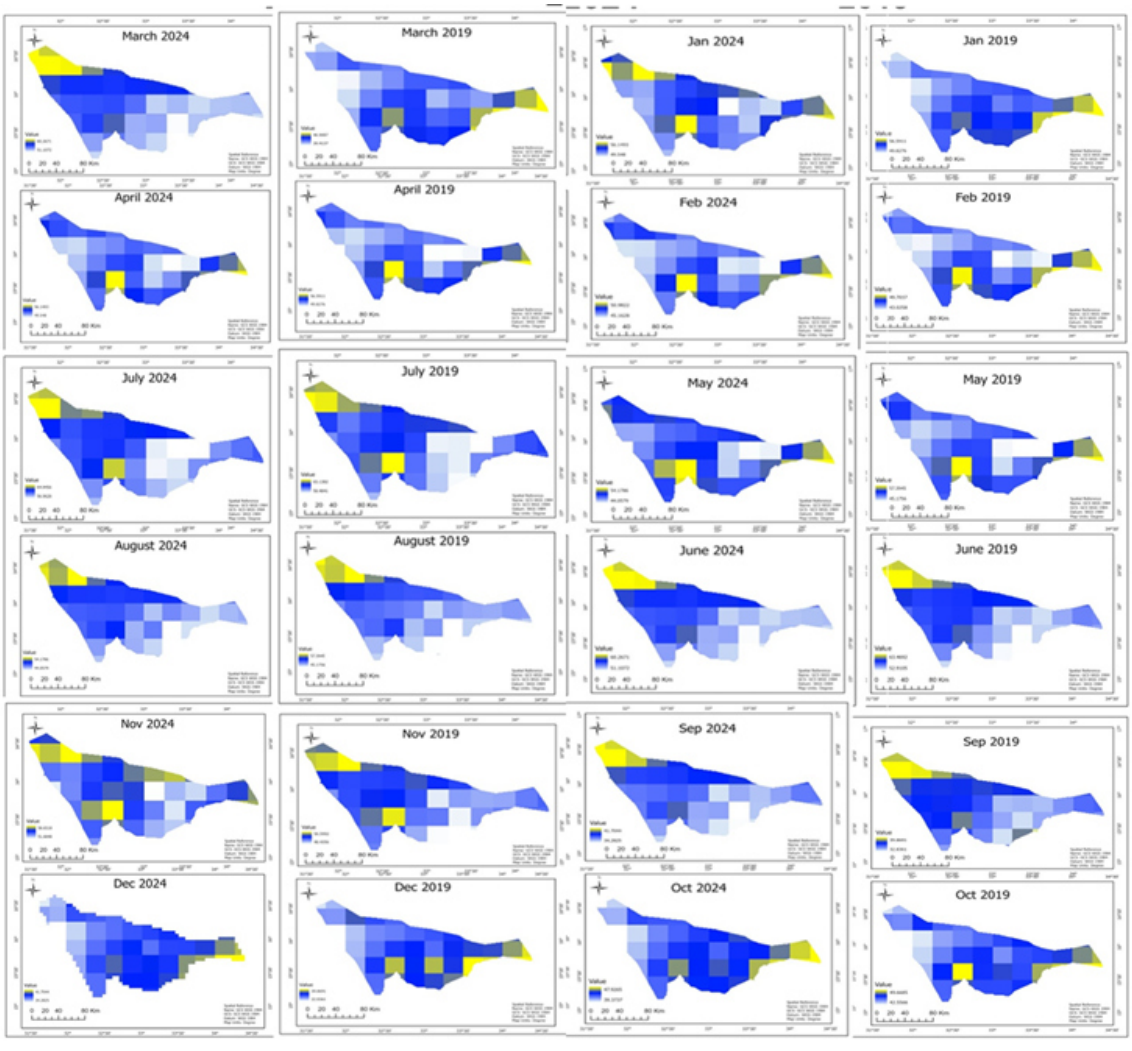

Figure 9: TCI values in Khartoum State in 2019 vs. 2024

To conclude, the TCI regression analysis shows that the relationship with CO concentrations of 2024 was lower in relation to the increase in temperature with 2024 and that in comparison with 2019, the correlation was higher in 2024. This suggests that increased heat stress coupled with vegetation loss and soil degradation have impacted the determinants of air quality in Khartoum State.

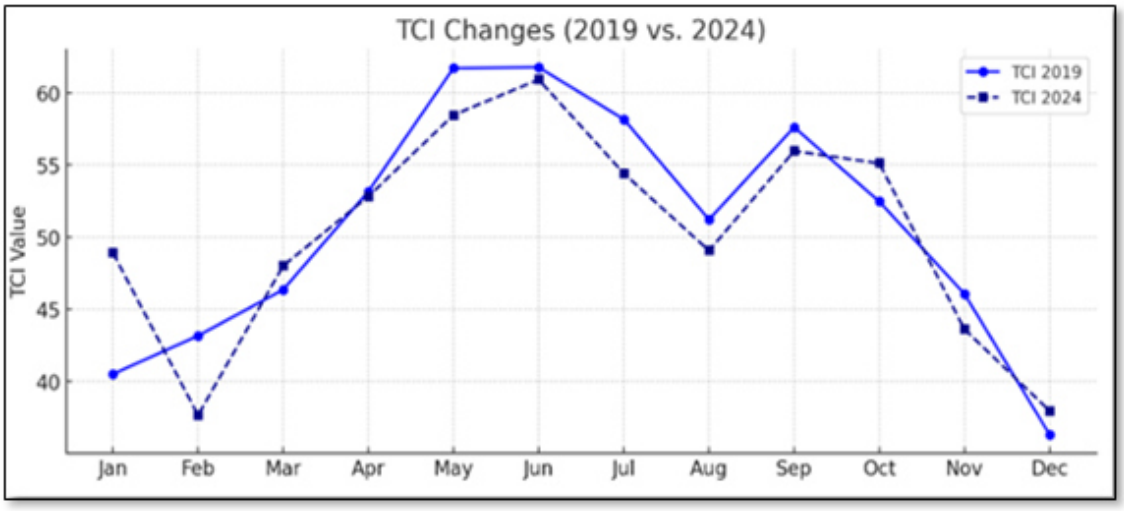

Figure 10: Changes in TCIvaluesin Khartoum State in 2019 vs. 2024

3.4. Regression Analysis

3.4.1. CO–NDVI Regression 2019 vs. 2024

The regression analysis, using CO concentrations as the dependent variable and NDVI as the independent predictor, was also conducted to explore the effect of vegetation on air quality. The 2019 model also showed a very weak correlation (R^2 = 0.017) suggesting that existing vegetation covered had no influence on CO distribution throughout Khartoum State. The evidence for this suggests that in this year, the CO levels from vegetation can be natural buffer of the natural world and, as a result, other factors such as traffic density, industrial emissions and localized human activities probably took larger roles than foliage was. The low accuracy reveals the complexity of the dynamic of urban air pollution as multiple anthropogenic and environmental variables interact at the same time (Figure,11).

By 2024, the CO–NDVI relationship reduced further, R^2 dropping to 0.0097. This loss may be due to the combined effects of more severe vegetation loss, land degradation, and increased emissions attributable to conflict-related disturbances such as fires, infrastructure loss, and population displacement. The further reduction in correlation suggests that this slowing effect of vegetation on the concentration of CO increased even less when under stressful environmental and social conditions. These findings suggest that green cover is becoming increasingly compromised in rapidly changing urban and conflict-affected landscapes, and CO pollution patterns are influenced more strongly by anthropogenic emissions and seasonal variables than by vegetation dynamics.

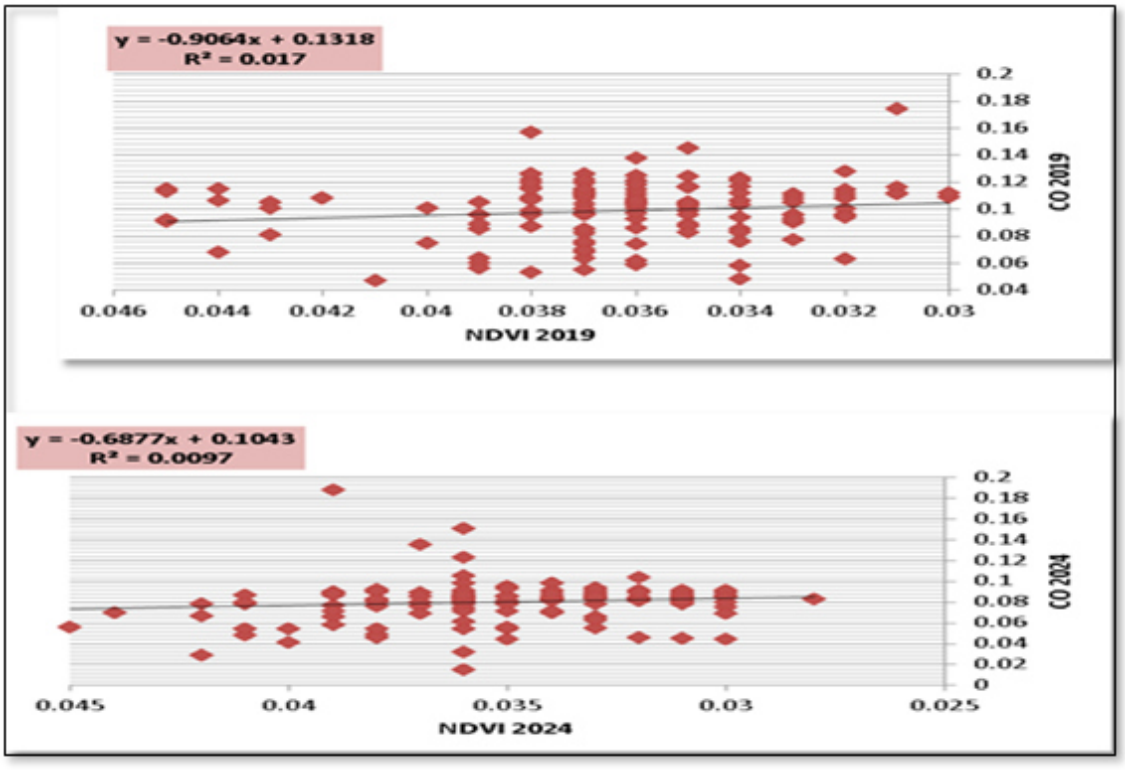

Figure 11: Khartoum State CO–NDVI Regression 2019 vs. 2024

3.4.2. CO–TCI Regression Analysis

The CO–TCI regression found that a negative relationship of the CO/TCI analysis between 2019 and 2024 was that lower TCI values (less thermal stress) were generally associated with slightly higher CO concentrations in 2019. But, the R2 value of 0.0379 indicated that TCI only explain only 3.79% of the variation in CO, indicating only that TCI explained only 3.79% of the variability in CO. this reflecting that other factors such as emission sources, wind patterns, and urban activities played the dominant role in shaping CO distribution. In 2024, the regression slope became flatter and the R^2 decreased to 0.0275, pointing out a further reduction in TCI's influence on CO levels(Figure, 12).

This weakening relationship is linked to the cumulative impacts of environmental degradation and vegetation loss, besides conflict-related disturbances, which might have disturbed the natural buffering role of the land surface. Seasonal changes, enhanced urban emissions, and local atmospheric dynamics seem to overwhelm the driving role of thermal stress on CO concentration. These findings all suggest that although surface temperature conditions might modulate air quality partially, anthropogenic and conflict-driven factors are increasingly influential in CO variability within Khartoum State.

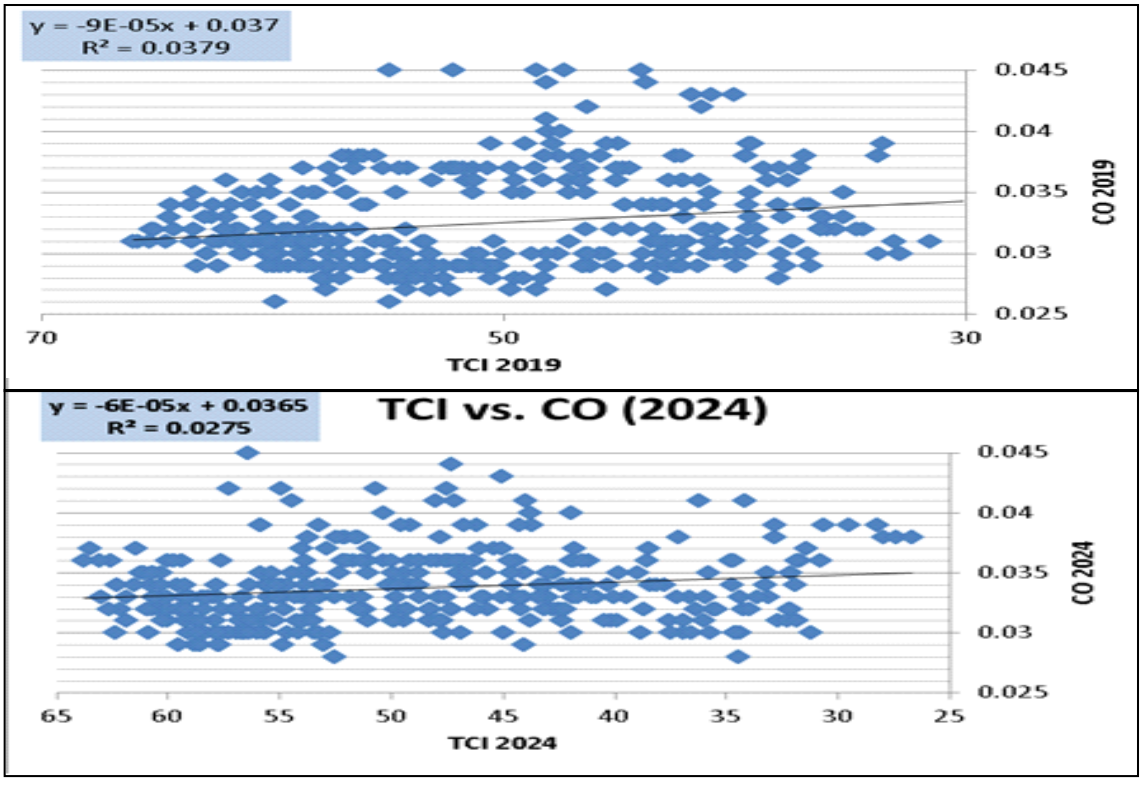

Figure 12: Khartoum State CO–TCI Regression 2019 vs. 2024

According to our results, CO concentrations were lower during the rainy months (July -August) and peaked during the dry season (May–June). This pattern is align with the findings of Anwer et al. (2025), who found that increased dust, decreased precipitation, and increased human activity were the causes of Khartoum's elevated CO and aerosol levels during the dry season,and similar seasonal patterns have been documented over North Africa and the Sahel, where CO concentrations peak during dry periods and decrease during the rainy season (Borsdorff et al., 2019).Additionally, our research found that CO levels gradually increased between 2019 and 2024, which is consistent with multi-year trends documented in Mohamed et al. (2025). This pattern might be a result of Khartoum State's increased deforestation and urbanization during that time.

The inverse relationship between CO concentrations and NDVI values, which suggests that regions with denser vegetation typically have lower CO levels, is one of our study's significant findings,where vegetation serves as a natural sink for air pollutants, reducing local CO accumulation. Similarly, TCI values demonstrated that pollutant dispersion is influenced by soil and surface moisture conditions, with lower TCI (drier conditions) corresponding to higher CO levels.

These findings align with regional research employing Sentinel-5P and GIS-based analysis (e.g., Sohag Governorate, Egypt; Mustafa, 2025), which found that surface conditions and land cover had a major impact on the distribution of pollutants. Kogan (1995) and other studies have reported similar findings, showing that better thermal conditions are linked to more favorable atmospheric dispersion conditions and better vegetation health.

4. CONCLUSION AND RECOMMENDATIONS

The research examined how carbon monoxide (CO) emissions impact vegetation and land surface stress in Khartoum State. They relied on data from Sentinel-5P, Sentinel-2, and GLDAS; all processed with Google Earth Engine, and visualized the findings using ArcGIS Pro. From 2019 to 2024, CO concentrations noticeably increased, but not dramatically. The TCI values declined along with NDVI and NDVI decreases. Both indicate environmental stress. They all come from factors such as climate change, urban development and constant conflict. As compared to contrasting correlations between CO, NDVI and TCI, the relationship was somewhat weak indicating that human activities and seasonal changes play a bigger role in pollution patterns. Finally, satellite monitoring can finally add value in low ground and unstable areas. This study further suggests that Khartoum State needs more air quality monitoring, better management and evidence-based policies to protect health and sustain ecosystems.

5. REFERENCES

Anwer, H. A., Hassan, A., &Anwer, G. (2025).Satellite-Based Analysis of Air Pollution Trends in Khartoum before and After the Conflict.Annals of Civil and Environmental Engineering.

Borsdorff, T., et al. (2019).Global and regional carbon monoxide trends observed by Sentinel-5P TROPOMI.Atmospheric Chemistry and Physics, 19, 12819–12835. https://doi.org/10.5194/acp-19-12819-2019

Enkhjargal, O., Tuyagerel, D., Tovuudorj, R., Khurelsukh, Z., &Sarangerel, E. (2024).Dispersion mapping of Carbon Monoxide (CO) derived Sentinel 5P and evaluation with LUR model during winter in Ulaanbaatar, Mongolia. Proceedings of the Mongolian Academy of Sciences, 64(01), 1–10. https://doi.org/10.5564/pmas.v64i01.3545

Hwang, J., Maharjan, K., Cho, H., (2023). A review of hydrogen utilization in power generation and transportation sectors: achievements and future challenges. Int. J. Hydrogen Energy 48 (74), 28629e28648.

KazemiGarajeh, M; Laneve, G; Rezaei, H; Sadeghnejad, M; Mohamadzadeh, N; Salmani, B (2023). Monitoring Trends of CO, NO2, SO2, and O3 Pollutants Using Time-Series Sentinel-5 Images Based on Google Earth Engine. Pollutants.3(2): 255 279.

Kogan, F. N. (1995). Application of vegetation index and brightness temperature for drought detection.Advances in Space Research, 15(11), 91–100. https://doi.org/10.1016/0273-1177(95)00079-T

Liu, Z., Chen, Y., & Chen, C. (2023).Analysis of the Spatiotemporal Characteristics and Influencing Factors of the NDVI Based on the GEE Cloud Platform and Landsat Images. Remote Sensing, 15(20), 4980.https://www.mdpi.com/2072-4292/15/20/4980.

Lorente, A; Boersma, KF; Eskes, HJ; Veefkind, JP; Van Geffen, JHGM; De Zeeuw, MB; Krol, MC (2019). Quantification of nitrogen oxides emissions from build-up of pollution over Paris with TROPOMI.Sci. Rep. 9(1), 20033.

Maurya, NK; Pandey, PC; Sarkar, S; Kumar, R; Srivastava, PK (2022). Spatio-Temporal Monitoring of Atmospheric Pollutants Using Earth Observation Sentinel 5P TROPOMI Data: Impact of Stubble Burning a Case Study. Int. J. Geogr. Inf.11(5): 301.

Mohamed, H., Hassan, A., &Elhag, A. (2025).A five year study using Sentinel 5P data observing seasonal dynamics and long term trends of atmospheric pollutants.International Journal of Engineering and Geosciences. Retrieved from https://dergipark.org.tr/en/pub/ijeg/issue/90140/1587122

Mustafa, A. A. (2025). Integration of Google Earth Engine and GIS for monitoring and mapping air pollutants (Sohag Governorate, Egypt).Egyptian Journal of Remote Sensing and Space Science. Retrieved from https://journals.ekb.eg/article_417301.html

OCHA, 2023; United Nations Office for the Coordination of Humanitarian Affairs (OCHA). Sudan: Khartoum State Population Estimate (2023). Available at: https://unocha.org/sudan.

Peel, M. C., Finlayson, B. L., & McMahon, T. A. (2007). Updated world map of the Köppen-Geiger climate classification.Hydrology and Earth System Sciences, 11, 1633–1644.

Uyar, N. (2024). Air Pollution and Plant Health: A Research on Tokat Province. Journal of New Results in Engineering and Natural Sciences, 21, 30–46. https://dergipark.org.tr/tr/pub/jrens/issue/88796/1503143

LAND SURFACE TEMPERATURE (LST) ANOMALIES AS POTENTIAL PRE-SEISMIC INDICATORS: A REMOTE SENSING INVESTIGATION IN SEISMO-TECTONIC REGIONS- SUDAN

Hanan M. Elawad [1], Khalid A. Elsayed Zeinelabdein [2],nonamoh31@yahoo.com,
Remote Sensing and Seismology Authority, National Center for Research, Khartoum, Sudan [1]
Professor at Department of Geology, Al Neelain University, Sudan [2]

ABSTRACT

This study investigates the correlation between **Land Surface Temperature (LST) anomalies** and seismic events, exploring the potential of LST as a pre-seismic indicator. The underlying hypothesis is that the development of tectonic stress prior to an earthquake induces physical changes in the Earth's crust that manifest as thermal anomalies on the surface. Remote sensing data from the **Moderate-resolution Imaging Spectroradiometer (MODIS)** Terra/Aqua and the **Sea and Land Surface Temperature Radiometer (SLSTR)** on Sentinel-3 were utilized to analyze LST time series for selected earthquakes in the study area, including events near Sinkat, Al Gadaref, and Almatma. Detailed analysis of the **Sinkat 2000 earthquake (Mw 2.78)** revealed the spatial and temporal evolution of significant LST anomalies, with high-temperature regions appearing and spreading up to 24 days before the seismic event. The results suggest a clear correlation between the observed LST variations and the impending earthquakes, supporting the use of satellite-derived LST monitoring as a critical component in integrated seismo-tectonics surveillance systems.

1. INTRODUCTION

1. Introduction

The monitoring of pre-seismic phenomena is a vital aspect of operational seismo-tectonics. Prior to a major earthquake, the region undergoes a long preparation phase characterized by the accumulation of tectonic stress, which can lead to various physical and electrical changes in the Earth's media [1]. Among the geophysical parameters investigated, **Land Surface Temperature (LST)** has emerged as a promising candidate for remote sensing-based pre-seismic monitoring [2]. The lithosphere-atmosphere coupling mechanism suggests that stress-induced changes in the crust, such as the release of latent heat or changes in ground emissivity, can cause measurable thermal anomalies on the surface.

The earthquake precursor that has been gaining a lot of attention and support from the scientific community across the world is thermal anomaly, i.e. a sudden rise in land surface temperature (LST) a few days or weeks before the earthquake occurrence [3].

Remote sensing offers a crucial advantage in this field by providing wide spatial coverage and continuous monitoring over remote and active fault systems. This study aims to:
1 Analyze the time series of LST data before and after selected earthquake events.
2 Identify and characterize the spatial and temporal evolution of LST anomalies.
3 Evaluate the effectiveness of satellite-derived LST as a pre-seismic signal in the study area.

2. MATERIALS AND METHODS

2.1 Study Area and Selected Earthquakes

The investigation focused on a region encompassing several seismic events. Four selected earthquakes were analyzed, as detailed in Table 1

No	Date	Time h:m:s	Lat. (°)	Long. (°)	Depth Km	Mw	Author	Sub Author	Locality
1	25.Dec. 2000	02:46:54	18.9	34.6	shallow	2.78	KSA		Sinkat
2	27.Jan. 2006	15:54:14	18.91	34.6	33	3.6	ISC	HLW	Sinkat
3	06.Sep. 2007	21:33:01	16.6	33.28	shallow	2.3	ISC	SSN	Matama
4	12.Oct. 2020	03:54:16	16.60	35.350833	10	4.2	GRASS		Gedaref

Table 1: *The earthquakes selected for LST investigation.*

Fig.1 Location of the earthquakes zone selected to study in Sudan.

2.2 Remote Sensing Data

The primary data sources for LST investigation were:
• **MODIS Terra/Aqua Land Surface Temperature/Emissivity (LST) product:** Used for time series analysis, particularly for the 2000, 2006, 2007, and 2020 events. Daily daytime MODIS LST (MOD11A1) scenes were utilized.
• **Sentinel-3 Sea and Land Surface Temperature Radiometer (SLSTR):** Used for the Al Gadaref 2020 event to supplement the MODIS data.

2.3 LST Analysis

A time series analysis of LST was conducted for a period before and after each earthquake. The analysis involved:
1 **Visual Interpretation:** LST images were visually interpreted, where high temperatures were represented by **Red** color and low temperatures by **light green** tones.
2 **Temporal and Spatial Tracking:** The evolution of LST anomalies was tracked over time to identify patterns preceding the seismic events.
3 **Classification (Sinkat 2000 Case):** For the Sinkat 2000 event, an **unsupervised classification** (cluster analysis) was performed to divide the image data into 5 distinct temperature classes, providing a thematic map to aid in the visual interpretation of the high anomaly areas.

3. RESULTS

3.1 Sinkat 2000 Earthquake (Mw 2.78)

The detailed analysis of the Sinkat 2000 event, using 15 scenes before and after the shock, demonstrated a clear pattern of pre-seismic LST anomalies Fig (2a,b).

• **Pre-Seismic Anomaly Evolution:**

◦ **24 Days Prior (Dec 1, 2000):** High LST (53.03-16.31˚C) was observed in the eastern part of the study area.

◦ **13 Days Prior (Dec 12, 2000):** The high LST region began to cover the location of the earthquake and spread to the northern area.

◦ **9 Days Prior (Dec 16, 2000):** The high and moderate anomalous LST spread to the western part of the image, with the anomaly covering the event location from all directions.

3 Days Prior (Dec 22, 2000): The high LST anomaly intensified and extended north of the earthquake location, with a range of 53.73-17.19˚C.

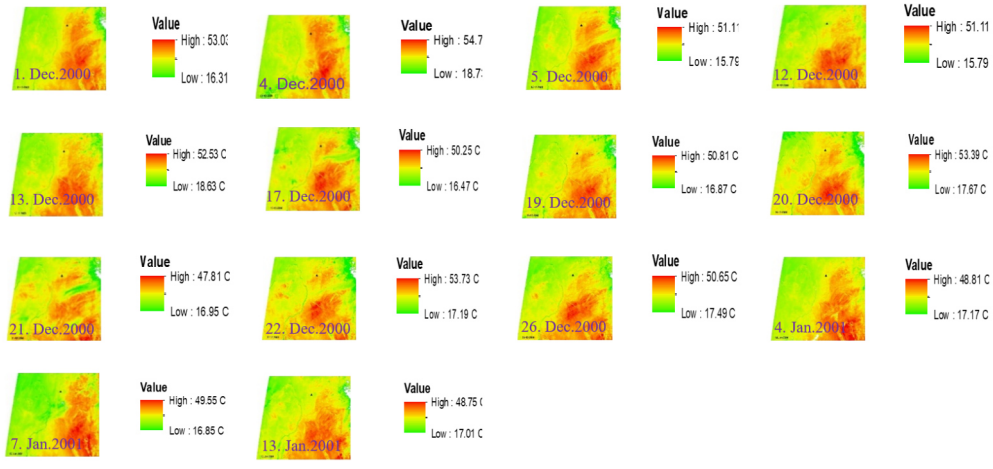

(a) •Red colour denotes region of high LST

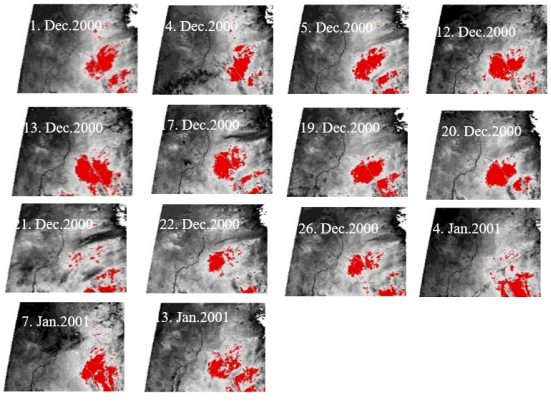

(b) *Fig.2 (a, b) The 25 Dec. 2000 Sinkat earthquake*

• **Post-Seismic Observation:**
◦ **1 Day after (Dec 26, 2000):** The high anomaly extended to the eastern part, but the event location itself was covered by moderate LST, indicating a decrease in the immediate vicinity of the epicenter.
◦ **10 Days after (Jan 4, 2001):** The high LST concentrated in the eastern part, with the western part showing moderate LST, suggesting a dissipation and shift of the thermal pattern.

3.2 Other Case Studies

Similar LST investigations were conducted for the other events, confirming the presence of thermal variations around the time of the earthquakes:
• **Sinkat 2006 (Mw 3.6):** The LST anomaly began developing to the south and southwest of the epicenter 10 days prior to the event.
• **Matama 2007 (Mw 2.3):** A very high LST anomaly (55.61-22.47˚C) was observed on the day of the earthquake, covering the northern and western areas.
• **Gedaref 2020 (Mw 4.2):**The LST anomaly showed a decrease from south to north in the days following the event, suggesting a post-seismic thermal adjustment

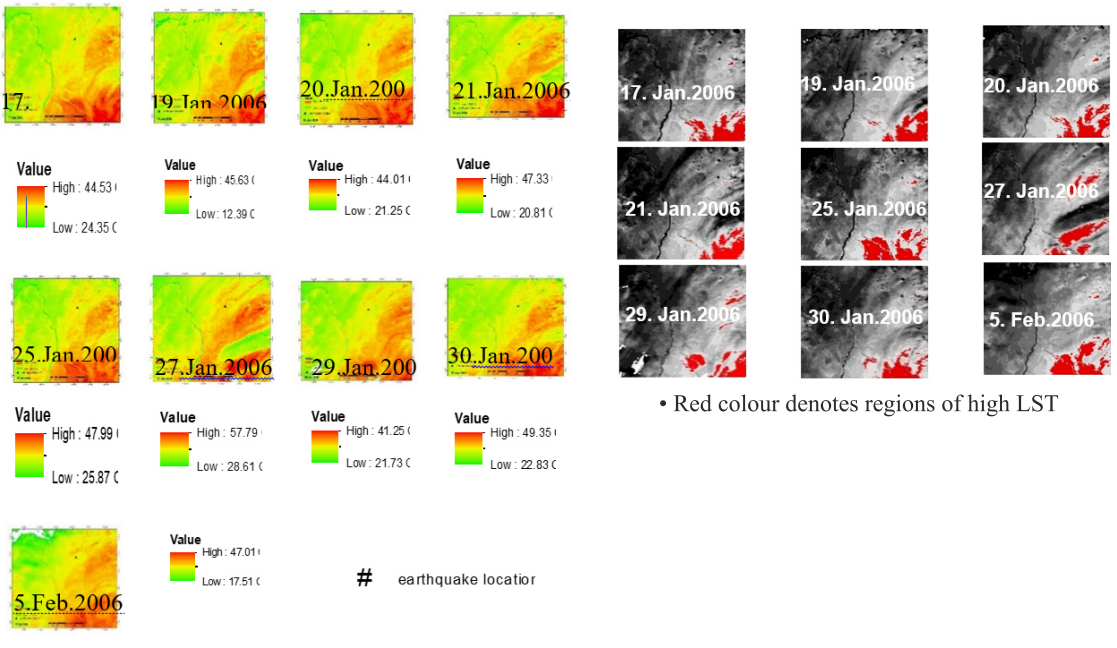

• Red colour denotes regions of high LST

Fig.3 (a, b) The 27. Jan.2006 Sinkat earthquake

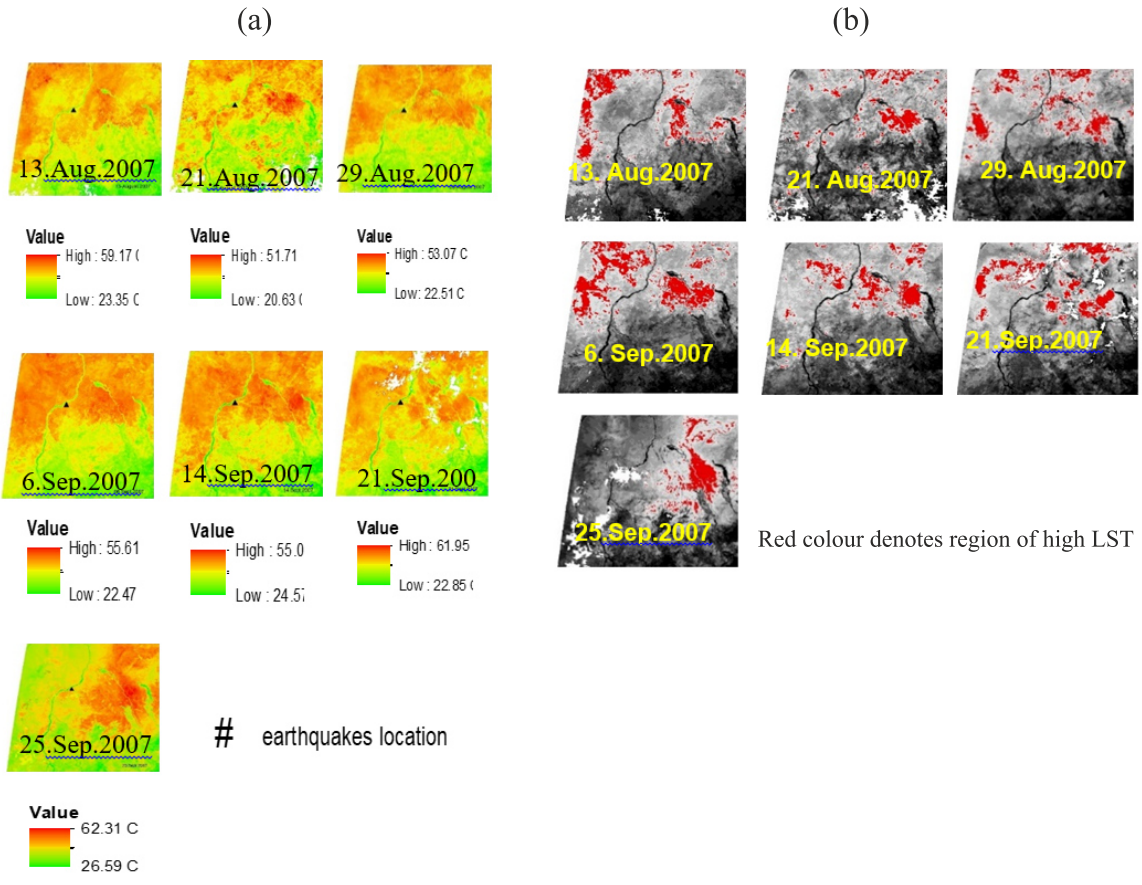

Fig.4 (a, b) The9.2007 River Nile earthquake

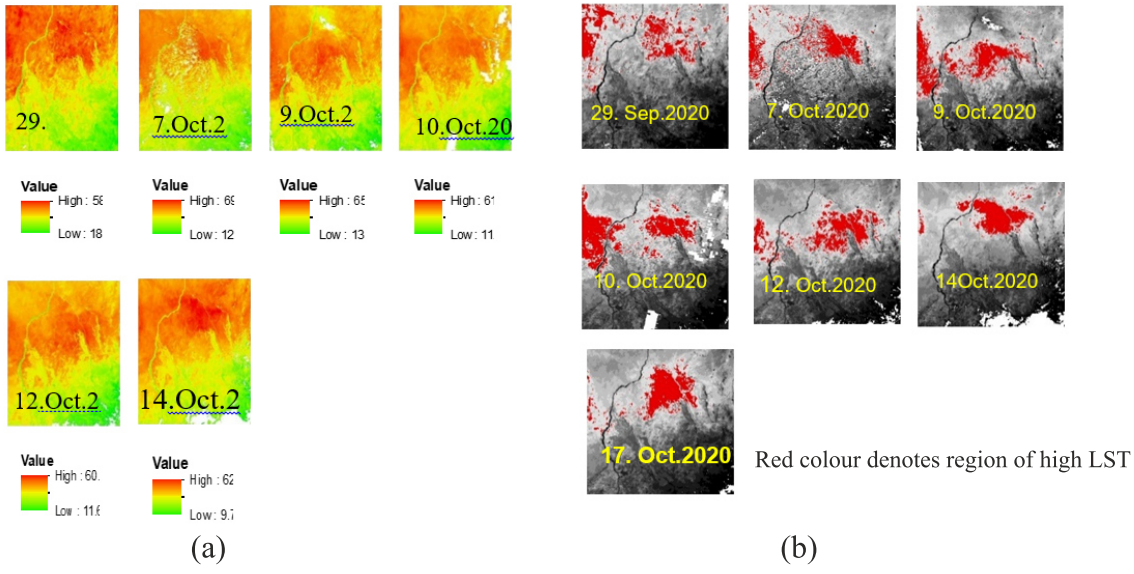

Fig.5 (a,b) The 12.10.2020 AlGadaref earthquake

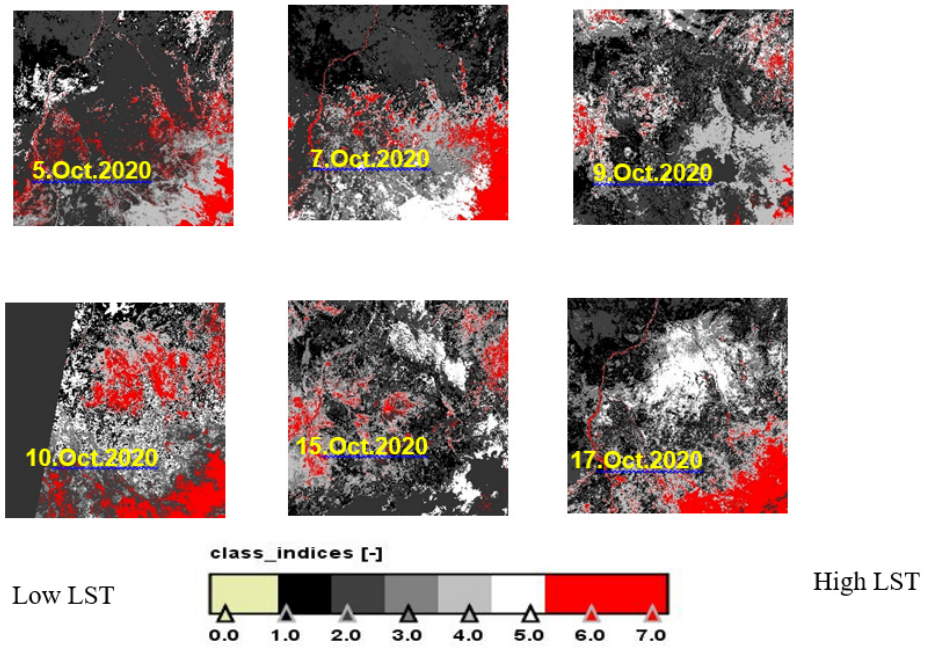

Fig.6AlGadareif 2020 earthquake via Sentinel 3 LST data

4. DISCUSSION

The consistent observation of significant LST anomalies preceding the seismic events, particularly the detailed temporal and spatial evolution observed in the Sinkat 2000 case, strongly supports the hypothesis of a **lithosphere-atmosphere coupling** mechanism. The spreading and intensification of high LST regions in the days and weeks leading up to the earthquakes align with models of pre-seismic stress accumulation and subsequent physical changes in the crust.

The use of unsupervised classification for the Sinkat 2000 data proved effective in isolating and tracking the high anomaly areas, which appeared as early as 24 days before the shock. This long lead time is crucial for the potential application of LST as a forecasting tool. The post-seismic decrease and shift in LST patterns further indicate that the observed thermal changes are directly linked to the tectonic activity rather than purely meteorological or seasonal variations.

While the results are compelling, it is important to note that LST data can be affected by factors such as cloud cover (as noted in the data analysis), atmospheric conditions, and land use changes. Future research should focus on developing robust algorithms to decouple these confounding factors from the genuine pre-seismic thermal signals.

5. CONCLUSION

This remote sensing investigation successfully demonstrated a strong correlation between pre-seismic activity and **Land Surface Temperature (LST)** anomalies derived from MODIS and SLSTR data. The temporal and spatial patterns of high LST observed before the Sinkat 2000, Sinkat 2006, Matama 2007, and Gedaref 2020 earthquakes suggest that LST is a viable geophysical parameter for monitoring seismo-tectonic activity. The findings advocate for the integration of satellite-based LST monitoring into comprehensive, multi-parameter systems for operational earthquake surveillance.

6. REFERENCES

[1] **Mari, Z. Roxana, S. and Dan Savastru., 2016.** Earthquake anomalies recognition through satellite and in-situ monitoring data. European Journal of Remote Sensing, 49: 1011-1032.

[2] **Alawad.M.H., 2022**.Chapter IX: LST and Surface Temperature Investigations. Integration of satellite gravity and multi-sensor remote sensing data for regional tectonic evaluation in central and eastern Sudan, Sudan Academy of Sciences, and Ph.D. unpublished.

[3] **Maria Zoran, Roxana Savastru and Dan Savastru., 2016.** Earthquake anomalies recognition through satellite and in-situ monitoring data. European Journal of Remote Sensing, 49: 1011-1032.

WAN, Z., 2006. MODIS land surface temperature products users' guide. Available on line at http://www.icess.ucsb.edu/modis/LstUsrGuide/usrguide.html (accessed on 1 June2006).

Wan, Z., 2014. New refinements and validation of the collection-6 MODIS land-surface temperature/emissivity product. Remote Sens. Environ. 2014, 140, 36–45.

A court Specialized regional scientific journal issued by CRTEAN in collaboration with the FASRC

CARTOGRAPHIEDES INONDATIONS ET VULNÉRABILITÉS TERRITORIALES DANS LA ZONE MÉRIDIONALE DU LITTORAL NORD-OUEST DU CAP-BON : ANALYSE COMPARATIVE DES ÉVÉNEMENTS DE 2018 ET 2025

Dalel Makhloufi, El Melki Taoufik
Univ. Manouba, FLAH, Géomatique des Géosystèmes (LR19ES07), campus Manouba, 2010, Tunisie

ABSTRACT

Floods are now one of the major natural hazards facing Mediterranean societies. Theyresult from a combination of extremer a in fall, local hydro-geographical constraints and land use patterns marked by rapid, oftenpoorlyplanned urbanisation. The Mediterranean basin, considered a climate change hotspot, isexperiencing an increase in short but violent rainfallevents, whichincrease the risk of flash floods. This trend reveals structural vulnerabilities: soil artificialisation, development in flood-prone areas, inadequate maintenance of drainage networks and hydraulic structures, as well as institutionalresponsesthat are oftenpunctual butunsustainable. In Tunisia, thesefindings are largelyconfirmed. The high rainfallvariability, combined within creasing an thropogenic pressures, increasesexposure to flooding. Numero us studies show thatuncontrolledurban expansion, weak territorial governance and the deterioration of drainage infrastructure greatly amplify the damage. The consequences go beyond the material level alone: humanlosses, infrastructure collapse, economic disruption and social in equalities between protected neighbour hoods and marginalised areas.
Tunisia'shydrological history is marked by significant events (1969, 1973, 1982, 2003, 2007), reflecting a long-standing and persistent vulnerability.
In thiscontext, Cap Bon appears to be a prime area for study due to its agricultural and tourist challenges, its high level of urbanisation and itsphysicalcharacteristics (lowcoastal plains, sebkhas, water sheds connecting the land and the sea, and wadiswithoftenoccasional flow) thatlead to the rapid concentration of runoff. The repeatedfloods of 2012, 2016, 2018 and 2025 illustrate the reoccurance of threats. This studyaims to compare the events of 22 September 2018 and 1 February 2025 in order to analyse the dynamics of the hazard, the persistence of vulnerabilities and the effectiveness of post-2018 public policies, using a multidisciplinaryapproachthatdraws on rainfall data, Sentinel-1 imagery, fieldsurveys and official archives.

Keys words: Flash floods, Territorial vulnerability, Rainfallevent, Uncontrolled urbanisation, Cap Bon (Tunisia)

1. INTRODUCTION

Les inondations représentent aujourd'hui l'un des aléas naturels les plus préoccupants pour les sociétés méditerranéennes (*Germain, 2022 ; Fiori, 2014 ; Alfieri, 2015 ;Merino, 2017 ; Zakaria, 2022 ; UNDRR, 2025*). Elles résultent d'une interaction complexe entre des précipitations extrêmes, des contraintes hydro-géographiques locales et des dynamiques d'occupation du sol marquées par une urbanisation rapide et souvent désordonnée (*MedECC. 2020 ; IPCC. 2022 ; UNDRR. 2025 ; World Bank. 2021 ; Tramblay, 2023 ; Fehri, 2014 ; Lahmar, 2024)*. La récurrence de ces événements dévoile des vulnérabilités chroniques profondément ancrées dans les territoires *(Llasat, 2016 ; Vinet, 2015 ; Aouissi, 2024 ; Khemir, i 2024 ; Tramblay, 2023 ; Dahri, 2020*). Le bassin méditerranéen, identifié comme un « hotspot » du réchauffement climatique (*GIEC, 2023*), connaît une intensification des épisodes pluvieux courts mais violents (*Panthou, 2014 ; Cantoni, 2022 ; IPCC. 2022 ; UNDRR. 2025 ; Tramblay, 2013*). Les pluies intenses accentuent le risque d'inondations soudaines, aggravées par l'extension urbaine dans des zones fragiles et par l'artificialisation des sols.

Les recherches menées dans l'espace méditerranéen confirment que la récurrence de ces évènements est avant tout liée à des facteurs structurels et institutionnels. Il a été montré en Espagne (*Llasat, 2016*) que les inondations répétées traduisent l'incapacité à maîtriser l'urbanisation en zones inondables. En France*Vinet* (*2010*) asouligné que les réponses post-catastrophes, souvent limitées à des interventions ponctuelles (consolidation de digues, curage des cours d'eau) ne suffisent pas à réduire durablement l'exposition au risque.

L'état actuel des connaissances en matière de risques urbains confirme l'aggravation des inondations dans les grandes agglomérations méditerranéennes (*Tramblay, 2018*). Le rapport (*MedECC, 2020*) confirme que la hausse des températures accentue les pluies brèves mais violentes, tandis que la densité des villes multiplie leurs effets destructeurs. Les rapports de l'Agence européenne pour l'environnement (2024) et du Plan Bleu (2019) rappellent que cette situation ne tient pas seulement au climat, mais à une vision de l'aménagement qui a longtemps privilégié la croissance urbaine à la sécurité des habitants.

Les recherches menées en Tunisie corroborent ces constats. Les choix d'aménagement et la faiblesse de la gouvernance territoriale accentuent la vulnérabilité chronique des territoires nationaux. Les travaux de (*Fehri, 2013 ; 2014 et 2020 ; Lahmar, 2024 ; Louhaichi, 2013 ; Makhloufi, 2021 ; Khemiri, 2024 ; Bourgou, 2018*) démontrent que la croissance urbaine nonmaîtrisée conjuguée à la faiblesse de la gouvernance territoriale locale constituent un facteur déterminant dans l'aggravation des dégâts induits par les inondations.Dans la plupart des villes les réseaux d'évacuation sont souvent plus ou moins obstrués, les lits des oueds sont transformés en dépotoirs d'ordures et l'imperméabilisation des sols réduit toute infiltrationnaturelle. Dans de telles circonstances chaque épisode pluvieux intense révèle les défaillances d'un modèle de développement territorial qui a longtemps ignoré les risques hydrologiques.

Pour la Tunisie, les conséquences dépassent le seul plan matériel : pertes humaines, effondrement d'infrastructures, paralysie économique locale, mais aussi fracture sociale entre les quartiers protégés et ceux livrés à eux-mêmes.

En Tunisie, la problématique est particulièrement aiguë. Le pays soumis à une forte variabilité pluviométrique interannuelle (*Henia, 2000*), combine des contraintes naturelles et des pressions anthropiques qui aggravent l'exposition aux inondations (*Makhloufi, 2021 ; Chourai, 2009 ; Fehri, 2013 ; Hemercha, 2015 ; Lahmar, 2024*). De nombreuses recherches réalisées au cours des dernières décennies confirment l'intensification des épisodes pluviométriques extrêmes, caractérisés par leurs fortes intensités et leurs courtes durées. Ils provoquent des ruissellements intenses et des crues soudaines (*Makhloufi, 2021 ; Bourgou, 2018 ; Daoud, 2013 ; Chouari, 2019*). Cette évolution climatique se superpose à des dynamiques territoriales marquées par une urbanisation rapide, souvent mal planifiée ou anarchique/ informelle, effectuée dans des milieux naturels inadaptés (sebkhas, lits oueds, bas-fonds). De telles pratiques d'aménagement, largement analysées (*Makhloufi, 2021 ; Bourgou, 2018 ; Fehri, 2013 ; 2014 ; Nasrallah, 2020 ; Mrabti, 2019*), transforment parfois un aléa, même de faible ampleur, en catastrophe humaine et économique.

De ce fait, les inondations tunisiennes traduisent une vulnérabilité ancienne/structurelle, amplifiée par des choix de développement urbain qui, faute de tenir compte des exigences du territoire, exposent en permanence la société aux événements pluviométriques intenses.

La mémoire hydrologique de la Tunisie est jalonnée d'épisodes parfois très marquants. Les crues de 1969 et 1973 ont touché une grande partie du pays, révélant pour la première fois l'ampleur des vulnérabilités urbaines. Celles de Sfax en 1982 et du Grand-Tunis en 2003 et en 2007 ont mis en évidence la précarité des réseaux de drainage des deux principales villes du pays,illustrée par leur saturation rapide (*Daoud. 2013*).

Dans ce contexte, le Cap-Bon constitue un terrain d'étude privilégié. Etant à la fois un espace agricole important, une destination touristique reconnue et une zone de forte urbanisation, il illustre bien les tensions entre une croissance urbaine rapide et des contraintes environnementales multiples. La région se caractérise par une topographie assez contrastée, marquée par la présence de vastes plaines littorales basses et jalonnées de sebkhas, de multiples bassins-versants reliant un arrière-pays montagneux à la mer, un réseau hydrographique souvent linéaire et des cours d'eau (oueds) à écoulement souvent occasionnel et rarement intermittent, ce qui favorise la concentration de l'écoulement en cas de pluies extrêmes. Ces caractéristiques naturelles (périodes sèches relativement longues, séparées par des averses intenses et de courtes durées, encourageant les citoyens à s'installer dans des zones à fort risque d'inondations), combinées à l'extension urbaine rapide sur des terrains vulnérables et à l'absence d'entretien régulier des ouvrages hydrauliques, expliquent la gravité des inondations dans la presqu'ile du Cap-Bon. Les évènements de 2012, 2016, 2018 et 2025 révèlent la forte répétitivité temporelle de ces menaces dans cette région.

Les événements du 22 septembre 2018 et du 1er février 2025 donnent un exemple éloquent de cette réalité. Par leur intensité, leur soudaineté et la gravité de leurs impacts, ils ont profondément marqué les localités de Soliman, Korbous, Aïn El Fakroun et Sidi Errayes. Bien que survenus après un écart temporel de sept années, ces deux épisodes révèlent,malheureusement, la persistance des vulnérabilités non encore résorbées de ces zones sinistrées. La présente étude a pour principal objectif d'analyser de manière comparative ces deux évènements, mettant en évidence la ressemblance des dynamiques de l'aléa et les raisons de la vulnérabilité territoriale de ces localités. Il s'agit d'évaluer les caractéristiques pluviométriques et hydrologiques de ces événements, d'une part, et d'autre part, la fragilité des dispositifs de protection et l'inefficacité des politiques publiques mises en œuvre après 2018. Pour ce faire, une approche pluridisciplinaire est adoptée, basée sur des données pluviométriques, des imageries satellitaires (Sentinel-1), des enquêtes de terrain et des archives officielles.

1. Secteur d'étude, données et méthodologie :

1.1. Secteur d'étude

La zone d'étude se situe dans la partie méridionale du littoral nord-ouest du Cap-Bon ; qui, correspond au gouvernorat de Nabeul et occupe l'extrémité nord-est de la Tunisie. La zone d'étude couvre les localités de Soliman, Korbous, Aïn El Fakroun et Sidi Errayes. Cette zone est marquée par des contrastes topographiques et environnementaux importants et manifeste une vulnérabilité commune face aux aléas hydrométéorologiques*(Fig1).*

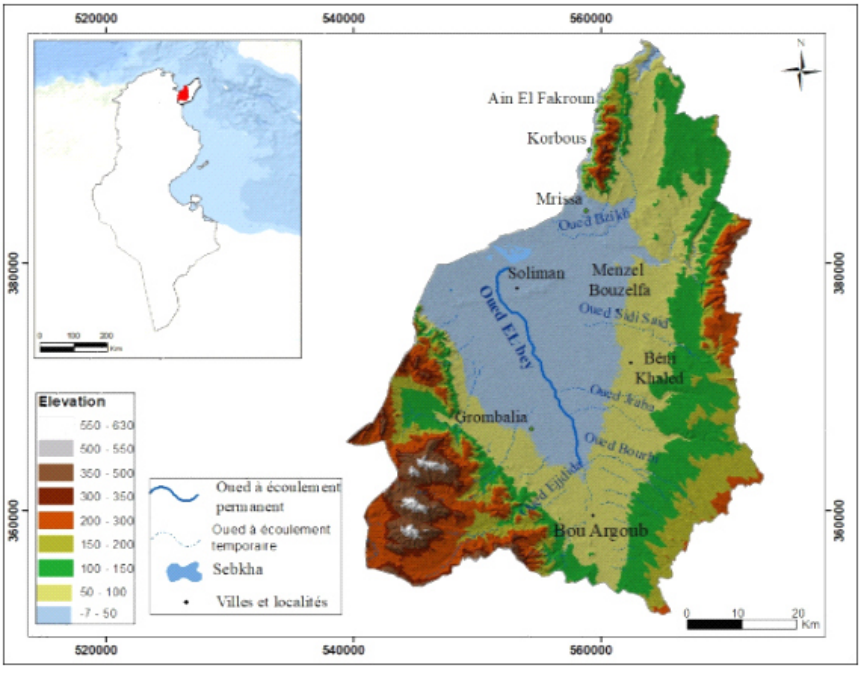

(Fig1). Localisation et topographie de la zone d'étude.

Cet espace représente un système topographique contrasté, constitué d'un arrière-pays montagneux encadrant des plaines littorales basses, particulièrement sensibles aux inondations.

La zone étudiée est dépourvue d'une station de mesures climatologiques. La station synoptique la plus proche et celle de Tunis-Carthage. Celle-ci, est située sur le littoral méridional duGolfe de Tunis tout comme la zone étudiée.Elles sont soumises, toutes les deux, aux mêmes influences atmosphériques et aux mêmes circulations régionales. Ceci en fait une station de référence suffisamment pertinente pour cette étude.

Leclimat méditerranéen de la région est marqué par une alternance nette entre un été chaud et sec et un hiver frais et pluvieux*(Fig2)*. L'automne, encore thermiquement chaud, favorise les circulations azonales de secteur Est (*El Melki*. 2014, *Makhloufi. 2021*), générant des épisodes pluvieux parfois très intenses. Ce mécanisme explique la forte variabilité des précipitations observée dans cette région et, plus largement, dans l'ensemble du climat tunisien(*Kassab, 1979 ;Henia, 1980 ;Bousnina, 1986 ;Hlaoui, 2001 ;Abdelkhalek, 2008 ;Dallel, 2007*). Il est bien visible alors (*Fig2*)que les normales mensuelles de septembre et de février sont bien en deçà des déluges enregistrés dans la zone d'étude durant les journées des 22/09/2018 et 01/02/2025.

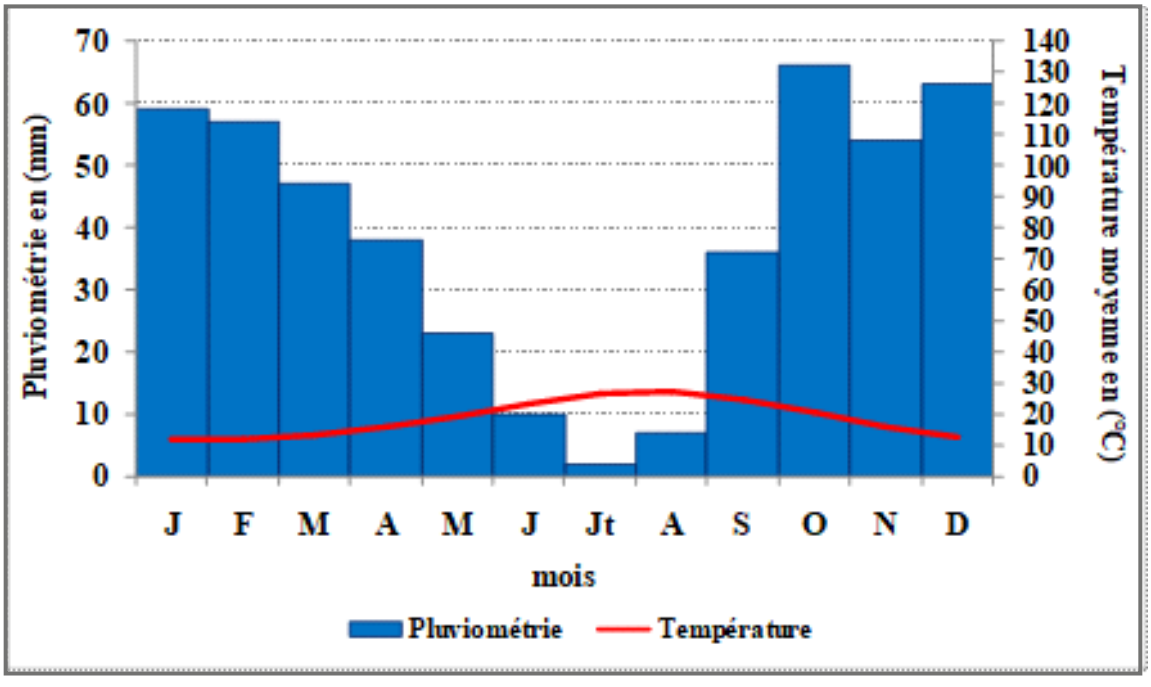

(*Fig*2). *Diagramme ombrothermique de Tunis-Carthage (1960-1990).*
Source des données brutes : I.N.M., Tunis.

Sur le plan topographique, deux ensembles principaux se dégagent *(Fig1)*: d'une part, une vaste plaine basse abritant les principales villes de la région (Soliman, Menzel Bouzelfa, BéniKhalled et Grombalia) et d'autre part, des reliefs fortement contrastésencadrant celle-ci, dont le JbelKorbous et Ain El Fakroun figurant dans cette étude.

Ainsi, Soliman se localise dans la partie la plus basse de ladite plaine littorale,là où la faiblesse des pentes ralentit l'évacuation des eaux de ruissellement, favorisant leur stagnation lors des événements pluvieux intenses. Cette plaine reçoit aussi les apports de l'Oued El Bey et de ses affluents, ce qui rend la région particulièrement vulnérable aux inondations (*Khadhar, 2013 ; ME, 2002 ; RAMSAR, 2016).*

La région de Korbous se caractérise par une topographie particulièrement contraignante, dominée par les versants abrupts du JbelKorbous (*El Aroui, 2020*). Ces pentes marquées se prolongent dans de petits vallons étroits où l'eau de pluie s'écoule rapidement vers le littoral. Théoriquement, cette configuration topographique ne pose pas de problèmes majeurs, puisque l'eau rejoint directement et rapidement la mer. Cependant, les aménagements réalisés au pied du versant (route littorale, remblais et divers ouvrages) ont perturbé les trajectoires d'écoulement. Le ruissellement se trouve alors freiné/bloqué ou artificiellement redirigée vers des zones habitées. Ainsi, ce sont des interventions humaines, bien plus que le relief lui-même, qui transforment des pluies intenses en véritables inondations.

1.2. Données et méthodologie

Pour effectuer ce travail, plusieurs types des données ont été mobilisés :

- ✓ Des relevés pluviométriques journaliers fournis par la DGRE pour les stations de Soliman et Korbous.

- ✓ Des données météorologiques :
  - Cartes synoptiques (pression atmosphérique au sol et altitude du géopotentiel 500 hPa) pour la caractérisation des situations atmosphériques relatives aux évènements étudiés
  - Carte du Courant Jet- Stream à 12h00mn pour les mêmes évènements.
  - Radiosondages de Tunis-Carthage (00H00mn)et de Trapani (12H00mn) en raison de la proximité de la Sicile.

- ✓ Des cartes topographiques aux échelles 1/25000 et 1/50000couvrant les zones sinistrées,

- ✓ Des images satellitaires :
  - Les images radar à synthèse d'ouverture (SAR) du satellite Sentinel-1, acquises les 21 et 27 septembre 2018 ainsi que les 23 janvier et 4 février, ont été utilisées pour identifier, délimiter et cartographier les zones affectées par les inondations.

Sentinel-1 offre une capacité d'observation tout-temps et jour/nuit, le rendant particulièrement adapté au suivi des phénomènes hydrologiques en période de conditions météorologiques défavorables, notamment lors des épisodes de forte couverture nuageuse caractérisant les épisodes de fortes pluies et crues.
La méthode de détection différentielle de la rétrodiffusion, appliquée aux images avant et pendant la crue, a été utilisée pour identifier les surfaces submergées. Cette approche repose sur la variation du coefficient de rétrodiffusion entre les deux acquisitions, la diminution notable de la rétrodiffusion traduisant la présence d'une lame d'eau homogène atténuant le signal radar
(https://scihub.copercus.eu)
- Images Google-Earth datées des 22/11/2017, 5/11/2018, 31/03/2024 et 22/03/2025

✓ Des archives officielles permettant de comprendre l'évolution des dispositifs de prévention et de protection contre les inondations, dont :
- Des notes internes auprès de plusieurs institutions publiqueslocales (Municipalités de Korbous et de Soliman, Délégation de Soliman, Croissant rouge de Soliman et de Nabeul),
- Documents juridiques issus des consultations effectuées par un huissier désigné par les instances juridiques, comprenant des images ainsi qu'un procès-verbal du constat relatif à l'explosion du tunnel de Korbous, daté du 29/09/2018.

✓ Des enquêtesde terrain :
Les enquêtes qui ont été menées auprès des habitants, des élus locaux et des techniciens municipaux concernent les hauteurs d'eau des inondations, la durée de la submersion et les impacts socio-économiques. Ces informations se sont révélées essentielles pour la validation des résultats obtenus à partir du traitement des données satellitaires.

Toutes ces données ont été intégrées dans un système d'information géographique (SIG), permettant la cartographie des zones vulnérables et la comparaison spatio-temporelle des événements de 2018 et 2025. Le croisement méthodologique adoptée garantit la validité des résultats et assure une base scientifique solide permettant l'analyse comparative des évènements étudiés.
L'approche méthodologique adoptée s'articule autour de trois principaux volets : l'analyse de l'aléa pluviométrique, l'exploitation des données satellitaires et le recoupement avec les observations de terrain et les archives officielles.
Cette méthodologie *(Fig3)* permet d'évaluer les différents facteurs de vulnérabilité propres à chaque localité étudiée : facteurs structurels, environnementaux et institutionnels.

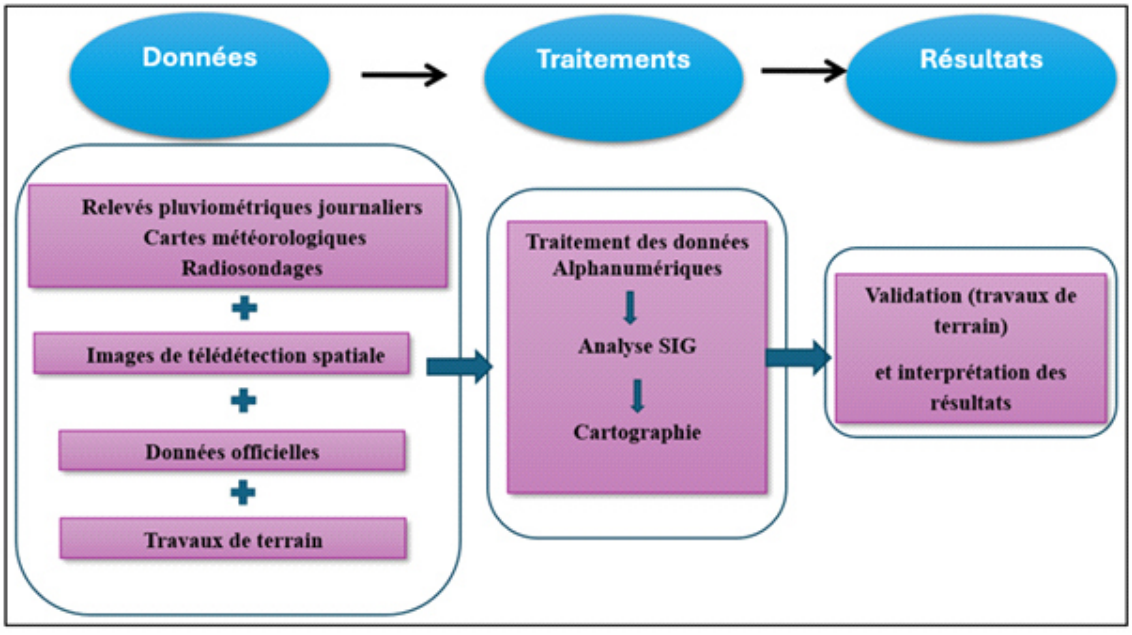

(Fig3). Organigramme de la démarche méthodologique suivie

2. Résultats

2.1. Caractérisation des événements pluviométriques

L'épisode pluvieux du 22 septembre 2018 constitue l'un des événements hydrométéorologiques les plus marquants des dernières décennies dans la région du Cap-Bon. La station de Béni Khalled a enregistré un cumul exceptionnel de 297 mm en moins de 24 heures : un record absolu pour toute la Tunisie (*DGRE, 2018 ; Gouvernorat de Nabeul, 2018 ; CRDA Nabeul, 2018*). Ce volume dépasse largement la normaleinterannuelle (*fig.2*) de la saison (280% selon le *DGRE, 2018*). Ce déluge survenu au cours d'une période de 6 heures, a provoquédes crues soudaines et destructrices (*MARHP. 2020 ;CRDA, 2018*).

L'évènement pluvieux du 1er février 2025 (126 mm dans la ville de Soliman, 124mm à Mrissa et 120mm dans la ville de Menzel Bouzelfa), bien que moins spectaculaire en termes de cumul journalier (*CRDA, 2025*)a eu des impacts similaires que celui de 2018, voire plus graves dans certaines zones. Le ruissellement a été particulièrement intense car les sols sont déjà saturés en raison des pluies précédentes de la saison hivernale.Effectivement, janvier 2025 selon l'INM affiche un excédent pluviométrique de 36 %.

L'étude de la répartition spatiale des précipitations révèle des contrastes marqués entre les deux épisodes. En 2018, les pluies se sont concentrées surtout sur le centre et le sud du Cap-Bon, tandis que l'événement de 2025 a touché de façon plus uniforme l'ensemble de la région.

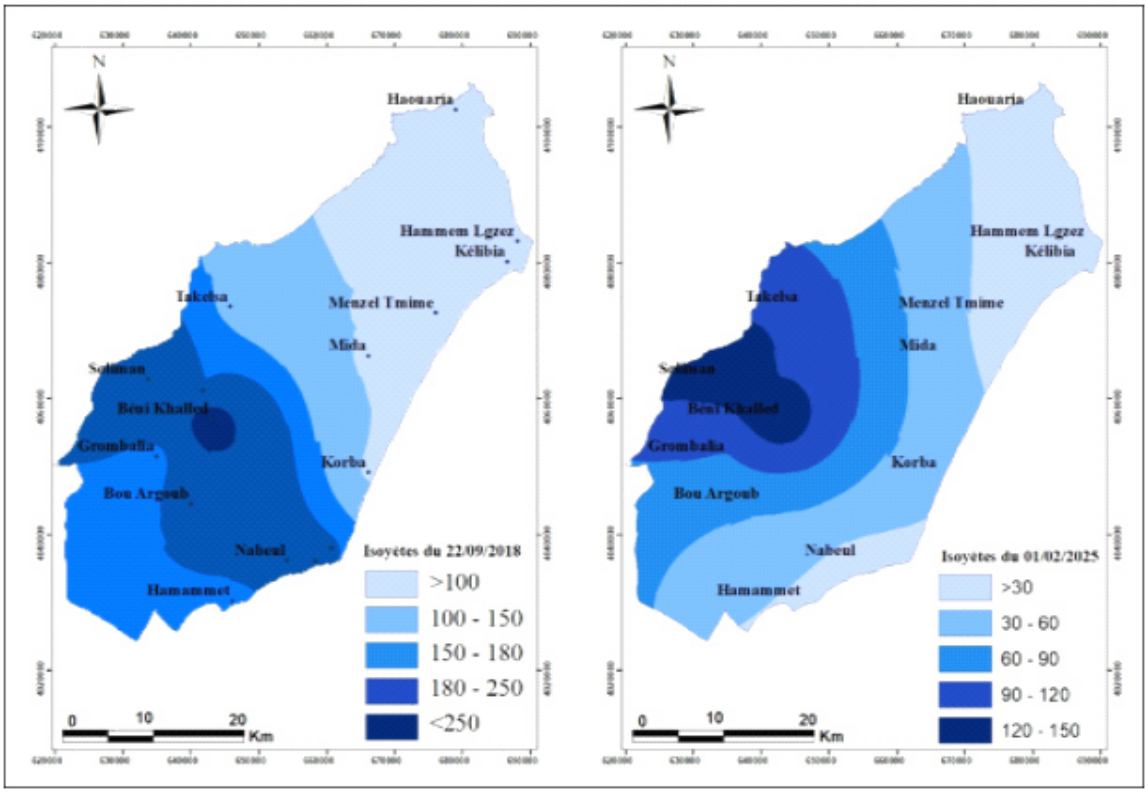

(Fig4). Les isohyètes du 22/09/2018 et du 01/02/2025

Les épisodes pluvieux intenses observés dans le bassin méditerranéen sont généralement liés à des phénomènes convectifs (*Henia, 2000*)de fortes intensités et dont l'envergure spatiale peut varier très sensiblement (*El Melki, 2014 et 2015*). Ils provoquent des inondations soudaines et parfois dévastatrices. Ces événements surviennent le plus souvent en fin d'été et au début de l'automne, périodes au cours desquelles les températures élevées favorisent beaucoup l'évaporation et l'instabilité des basses couches de l'atmosphère initiant la formation des cellules orageuses (*Llasat, 2016 ; El Melki, 1997,2014 et 2015*). Ces orages sont souvent localisés, de courtes durées, mais potentiellement dévastateurs, pouvant entraîner des crues catastrophiques (*Jansà, 2001*).

Les précipitations extrêmes observées au cours de cette période de l'année sont fréquemment associées à des systèmes convectifs violents associés à des lignes de grains ou des complexes convectifs de méso-échelle. Ces phénomènes sont capables de produire de très forts cumuls en des laps de temps réduits (*Zhou, 2017 ; El Melki, 2014 et 2015*).

C'est dans cette dynamique atmosphérique que s'insèrent les deux évènements analysés dans cette étude.

Les cartes de la pression atmosphérique en surface révèlentdes champs barométriques dépressionnaires en Tunisie*(fig.5)*. C'est le premier élément indispensable à tout évènement pluviométrique important dans le pays :

- En 2018, une dépression minuscule et peu creuse (1013 hPa) centrée entre les iles italiennes (Sardaigne et Sicile) dirige vers la Tunisie un flux de secteur NE. Un front secondaire longe les côtes nord de la Tunisie. Cette configuration révèle une incursion d'air frais sur la Méditerranée encore très chaude à cette période (septembre). Le contraste thermique entre ces deux milieux favorise la convection et les ascendances. Les petits reliefs de la région peuvent accentuer ces dernières.
- En 2025, dépression saharienne plus grande et plus creuse (1007 hPa) est centrée sur le SE de l'Algérie. Elle dirige vers la Tunisie un flux maritime de SE. La Méditerranée plus chaude que l'atmosphère en hiver, réchauffe et humidifie sensiblement les masses d'air au-dessus d'elle.

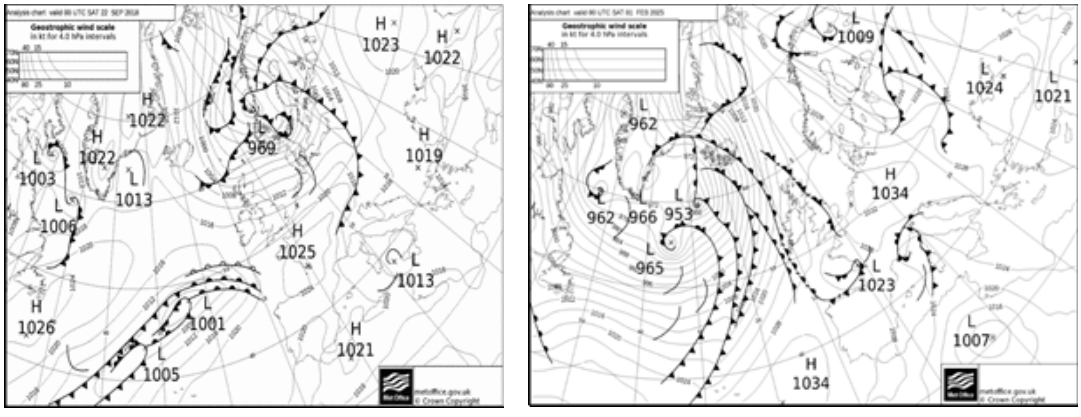

(Fig5). (À gauche) Champs barométrique de surface du 22/09/2018 à 00h00mn. Source : www.wtterzentrale.de
(À droite) Champs barométrique de surface du 1er/02/2025 à 00h00mn. Source : www.wtterzentale.de

Les altitudes de la surface 500 hPa*(Fig6)*, révèlent pour chacun des deux évènements la configuration d'une large vallée barométrique. Ce fait est synonyme d'infiltration d'air frais/froid en altitude, ce qui favorise parfaitement les ascendances issues des basses couches. La formation des nuages à grand développement vertical (Cumulus et cumulonimbus) est possible. Toutes ces propriétés caractérisent une atmosphère très orageuse.

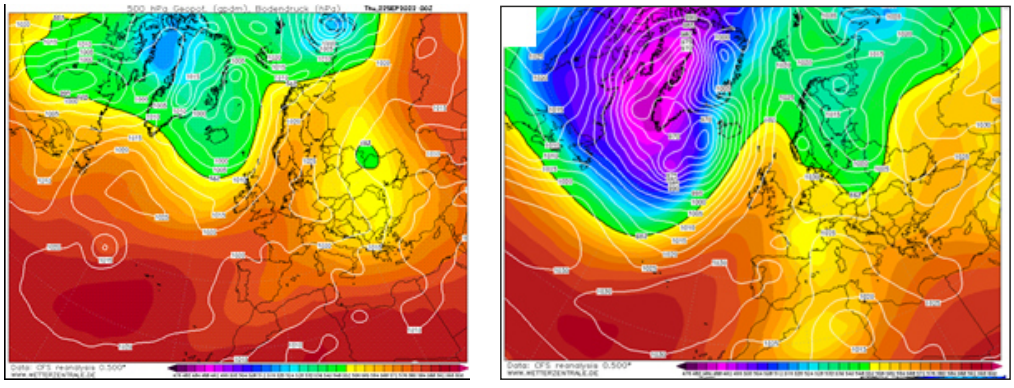

(Fig6). (Gauche) : Altitudes du champ barométrique 500 hPa du 22/09/2018 à 00h00mn. Source :www.wtterzentale.de
(Droite) : Altitudes du champ barométrique 500 hPa du 01/02/2025 à 00h00mn. Source : www.wtterzentale.de

La position d'une branche très active (épaisseur importante et vitesses élevées du courant) du « Jet-stream » sur la Tunisie *(Fig7)* renforce les instabilités verticales et exacerbe les ascendances orageuses (*El Melki, 2014 et 2015*).

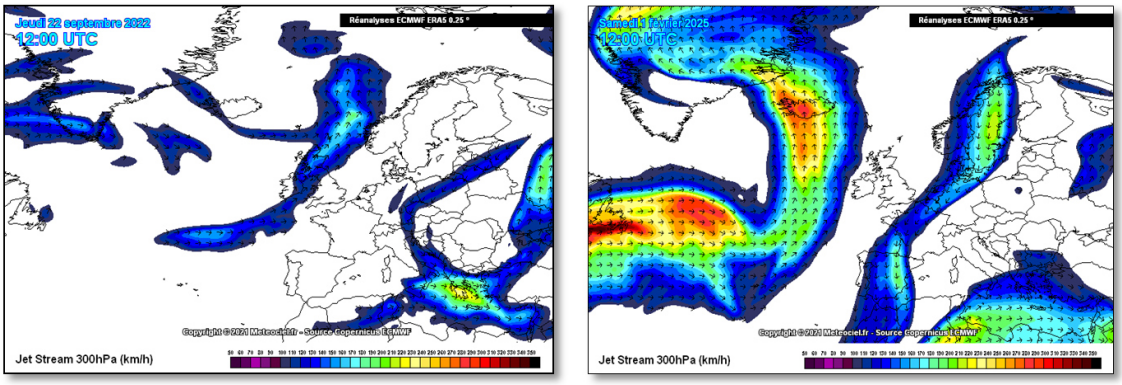

(Fig7). (Gauche) : position du courant Jet-stream, le 22/09/2018 à 12h00mn. Source : https://images.meteociel.fr
(Droite) : position du courant Jet-stream, le 1er/02/2025 à 12h00mn. Source : https://images.meteociel.fr

Les documents précédents donnent un aperçu des propriétés de l'atmosphère dans deux plans horizontaux, très vastes certes, mais distincts : au niveau du sol et au niveau de la surface 500 hPa. Ces deux niveaux sont séparés en moyenne par 5600 mètres d'altitude. Seuls les sondages atmosphériques (effectués par radiosondages ou lidar) peuvent donner un aperçu des propriétés de l'atmosphère à la verticale, mais uniquement au niveau d'un lieu donné : la station de mesure qui les effectue. Une analyse de cas spatialement limités, à l'image de cette étude, doit mobiliser les deux moyens.

Les radiosondages relatifs aux deux évènements étudiés*(Fig8).* Montrentdes profils de troposphères humides et instables.

L'humidité d'une masse d'air se traduit sur les radiosondages par le rapprochement des courbes rouge (température de l'air) et bleue continue (température du point de rosée : température à laquelle on doit amener la masse d'air pour qu'elle soit saturée). Plus elles sont rapprochées, plus la masse d'air est humide.

Les humidités relatives maximales observées sont égales à 100% à Tunis-Carthage (enregistrées entre 820m et 970 m) et à Trapani : 91% (au niveau 6077m).

À Tunis-Carthage les humidités relatives sont comprises entre 70% et 100% entre le niveau du sol et l'altitude 3812 m. Elles sont supérieures ou égales à 62% jusqu'à la hauteur de 5155m. À Trapani les humidités relatives sont variables avec l'altitude : 63% au niveau du sol, 90% à 787 m, 22% à 2343 m et 70% à7296 m. Il faut rappeler que le radiosondage de Trapani est effectué à 12h00mn : en phase diurne, les humidités relatives décroissent naturellement par effet du réchauffement causé par l'irradiation solaire, contrairement à une situation nocturne où l'inverse se produit.

L'importance de la quantité d'eau précipitable (hauteur d'eau qu'on recueillerait si toute l'eau de la colonne d'air sondée précipite) confirme cette réalité surtout pour le cas du 22-09-2018 (*Tableau : 1)*.

L'instabilité, quant à elle, se traduit par le réchauffement des basses couches tangentes au sol.

Celles-ci sont clairement convectives (lignes rouges, des températures de l'air, inclinées vers la gauche près du sol). Ce fait est relatif à une incursion d'air frais ou froid qui se réchauffe par la base au contact du substrat plus chaud ; fait qui persiste encore même pendant la nuit (radiosondage de Tunis-Carthage du 22/09/2018 à 00h TU) en dépit du rayonnement thermique nocturne. Le même fait est encore plus net sur le radiosondage de Trapani (Sicile, Italie) de 12h00mn (1er /02//2025). Celui-ci est pris à titre juste indicatif pour assurer la comparaison : la station météo de l'INM de Tunis-Carthage n'effectuant plus depuis des années des radiosondages. Alors, Trapani est la station météorologique la plus proche de la zone étudiée. Au fait dans les détails, un radiosondage n'est vraiment représentatif que du site de la station qui l'effectue ; mais les propriétés fondamentales d'une masse d'air (stabilité/instabilité, humidité, convergence/divergence…) ne changent pas significativement sur de courtes distances en dehors des régions montagneuses très élevées.

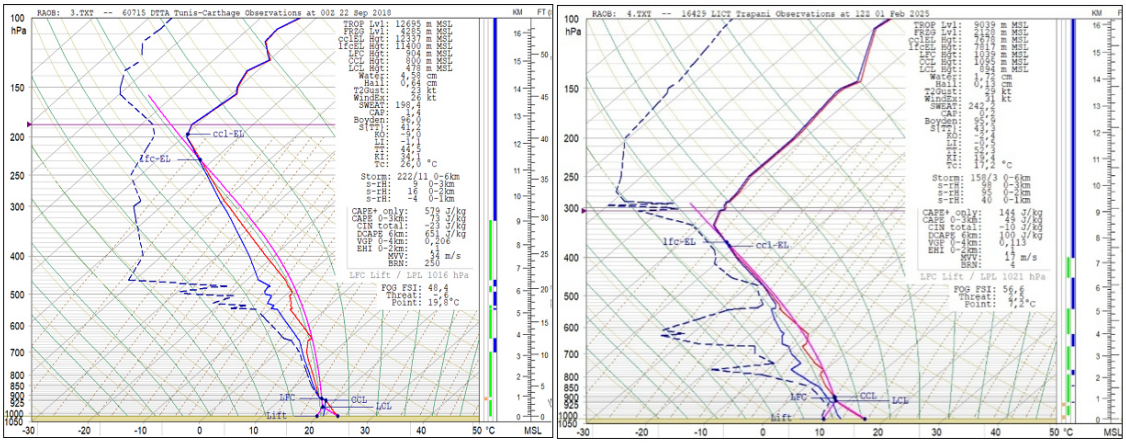

(Fig8). (À droite) Radiosondage de Tunis-Carthage du 22/09/2018 à 00h TU.
(À gauche) Radiosondage de Trapani du 1er /2/2025 à 12h00mn.
Source des données brutes : http://weather.uwyo.edu/upperair/sounding.html
Graphiques des radiosondages (Émagramme, ou, Diagramme 761) produits sous « RAOB program ».

L'instabilité des masses d'air caractérisant ces deux évènements est révélée aussi par certains des indices des radiosondages calculés sous le « RAOB program » (*Tableau : 1*). L'instabilité atmosphérique est toutefois plus importante pour le cas du 22/09/2018 ; ce qui explique parfaitement l'énormité du déluge abattu sur la région étudiée durant cet évènement. En fait, la CAPE est importante. Les niveaux LFC et LCL (niveaux de base des ascendances libre et convective) sont très bas favorisant des plafonds nuageux (bases des nuages) très bas. Les niveaux d'équilibre thermiques relatifs à ces deux indices (« equilibriumlevel ») au niveau desquels les ascendances libre et convective prennent fin sont très élevés ; ce qui permet la formation de nuages orageux à grand développement vertical (cumulus et cumulonimbus).

A Tunis-Carthage (22/09/2018), la différence d'altitude entre « LFC » et « lfc-EL » est de 10496 m ; et elle est de 11537 m entre « CCL » et « ccl-EL ». Ces deux valeurs sont respectivement de 6778 m et de 6583 m à Trapani (1er /02/2025).

Tableau : 1. Quelques indices de radiosondages affirmant l'instabilité et l'humidité atmosphériques des situations étudiées, obtenus sous « RAOB Program ».

Indices du sondage	Unités	Tunis-Carthage 22 Sep 2018 00h00mn	Trapani 31-janv-25 12h00mn
CAPE : Convective Available Potential Energy: Energie potentielle disponible pour la convection	Joule/Kg	579	144
Pw : Precipitable water for entire sounding: Eau précipitable de la colonne d'air sondée,	mm	45,8	17,2
LFC : Level of free convection : Niveau de convection libre	m	904	1039
LCL : Lifting condensation level: Niveau d'ascendance convective	m	478	894
CCL : Convective condensation level : Niveau de condensation convective	m	800	1095
lfc-EL : LFC Based equilibrium level: Niveau d'équilibre basé sur LFC	m	11400	7817
ccl-EL : CCL Based equilibrium level: Niveau d'équilibre basé sur CCL	m	12337	7678

2.2. Zones sinistrées et dégâts observés

Les observations de terrain, consolidées par l'imagerie satellitaire, révèlent une remarquable similitude entre les zones inondées lors des évènements présentés dans cette étude. Cette similitude révèle que les vulnérabilités structurelles identifiées après le premier événement de septembre 2018 n'ont pas été traitées de manière efficace.Ainsi, le second épisode survenu après une période suffisamment longue de sept années, confirme l'absence quasi-totale de toute mesure de protection efficacecontre les inondations ; ce qui a maintenu les zones étudiées dans un état de vulnérabilité chronique.

2.2.1. Soliman : une vulnérabilité structurelle persistante face aux inondations

En 2018, la rupture d'une digue de l'oued El Bey, à proximité de la cité El Bhira a favorisé le débordement du cours d'eau eta provoqué la catastrophe. La submersion a commencé six heures après le début des pluies torrentielles du 22/09/2018 (297 mm en 24 heures). La défaillance du réseau de drainage urbain a amplifié l'ampleur du phénomène, facilitant la montée des eaux et la submersion de zones névralgiques : la rocade, les quartiers d'El Bhira et de l'Oued En-Namous, ainsi que la zone industrielle où convergent les écoulements des oueds El Bey et Sidi Saïd. Les hauteurs d'eau de submersion, supérieures à trois mètres dans certains secteurs stratégiques, à l'instar des alentours de la Maison des Jeunes, témoignent de la brutalité du phénomène et de l'inadaptation de la ville.

Les impacts de l'évènement de 2018 se sont manifestés à plusieurs échelles. Les infrastructures sanitaires et éducatives ont été fortement perturbées : l'hôpital de Soliman a dû être évacué, les établissements scolaires tels que le lycée secondaire, l'école Habib Thameur et le centre sectoriel de formation ont interrompu leurs activités. La bibliothèque municipale de la cité Er-Rommana a perdu plus de 80 % de ses acquis. C'était la conséquence directe de son implantation dans une zone vulnérable et de l'absence de dispositifs de protection adaptés. Par ailleurs, les infrastructures routières stratégiques, comme la route du 14-Janvier, l'axe menant au technopôle de Borj Essedria et la MC26 vers Korbous au niveau du parc JinéneLoizir*(Fig9)*, ont été coupées, isolant temporairement la ville et accentuant les difficultés socio-économiques des habitants.

(Fig9). Photo 1 : Coupure de la route MC26 vers Korbous au niveau du parc JinéneLoizir en 22/09/2018
Photo 2 : Interruption de la route MC26 vers Korbous au niveau du parc JinéneLoizir en01/02/ 2025
Source (clichés personnels)

L'évènement de 2025, bien que moins important en termes de cumul pluviométrique (126 mm en 12 heures) a été non moins graves en termes d'intensité pluviométrique. Il a déclenché un ruissellement urbain fort, déterminant des dégâts quasi identiques à ceux de 2018. Les mêmes quartiers, les mêmes infrastructures publiques et privées et les mêmes voies de communication ont été touchés *(Fig10).*

Le renouvellement des inondations dans les secteurs d'El Bhira, et surtout dans les alentours de la sebkha de Soliman souligne la persistance des vulnérabilités structurelles et l'absence d'action efficace depuis 2018. En 2025 aussi, les activités scolaires ont été de nouveau suspendues, l'hôpital de la ville a connu une fermeture partielle, et certaines unités industrielles ont suspendu provisoirement leurs activités. C'est les cas de sociétés comme HaierTechnology International (*HMIDI, 2019*) et Delice-Danone dont les entrepôts ont subi des pertes comparables lors des deux évènements. Ce qui confirme que les mesures post-crises demeurent fragmentaires et insuffisantes. En fait, l'intensité des précipitations n'explique pas toute l'ampleur des catastrophes : ce sont surtout les spécificités et les caractères du territoire qui jouent un rôle déterminant dans le déclanchement du risque. L'urbanisation non planifiée sur des zones inadaptées, tel que les alentours de la sebkha de Soliman et dans le lit mineur d'Oued el Bey à l'image de cité El Bhira, l'imperméabilisation croissante des sols due à l'urbanisation excessive, la fragilité des infrastructures hydrauliques et l'absence d'entretien régulier sont les raisons profondes de la crise. Ces facteurs permettent à un aléa climatique, même de faible intensité de provoquer une catastrophe. La ville de Soliman illustre ainsi l'effet cumulatif des vulnérabilités physiques, sociales et institutionnelles. Les habitants, confrontés à deux événements hydrologiques intenses en moins d'une décennie, se sentent abandonnés par les autorités locales et régionales, et expriment un sentiment d'indignation et de perte de confiance envers eux, les accusant de ne pas avoir mis en œuvre des actions de protection durable depuis 2018. Cependant, la question que les citoyens doivent se poser aussi : les autorités sont-elles l'unique responsables dans ce contexte ?

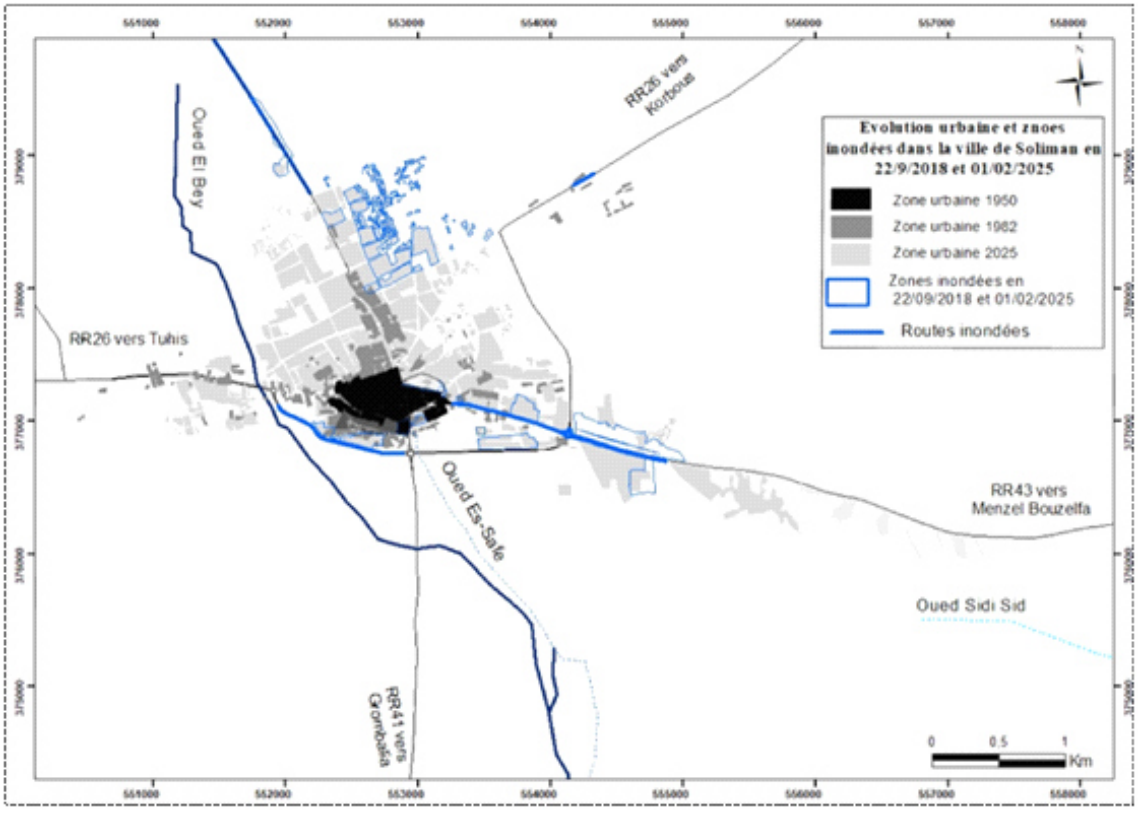

(Fig10) Quartiers inondés le 22/09/2018 et 01/02/2025.

2.2.2. Korbous et Ain El Fakroun: vulnérabilité multidimensionnelle

Korbous et Ain El Fakroun sont deux petites villes encollées au versant NW du JbelKorbous. Ce versant, très abrupt descend en vraie falaise vers la mer ; et domine des bassins de réception minuscules qui abritent les deux villes. A premier abord, cette configuration topographique ne devrait pas être le théâtre d'inondations catastrophiques et répétitives. Ce sont les défaillances humaines qui sont à l'origine de la crise.

A. Korbous : entre vulnérabilité environnementale et fragilité socio-économique

Dans cette petite ville réputée exclusivement pour ses sources thermales, la station thermale qui présente le principal pilier de l'économie locale, se trouve régulièrement menacée par les crues ; révélant la fragilité d'un territoire dont l'économie repose sur une ressource à la fois attractive et vulnérable.

L'épisode pluvieux du 22 septembre 2018 a profondément marqué la mémoire collective locale. La rue commerçante, principale et unique artère de la ville, s'est transformée en véritable torrent.

Conçu par Carpentier pour canaliser un ancien cours d'eau et évacuer les eaux de ruissellement vers la mer, ce tunnel avait longtemps protégé la ville contre les inondations.

Cependant, à partir des années 1990, diverses interventions telle que l'utilisation pour l'évacuation des eaux usées, enrochements côtiers, dérivation des eaux thermales vers les établissements touristiques, ce qui ont entraîné un rétrécissement critique de l'ouvrage, réduisant sa section à moins de 1,5 m en amont et à moins de 1 m en aval. À cette réduction s'est ajoutée l'obstruction progressive par des déchets, compromettant encore davantage sa capacité hydraulique.

Lors de l'épisode pluvieux exceptionnel du 22 septembre 2018, cette combinaison de sous-dimensionnement et de manque d'entretien a provoqué un débordement massif du canal et l'effondrement du tunnel dans un atelier artisanal, constaté officiellement par un huissierdésigné par les instances juridiques,(*fig11*).

Le torrent qui s'est engouffré dans la rue commerçante de Korbous, pourtant sans précédent selon les témoignages locaux, a entraîné des dégâts considérables : une vingtaine de véhicules emportés, des constructions légères détruites, ainsi qu'une explosion dans un local commercial.

Le poste de police a été submergé sous près de deux mètres d'eau, entraînant la perte d'archives et l'endommagement des équipements informatiques.

L'emblématique station thermale a également été gravement touchée : l'eau a atteint le toit du rez-de-chaussée, voire le deuxième étage, provoquant l'arrêt durable des activités sanitaires et touristiques et l'effondrement fonctionnel du système hospitalier thermal.

Sept ans plus tard, en février 2025, un épisode similaire s'est produit, malgré les réaménagements entrepris après la catastrophe de 2018. Le tunnel de drainage a de nouveau cédé, provoquant des débordements comparables à ceux observés auparavant. Le poste de police a subi une nouvelle infiltration (limitée cette fois à une vingtaine de centimètres), mais révélatrice de la persistance des vulnérabilités du système d'évacuation.

Les eaux de ruissellement ont arraché les accotements routiers, emporté plusieurs véhicules et provoqué l'effondrement du même local commercial déjà identifié comme très vulnérable depuis 2018. La station thermale, à nouveau inondée, a dû interrompre ses activités.

Cette récurrence confirme la fragilité structurelle de l'ouvrage : le tunnel principal, ayant déjà subi un effondrement en 2018 au niveau de ce même local commercial situé en aval, a connu en 2025 une nouvelle rupture au même emplacement, révélant l'aggravation d'un dysfonctionnement jamais traité de manière satisfaisante *(Fig11)*.

Ces clichés ont été pris dans le même endroit
(Fig11). Cliché1 : L'effondrement partiel du tunnel dans un local commercial en 2018
(Cliché pris par un huissier désigné par les instances juridiques).
Cliché2 : L'effondrement partiel du tunnel au même endroit en 2025(Photo personnelle)

B. Aïn El Fakroun : vulnérabilité sociale et insuffisance des infrastructures hydrauliques

A quelque kilomètre de la ville de Korbous, l'analyse des inondations dans la localité d'Aïn El Fakroun met en évidence, à la fois une fragilité environnementale et sociale, qui explique la récurrence des dommages observés en 2018 et en 2025. Établie dans l'embouchure d'un petit bassin versant, la petite ville a été marquée par une urbanisation non planifiée sur des zones sensibles. Elle a été édifiée sur un ancien cours d'eau remblayé, clairement identifiable sur la carte topographique de la région. Cette configuration topographique, combinée à une densification récente et mal maîtrisée de l'urbanisation, explique le fait que chaque épisode pluvieux intense y déclenche une catastrophe urbaine.

Les quartiers populaires ont été les plus durement touchés, révélant la dimension sociale de la crise. En 2018, plusieurs habitations avaient été partiellement ou totalement détruites. En 2025, le phénomène s'est amplifié : plus d'une dizaine de logements ont été entièrement effondrés et d'autres rendus inhabitables, les eaux ayant atteint par endroits plus d'un mètre de hauteur. La stagnation prolongée, observée lors des deux épisodes, a non seulement aggravé les dégâts matériels mais aussi accru la précarité des ménages à faibles revenus, déjà fragilisés par un manque de moyens de reconstruction et d'adaptation.

Sur le plan technique, les infrastructures hydrauliques se sont révélées défaillantes. Les ouvrages de rétention ont été submergés et le système d'évacuation, sous-dimensionné, n'a pas pu absorber le volume de ruissellement.

2.2.3. Sidi Errayes : artificialisation du paysage et vulnérabilités récurrentes face aux inondations

L'étude des inondations de 2018 et de 2025 à Sidi Errayes met en évidence une interaction marquée entre urbanisation non maîtrisée, artificialisation des milieux naturelle ce qui provoque une aggravation des risques hydrologiques.

Les images Google Earth révèlent, dès 2018 *(Fig12),* une implantation anarchique de constructions dans le chenal principal de l'oued, ainsi que la présence d'un pont édifié directement dans le lit d'étiage.

À Sidi Errayes, l'implantation anarchique de constructions dans le chenal principal de l'Oued El Mrissa, combinée à l'édification d'ouvrages inadaptés dans le lit d'étiage, accentue fortement le risque d'inondation. Parmi ces aménagements, la construction d'un pont informel par les habitants pour faciliter la traversée entre les deux rives constitue un facteur aggravant majeur.

En obstruant la circulation naturelle des eaux, cet ouvrage bloque partiellement l'écoulement, provoquant le débordement du cours d'eau dans le quartier avoisinant et entraînant d'importants dégâts matériels.

Cet aménagement inadapté a contribué à modifier la dynamique hydraulique, favorisant l'érosion des berges et l'accumulation de sédiments.

L'inondation du 22 septembre 2018 s'est traduite par l'effondrement du pont en question et par l'affectation de plusieurs habitations riveraines.

En 2025, un phénomène similaire s'est reproduitau niveau du lotissement Yassine, à quelques centaines de mètres du pont(point initial de débordement).

L'Oued El Mrissa, auparavant caractérisé par une végétation dense et un fonctionnement hydrologique relativement stable, a connu une artificialisation rapide en lien direct avec la construction de la route régionale Rr128.

La disparition de la couverture arborée et l'ouverture de pistes ont modifié le tracé naturel du cours d'eau, provoquant un débordement plus étendu et accentuant l'érosion des berges (*fig.10 image 3 et4*).

Cette transformation paysagère, couplée à l'absence de mesures de régulation, a entraîné une intensification des inondations et des dommages humains et matériels.

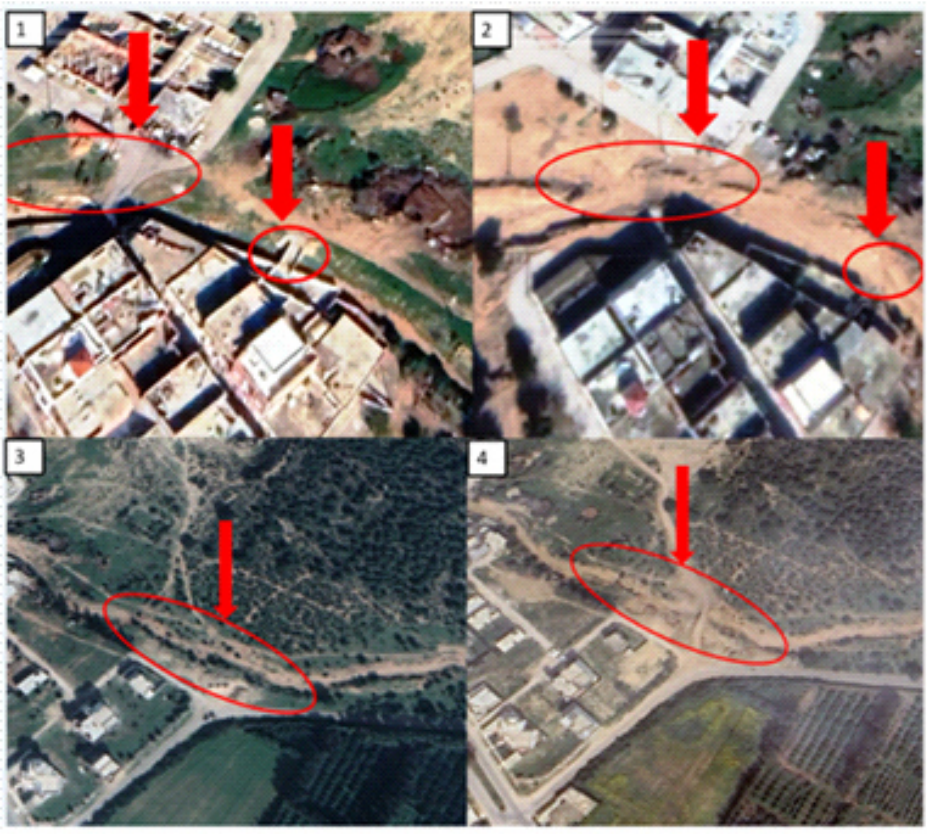

(Fig12).Images Google Earth, Situations d'Oued El Mrissa et localité Sidi Errayes avant et après les événements de 2018 et 2025. Source (Photos personnelles)
Image 1 : Situation au niveau du pont de l'oued El Mrissaavant 22 septembre 2018.
Image 2 : Situation au niveau du pont de l'oued El Mrissaaprès l'événement du 2018.
Image 3 : Situation de densification végétale constatée sur les berges de l'oued Le Mrissa, au niveau du lotissement Yassine, à quelques centaines de mètres du pont mentionné plus haut. Avant l'événement du février 2025.
Image 4 : Situation de déboisement observée sur les berges de l'oued El Mrissa, au niveau du lotissement Yassine, à quelques centaines de mètres du pont précédemment cité. Après l'événement du février 2025

Les impacts sur la population locale témoignent d'une vulnérabilité sociale récurrente *(fig.13)*. En 2018 (*cliché1)* comme en 2025*(cliché4)*, plusieurs logements ont été envahis par les eaux, dont certains sont devenus totalement inhabitables. Des équipements domestiques ont été détruits, un véhicule emporté (*cliché2)*, et une dizaine d'habitations touchées par les infiltrations (*cliché3)*. L'épisode de 2025 a également causé l'isolement d'un troupeau de moutons, dont plus d'une dizaine de têtes ont péri (*cliché6)*, aggravant les pertes pour les ménages ruraux. Ce phénomène a été accentué par l'abandon, dans le lit de l'oued, de résidus d'abattage d'eucalyptus issus de travaux de l'Office des Terres Domaniales (*cliché5)*, lesquels ont obstrué partiellement le chenal et perturbé l'écoulement des eaux.

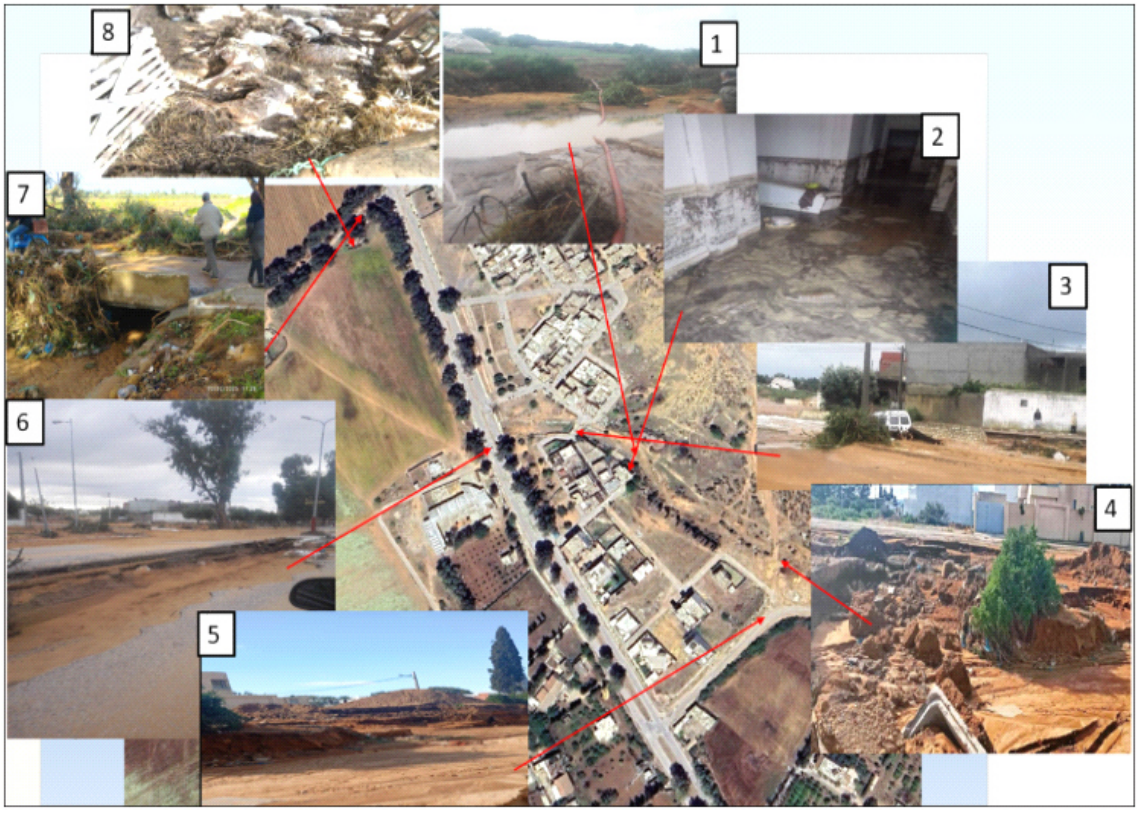

*(Fig13).*Artificialisation de l'Oued El Mrissa et dégâts induit par le débordement. Source (Photos personnelles)
Cliché1 : Débordement d'oued El Mrissa en 2018 et dégâts observés.Clichés 2 : maison inondée.Clichés 3 :véhicule emporté.

Clichés 4 : Point de débordement de l'oued El Mrissa, situé à quelques centaines de mètres du site du débordement de 2018. Cliché 5 : Dégâts induits par le débordement d'oued El Mrissa en 2025 : Cliché 6 : érosion des berges et de la route.Clichés7 : Transports de déchets divers empêchant l'écoulement normal des eaux. Clichés8 : submersion d'une étable et pertes de têtes d'ovin.

2.3. Apports de l'imagerie radar Sentinel-1 à la détection et à la cartographie des inondations (2018–2025)

L'utilisation des données radar Sentinel-1 a constitué un apport méthodologique essentiel pour la délimitation des surfaces inondées dans la zone étudiée, en particulier dans les zones périurbaines de Soliman et sur le littoral de Korbous. Le principe repose sur une approche différentielle de la rétrodiffusion, comparant des images acquises avant et après les événements extrêmes. Les plans d'eau génèrent une forte atténuation du signal radar en bande C (polarisation VV), traduite par un assombrissement marqué des pixels, ce qui permet d'identifier rapidement les surfaces submergées (*https://dataspace.copernicus.eu/*).

Ce procédé a déjà montré son efficacité en contexte méditerranéen (*Hostache,* 2007 ; Lahmar, 2018)et son application au Cap-Bon confirme la pertinence de la télédétection radar dans des régions où l'urbanisation et la pression foncière limitent l'accès aux données de terrain.

Lors de l'épisode du 22 septembre 2018, les images Sentinel-1 acquises le 21 septembre (pré-événement (*fig.14, image 1)* et le 27 septembre (post-événement) révèlent une extension notable des surfaces sombres, particulièrement au sud de Soliman (*fig.12, image 2)*. Ces signatures correspondent à la stagnation d'eau dans les zones agricoles basses, sur les abords de la sebkha et dans les plaines alluviales alimentées par les oueds El Bey et Sidi Saïd.

Le décalage de cinq jours entre l'inondation et la prise de vue a toutefois limité la détection dans certains secteurs urbains où l'assèchement est intervenu rapidement, suggérant une sous-estimation des surfaces réellement submergées (*Cantoni, 2022*).

Malgré cette contrainte temporelle, l'imagerie radar a permis de confirmer les observations de terrain relatives à l'inondation des infrastructures publiques et à l'interruption de plusieurs axes routiers.

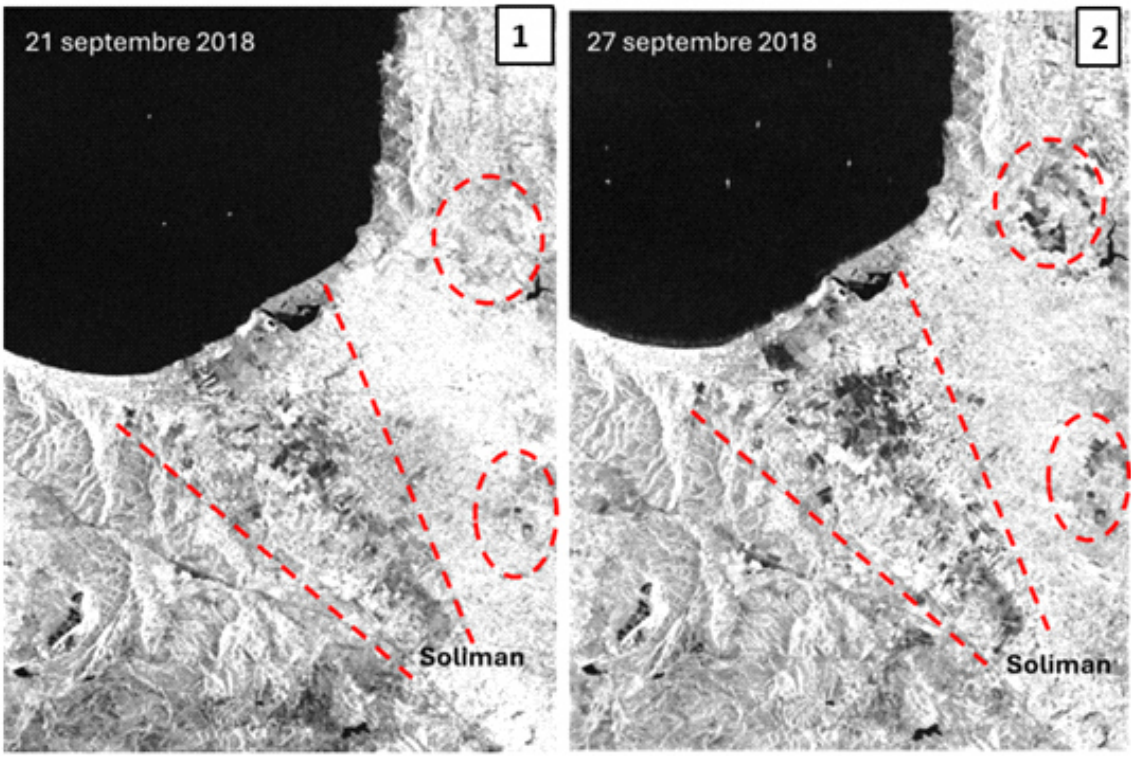

(Fig14). Image1 : image Radar avant l'événement de 22 septembre
Image2 : image Radar après l'événement de 22 septembre

En 2025, la disponibilité d'une image post-événement dès le 4 février, soit le lendemain de la crue, a renforcé la précision des analyses. Les zones sombres identifiées correspondent aux périmètres déjà affectés en 2018, révélant une forte récurrence spatiale des inondations, (*fig.14, image 1 et 2)*. Les abords du Technopôle de Borj Essedria, la route C26 et les zones agricoles situées en aval de la sebkha apparaissent particulièrement vulnérables, confirmant l'hypothèse d'une fragilité territoriale persistante. À Korbous, l'analyse radar met en évidence le débordement récurrent du tunnel principal, déjà signalé en 2018, ainsi que la réactivation des flux torrentiels vers la station thermale. Ces signatures confirment les dégâts rapportés sur le terrain (véhicules emportés, ateliers et locaux commerciaux inondés, interruption du service thermal), illustrant la capacité des données satellitaires à documenter la dynamique des inondations en complément des enquêtes de terrain*(Fig15)*.

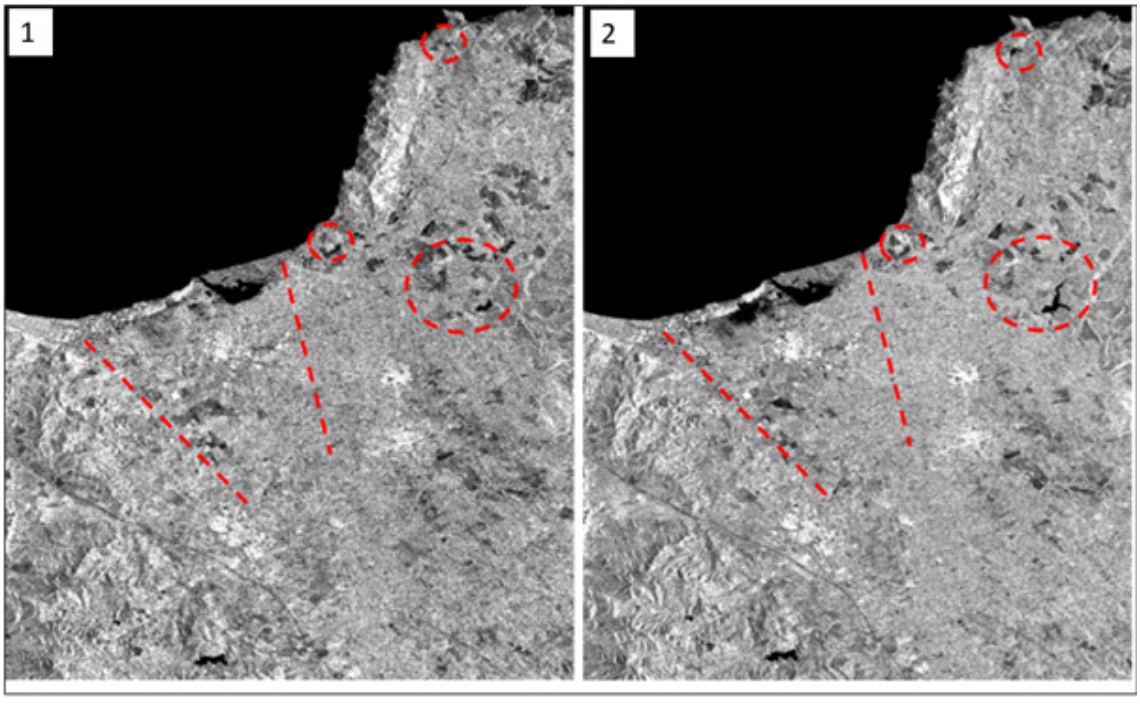

(Fig15). Image1 : image Radar du 23 janvier 2025
Image 2 : image Radar du 04 février 2025

De manière générale, la comparaison multi-temporelle entre 2018 et 2025 souligne trois points majeurs. Premièrement, la continuité spatiale des zones inondées autour de la sebkha et dans les basses plaines agricoles traduit la permanence de foyers de vulnérabilité structurelle, confirmant que les catastrophes hydrologiques résultent moins de l'intensité pluviométrique que de facteurs territoriaux persistants (*Makhloufi, 2021*).

Deuxièmement, la disponibilité rapide des images post-événement améliore la capacité de détection et limite les biais liés à l'assèchement rapide en milieu urbain, ce qui renforce l'intérêt opérationnel des missions Sentinel-1 pour l'alerte et la gestion de crise. Troisièmement, l'imagerie radar permet de dépasser les limites des observations ponctuelles de terrain en offrant une vision synoptique et reproductible des dynamiques de submersion. En ce sens, elle constitue un outil indispensable pour la compréhension des logiques spatiales du risque et pour la mise en place d'une gouvernance territoriale intégrée (*UNDRR, 2019*).

Ainsi l'apport des données radar au suivi des inondations dans le Cap-Bon dépasse la simple cartographie post-événement : il permet de mettre en évidence la persistance des vulnérabilités, de documenter les interactions entre dynamique hydrologique et occupation du sol, et d'ouvrir la voie à des dispositifs opérationnels de prévention et de planification plus efficaces. Leur intégration dans les politiques locales de gestion du risque représente un levier stratégique pour renforcer la résilience face à la récurrence annoncée des épisodes extrêmes en Méditerranée (*Barredo, 2009 ; Llasat, 2016*).

Synthèse et discussion des vulnérabilités de la zone étudiée

L'analyse des crues dévastatrices, induites par les évènements pluviométriques intenses des années 2018 et 2025, présentée dans les paragraphes précédents révèle une vérité inquiétante : une vulnérabilité persistante et multidimensionnelle, structurelle, institutionnelle, économique et sociale qui dévoile la fragilité des territoires concernés et la précarité des populations qui les occupent. Paradoxalement, par des pratiques quotidiennes irresponsables, ces populations contribuent d'une certaine manière à perdurer/aggraver cette fragilité et cette précarité.

3.1 Interactions entre dynamiques naturelles et défaillances d'aménagement : une vulnérabilité structurelle persistante

Sur le plantopographique, l'implantation des localités étudiées les soumet inévitablement au risque d'inondations.

La ville de Solimaninitialement installée sur la rive droite de l'Oued El Beycollecte les eaux de ruissellement issues d'une grande partie des hauteurs environnantes (*fig1*) et qui transitent du sud vers le nord pour se jeter enfin dans la Sebkha de Soliman, occupant une cuvette fermée, et ne communiquant avec la mer que lors des fortes crues.L'Oued Es-Safa, affluent sud de l'Oued El Bey, apparaissait clairement sur les anciennes cartes topographiques. Toutefois, sa partie méridionale a été entièrement remblayée pour permettre l'édification de la cité administrative (*Mehdouani, 2020*). Lors des pluies exceptionnelles, l'ancien lit de l'oued se retrouve largement inondé. Cette zone urbanisée présente une forte prédisposition aux inondations.

D'autre part, la partie sud-est de Soliman est traversée par l'Oued Sidi Sid, affluent droit de l'Oued Al'Anib. Cet oued prend naissance entre JbelMasaouda, JbelAl'Arka et Jbel Bou Daba, puis traverse HanchirAj-Jwaj, contourne la ville de Menzel Bouzelfa et longe la route R43 avant de se déverser dans la plaine agricole au sud-est de Soliman. Cependant, lors de l'épisode du 22 septembre 2018, les ruissellements torrentiels ont entraîné un débordement de l'Oued Sidi Sid, dont les écoulements ont atteint la zone industrielle puis le centre-ville, où ils ont convergé avec les eaux en provenance de l'Oued Le Bey.

La vulnérabilitétopographique de Korbous tout comme celle d'Aïn El Fakroundécoule de leurs sites respectifs très semblables. Elles sont implantées, chacuned'entre elles, à l'aval d'un bassin versant étroit et enserré entre des versants raids,dépassant parfois 200 m d'altitude. En contrebas de ces derniers, les écoulements convergent rapidement vers les installations urbaines des deux localités, édifiées sur des chenaux d'écoulement et dans des zones suffisamment planes pour permettre la stagnation des eaux. Ce contexte topographique conjugué à une urbanisation anarchique ou mal planifiée et à des pluies exceptionnelles, explique les inondations de 2018 et 2025. L'aléa étant présent et récurrent avant même l'installation des hommes, la faute revient en particulier aux défaillances d'ordre anthropique, ne tenant pas compte des contraintes naturelles du milieu*(Fig16)*.

(Fig16).Dégâts observés dans la rue commerciale de Korbous à la suite de l'événement de septembre 2018 Cliché1 : Débordement du tunnel en 2018 et quelques dégâts observés. Clichés 2 : des constructions en léger totalement détruites.Clichés 3 :Nettoyage du poste de police.Clichés 4 :Clichés 5 : Véhicules emportés par les eaux:Clichés 6 Véhicules endommagés.Clichés 7 : Deuxième effondrement du tunnel de Korbous au niveau de Ain Essbiya.

Sur les plans structurel et institutionnel, certaines des infrastructures des zones étudiées se sont trouvées affectées par ces deux évènements successifs, de la même manière ou à des degrés différents, en dépit de la période de sept ans qui les a séparés. Cette période est, en principe, suffisante pour que de bonnes décisions soient prises ; pour que les dispositifs de prévention/protection contre les inondations soient installées et/ou renforcés ; et, pour que les pratiques individuelles et collectives soient adaptées et plus respectueuses de l'environnement.

À Soliman, les mêmes établissements publics ont été touchés : Lycée secondaire, l'école Habib Thameur et la CNAM. Les réponses initiées après 2018se sont révélées insuffisantes. Aucune mesure sensible n'a été prise pour freiner les extensions urbaines massives sur les berges de la Sebkha et dans les zones topographiquement les plus basses et les plus vulnérables *(Fig16),* sans dispositifs de protection adaptés.

À Korbous et à Aïn El Fakroun, des programmes de réaménagement et de protection hydrauliques ont été mis en place sous l'égide du ministère de l'Équipement et du Conseil Régional de Développement. Ces programmes comprenaient la restauration du tunnel de drainage de Korbous et la construction d'ouvrages de protection à Aïn El Fakroun *(Fig18, cliché 1*). Toutefois, lors de l'épisode de 2025, ces aménagements ont révélé leurs limites : les bassins de rétention des eaux de capacité insuffisante ont été submergés et ont débordé *(Fig18, cliché 2*).Les volumes d'eau excédentaires ont submergé les rues (*Fig18, cliché 3*) et les habitations et biens des populations. (*Fig17, cliché 4*).

(Fig17).Cliché 1 : L'effondrement d'un mur de soutènement A Ain El Fakroun, édifié sur un conduit pluvial après la catastrophe de 2018, a été provoqué par un volume d'eau exceptionnel.
Cliché2 : Débordement et dispersion de matériaux solides en zone habitée à la suite de l'effondrement d'ouvrages hydrauliques.
Cliché 3 : Rues fortement encombrées par la boue, résultant à la fois de l'effondrement des ouvrages édifiés après la catastrophe de 2018 et des ruissellements torrentiels.
Cliché 4 : Submersion et destruction des biens des populations, avec un niveau d'eau dépassant un mètre dans certains secteurs. Source (Photos personnelles)

À Sidi Errayes, certaines pratiques officielles ont accentué la vulnérabilité locale ; dont le pont problématique édifié dans le chenal d'étiage d'oued El Mrissa qui n'a pas été réaménagé ; de même, aucune mesure dissuasive empêchant l'abandon des déchets pouvant aggraver les crues n'a été prise. De surcroît, les opérations d'abattage d'eucalyptus par les ouvriers de l'Office des Terres Domaniales, dont les résidus ont été laissés dans le lit de l'oued, ont contribué à colmater son chenal d'écoulement et à aggraver sont débordement. Ces insuffisances d'ordres structurel et institutionnel ont aggravé la fragilité des zones étudiées qui sont, naturellement, plus ou moins vulnérables aux inondations.

3.2 La vulnérabilité socio-économique : des populations simultanément touchées par la catastrophe et impliquées dans son aggravation.

Les vulnérabilités *économiques* sont particulièrement perceptibles à Soliman et à Korbous. Dans la première ville, Soliman, la zone industrielle a subi des pertes considérables. Des sociétés comme Hait et Délice-Danone ont subides dégâts importants : destruction de stocks (matières premières et/ou produit manufacturés) et suspension provisoire d'activités en 2018 puis en 2025. À Korbous, le thermalisme constitue la colonne vertébrale de l'économie locale. Le disfonctionnement provisoire de la station thermale affectée lors des deux évènements de 2018 et 2025 a affecté, en conséquence, la dynamique touristique et le commerce artisanal local. Dans les autres localités, les pertes de cheptel, les dégâts dans les infrastructures agricoles (petites exploitations) et les pertes de véhicules (moyens de production) créent davantage de difficultés économiques pour les populations locales.

Sur le plan social, l'ensemble des vulnérabilités présentées dessus aggrave les difficultés des populations touchées.Les logements partiellement ou totalement détruits par les crues et les pertes de biens domestiques (meubles, couvertures, ustensiles ...) chaque fois que des logements sont submergés, aggravent la précarité des ménages à faibles revenus et aux conditions de vie déjà précaires.

La suspension totale ou partielle des services éducatifs (école et bibliothèque municipale) et sanitaire ont profondément perturbé la vie quotidienne des populations locales subissant des pressions supplémentaires.

La perte ou l'endommagement de véhicules (de service) privés, la destruction des petits commerces, les pertes de bétail et le chômage forcé suite aux suspensions de travail dans les établissements industriels présentent autant de pertes de revenus et de moyens de subsistance pour les ménages/individus concernés. Ainsi, les populations locales constituent le maillon le plus exposé au risque et se sentent victimes ; certes, mais réellement, elles sont loin d'être exemptes de toute responsabilité. En fait, le comportement irresponsable de ces populations envers les cours d'eau, grignotés par les constructions à usages divers, transformés en décharges d'ordures ménagères et en dépotoirs de restes de matériaux de construction gène l'écoulement et aggrave le risque d'inondations.

Les résultats obtenus confirment ainsi que les catastrophes hydrologiques ne relèvent pas uniquement de l'exceptionnalité des aléas, mais aussi de la combinaison de facteurs multiples et imbriqués (*Vinet, 2010 ; Llasat, 2016*).

Les dommages de 2018 et 2025 révèlent la faiblesse des infrastructures hydrauliques dans la zone d'étude et la non-prise en compte des contraintes hydro-géographiques dans l'aménagement urbain. L'implantation d'équipements publics dans d'anciens lits d'oueds en est la meilleure démonstration.

L'effondrement de certains ouvrages (cas du tunnel de Korbous, par exemple) reconstruits/consolidés après la catastrophe de 2018 illustre également une réponse institutionnelle insuffisante / inefficace et fragmentée.

Plusieurs études confirment que l'urbanisation en zones inondables reste l'un des principaux facteurs aggravants le risque en Tunisie (*Fehri, 2013 ; 2014; Lahmar, 2020 ; Louhaichi, 2013 ; Makhloufi, 2021 ; Khemiri, 2024 ; Bourgou, 2018*).

L'extension urbaine informelle sur berges de la « Sebkha de Soliman » illustre bien l'absence de règlementationou de contrôle efficaces.L'évènement de 2025 montre ainsi que, faute d'une planification intégrée et cohérente, certaines pratiques institutionnelles peuvent elles-mêmes constituer des facteurs aggravants du risque.

3.3 Pour une gouvernance intégrée des risques hydrologique

Les analysesprésentées dessus montrent que la gravité des inondations se traduisant par des vulnérabilités complexes et récurrentesest la conséquence de choix d'aménagements inadaptés, d'un déficit d'entretien des infrastructures et d'une faiblesse institutionnelle persistante (*UNDRR, 2019*). Les réponses postérieures à 2018 confirment ce constat.

Elles sont souvent limitées à des mesures techniques ponctuelles et dépourvues d'un véritable retour d'expérience, raison pour laquelle elles n'ont pas permis de rompre le cycle des catastrophes. Face à ce constat, une approche intégrée et anticipative apparaît indispensable, combinant la réglementation stricte de l'urbanisation, la restauration écologique des territoires concernés et l'entretien rigoureux des ouvrages hydrauliques.

Les inondations de 2018 et 2025 révèlent une vulnérabilité systémique où se croisent des facteurs structurels, sociaux, économiques et institutionnels.

Dans ce contexte, seule une approche systémique et intégrée, tenant compte de tous les facteurs et impliquant les populations locales, peut briser le cycle des vulnérabilités chroniques et renforcer la résilience face aux aléas climatiques (*UNDRR, 2019*).

2. CONCLUSION

L'analyse comparée des inondations de 2018 et de 2025 dans la région du Cap-Bon met en lumière la complexité des catastrophes hydrologiques en Tunisie et, plus largement, dans l'espace méditerranéen. Les résultats montrent que la gravité des impacts ne dépend pas uniquement de l'intensité des précipitations, mais surtout de la vulnérabilité, notamment structurelle et institutionnelle, des territoires. Les aléas, aussi violents soient-ils, ne provoquent des catastrophes que lorsqu'ils touchent un milieu fragilisé par des pratiques et des choix d'aménagement inadaptés dénotant d'une mauvaise gouvernance.

L'enseignement majeur tiré de cette étude réside dans la confirmation du fait que le rôle de la vulnérabilité territoriale est plus déterminant que celui de l'aléa pluviométrique dans le déclenchement des crises.

L'épisode de 2025, pourtant moins intense en termes de cumul pluviométrique, a causé des dommages comparables à ceux de 2018. Ce fait illustre que l'ampleur des impacts dépend avant tout de la manière dont le territoire est occupé et géré : urbanisation anarchique, artificialisation des sols, infrastructures sous-dimensionnées ou mal entretenues. Alors l'aléa climatique ne fait que révéler les fragilités préexistantes, induites par des pressions urbaines mal gérées et par l'absence/insuffisance d'entretien systématique des ouvrages hydrauliques.

Les zones sinistrées dans un territoire donné se recoupent largement d'un épisode pluvieux à un autre : les mêmes quartiers, infrastructures et établissements économiques sont affectés en 2018 puis en 2025. Cette récurrence spatiale souligne le manque d'efficacité des mesures post-catastrophes, souvent limitées à des réparations ponctuelles, sans réelle stratégie de prévention. Elle traduit également une faible capitalisation de l'expérience : la mémoire des catastrophes demeure fragile ou absente, et les constats établis après 2018 ne se sont pas traduits en politiques publiques durables. En 2025, les mêmes défaillances se sont répétées, révélant la persistance d'une logique de gestion post-crise plutôt que d'une réelle politique de prévention des risques.

Ces constats dépassent le cadre tunisien. De nombreux pays du pourtour méditerranéen – notamment la France, l'Espagne, le Maroc et l'Algérie – rencontrent des problématiques similaires. La littérature scientifique (*Vinet, 2010 ; Llasat, 2016)* converge vers une même conclusion : les catastrophes hydrologiques récurrentes découlent moins de la fréquence des aléas que d'une vulnérabilité chronique nourrie par l'urbanisation non maîtrisée et l'insuffisance des politiques de prévention.

Au-delà du diagnostic, cette étude appelle à repenser la gestion des inondations à travers une approche territoriale et intégrée. La régulation de l'urbanisation dans les zones à risque, la protection des lits majeurs des oueds et la maîtrise de l'expansion des zones industrielles constituent des priorités.

L'entretien régulier des ouvrages de drainage, digues et ponts doit être inscrit dans la durée, car la pérennité des infrastructures conditionne directement la résilience territoriale. Parallèlement, des solutions fondées sur la nature (restauration des zones humides, reforestation des berges, réhabilitation des plaines inondables) offrent des alternatives durables et complémentaires aux approches techniques.

Enfin, les inondations de 2018 et 2025 dans le Cap-Bon ne peuvent être réduites à la simple gravité des événements climatiques.

Elles révèlent surtout les limites d'un modèle d'aménagement peu résilient et la nécessité urgente d'une gouvernance préventive du risque. Seule une stratégie intégrée et systémique, combinant prévention, entretien, aménagement raisonné et participation citoyenne, permettra de réduire durablement les effets de l'exposition aux aléas hydrologiques et de renforcer la résilience des territoires tunisiens.

BIBLIOGRAPHIE

Abdelkhalek, A. (2008). Les intensités des pluies dans la Tunisie orientale. FS HST, 306 p.
Alfieri, L., Thielen Del Pozo, J. A. (2012). Europeanprecipitation index for extremerain-storm and flash flood early warning. Meteorological Applications. JRC68363.
Alfieri, L., Burek, P., Dutra, E., Krzeminski, B., Muraro, D., Thielen, J., &Pappenberger, F. (2013). GloFAS – Global ensemble streamflowforecasting and flood early warning. HAL Id : hal-03483619.
Aouissi, J., Nsiri, I., & Ahmed, A. (2024). Evaluation of flood risk in an aridregion of southernTunisia: Couplinghydrological and hydraulic modeling. Moroccan Journal of Agricultural Sciences, 5(2), 118–129.
Ashley, S. T., & Ashley, W. S. (2008). Flood fatalities in the United States. Journal of AppliedMeteorology and Climatology, 47, 805–818. https://doi.org/10.1175/2007JAMC1611.1
Bárdossy, A., &Filiz, F. (2005). Identification of flood producingatmospheric circulation patterns. Journal of Hydrology, 313(1–2), 48–57. https://doi.org/10.1016/j.jhydrol.2005.02.006
Barredo, J. I. (2009). Normalised flood losses in Europe (1970–2006). Natural Hazards and Earth System Sciences, 9, 97–104. https://doi.org/10.5194/nhess-9-97-2009
Bourgou, M. (2018). Urbanisation et aléas hydrologiques dans le Cap Bon. Revue Tunisienne de Géographie, 41(2), 77–94.
Bousnina, A. (1986). La variabilité des pluies en Tunisie. Publications de l'Université de Tunis, 308 p.
Cantoni, E., Tramblay, Y., Grimaldi, S., Salamon, P., Dakhlaoui, H., Dezetter, A., &Thiemig, V. (2022). Hydrological performance of ERA5 reanalysis for flood modeling in Tunisiausing LISFLOOD and GR4J models. Journal of Hydrology: RegionalStudies, 42, 101169. https://doi.org/10.1016/j.ejrh.2022.101169

Chouari, W. (2009). Environnement et risques naturels dans le Grand Tunis : approche cartographique. Thèse de doctorat, Université Paris-Diderot, 395 p.
Chouari, W. (2019). Le bassin versant de l'oued El Kébir (Tunisie orientale). Geo-Eco-Trop, 43(1), 103–117.
Chouari, W. (2020). Pluviométries exceptionnelles et occupation des sols mal maîtrisée : l'exemple des inondations de septembre 2016 dans le Sahel de Sousse. La Houille Blanche, 106(1), 50–59. https://doi.org/10.1051/lhb/2019062
Commission Régionale de Développement Agricole de Nabeul (CRDA). (2018). Les inondations du gouvernorat de Nabeul – 22 septembre 2018.
Daoud, A. (2013). Retour d'expérience sur les inondations dans l'agglomération de Sfax (1982–2009). Revue Géographique de l'Est, 53(1–2).
Dahri, N., &Abida, H. (2020). Causes and impacts of flash floods: Case of Gabes City, SouthernTunisia. Arabian Journal of Geosciences, 13, 176. https://doi.org/10.1007/s12517-020-5149-7
Dallel, J. (2007). Les événements pluviométriques exceptionnels en Tunisie. FS HST, 344 p.
Direction Générale des Ressources en Eau – Direction des Eaux de Surface. (2018). Crue du 22 septembre 2018 dans le gouvernorat de Nabeul, 29 p.
El Aroui, O. (2020). Risques géomorphologiques et aménagement dans le sud-est du golfe de Tunis : le versant de JbelKorbous. Géo-Eco-Trop, 44, 631–650.
El Melki, T. (1997). Les masses d'air sur la Tunisie. Thèse de doctorat, 320 p.
El Melki, T. (2014). Climatologie dynamique de la Tunisie. Université de la Manouba, 438 p.
El Melki, T. (2015). Dynamique atmosphérique et événements pluviométriques intenses en Méditerranée occidentale : cas de la Tunisie. FLSH Saïe-Fès, 52, 21–30.
Fehri, N. (2013). Extension urbaine et risque d'inondation autour du Jebel Bou Garnine (Grand Tunis). Revista de Geomorfologie, 15, 13–26.
Fehri, N. (2014). L'aggravation du risque d'inondation en Tunisie : éléments de réflexion. Physio-Géo, 8, 149–175.
Fiori, E., et al. (2014). Analysis and hindcast of an extremerainfallevent in the Mediterraneanarea : The Genoa 2011 case. AtmosphericResearch, 138, 1–32.
Gaume, E., et al. (2009). A compilation of data on European flash floods. Journal of Hydrology, 367, 70–78.
Gilabert, J., &Llasat, M. C. (2017). Circulation weather types associatedwithextreme flood events in the NorthwesternMediterranean. International Journal of Climatology, 38(4).
Gouvernorat de Nabeul. (2018). Les inondations du gouvernorat de Nabeul du 22 septembre 2018, 66 p.
Henia, L. (1980). Les précipitations pluvieuses dans la Tunisie tellienne. FS HST, 262 p.
Henia, L., & El Melki, T. (2000). Circulation de « Retour d'Est » et pluies diluviennes sur la Tunisie orientale. Actes du XIIIe Colloque AIC, Nice, 120–127.
Hmidi, N., Fehri, N., &Baccar, A. (2019). Inondation dévastatrice à Soliman lors de l'événement du 22 septembre 2018. XXXIIe Colloque AIC, Thessalonique, 199–204.
Hostache, R., Puech, C., &Raclot, D. (2007). Caractérisation spatiale de l'aléa inondation à partir d'images radar. Cybergeo. https://doi.org/10.4000/cybergeo.7722
IPCC. (2022). AR6 – Working Group II: MediterraneanRegion.
IPCC. (2023). Rapport de synthèse.
Jansà, A., et al. (2001). Western Mediterranean cyclones and heavyrain – Part 2. Meteorological Applications, 8(1), 43–56.

Kassab, F. (1979). Les très fortes pluies en Tunisie. Université de Tunis, 234 p.
Khemiri, L., et al. (2024). Flood mapping of the lowerMejerda Valley using Sentinel-1 SAR. Frontiers in Earth Science, 11, 1332589.
Lahmar, L. (2018). Caractérisation et cartographie des espaces inondés en Tunisie centre-orientale. Revue Tunisienne de Géographie, 49–50.
Lahmar, L. (2024). Interférence des données naturelles et anthropiques dans l'évolution récente du risque d'inondation sur le littoral tunisien. Dynamiques Environnementales, 53.
Louhaichi, M., Hassan, S., &Etteieb, S. (2013). Assessing the risk of flooding in Central Tunisia. Australian Journal of Basic &Applied Sciences, 7(8), 868–874.
Makhloufi, D. (2021). Les événements pluviométriques intenses dans le Grand-Tunis. Thèse de doctorat, 282 p.
MedECC. (2020). Climate and Environmental Change in the Mediterranean Basin (MAR1).
Mehdouani. (2020). Contribution à l'étude des inondations du 22 septembre 2018 dans le Cap Bon. Revue Tunisienne de Géographie, 52–53.
Min, S. K., et al. (2011). Human contribution to more-intense precipitationextremes. Nature, 470, 378–381.
Ministère de l'Agriculture, des Ressources Hydrauliques et de la Pêche (MARHP). (2020). Rapport national du secteur de l'eau, 147 p.
Mrbati, M., et al. (2019). Les inondations catastrophiques de septembre 2018 dans le Cap Bon. XXXIIe Colloque AIC, 241–246.
Nasrallah, W. (2019). Hydroclimatologie des zones urbaines de Kairouan et Sidi Bouzid. Thèse de doctorat, 306 p.
Panthou, G., et al. (2014). Recent trends in extremerainfall in the Central Sahel. International Journal of Climatology, 34.
Tarolli, P., & Sofia, G. (2016). Human topographic signatures and geomorphicprocesses. Geomorphology, 255, 140–161.
Tramblay, Y., et al. (2013). Non-stationaryfrequencyanalysis of heavyrainfallevents. Hydrological Sciences Journal, 58, 280–294.
Tramblay, Y., &Somot, S. (2018). Évolution future des précipitations extrêmes en Méditerranée. Climatic Change, 151, 289–302.
Tramblay, Y., et al. (2023). Changes in Mediterranean flood processes and seasonality. Hydrology and Earth System Sciences, 27, 2973–2987.
Trenberth, K. E. (2011). Changes in precipitationwithclimate change. ClimateResearch, 47, 123–138.
Trenberth, K. E., et al. (2003). The changingcharacter of precipitation. BAMS, 84, 1205–1217.
UNDRR. (2019). Global Assessment Report on Disaster Risk Reduction.
UNDRR. (2025). Global Assessment Report on Disaster Risk Reduction.
Vinet, F. (2010). Le risque inondation : diagnostic et gestion. Lavoisier, 232 p.
Vinet, F., et al. (2015). Protection du bâti individuel contre l'inondation. Norois, 236.
World Bank. (2021). An EPIC Response: Innovative Governance for Flood and Drought Risk Management.
Zakaria, S., et al. (2022). Analyse du risque d'inondation de l'agglomération de Tindouf. Études Caribéennes, 53.
Zhou, Y., & Lau, W. K.-M. (2017). Trends of mean and extremeprecipitation. International Journal of Climatology, 37(10).

AN APPROACH FOR SUDAN'S FLOOD RISK MAPPING

Kamal A. SamiTarig Abu Obeida A. Ali &Ahmed Osama J. Mohammed
Kamal.Sami@uofk.edutarigabuobeida@gmail.com
Department of Surveying Engineering, Faculty of Engineering, University of Khartoum

ABSTRACT

Sudan has faced a series of severe floods along the Nile and its tributaries, as well as flash floods in the Wadi system, over the past several decades. These floods significantly impact human lives, livestock, agriculture, buildings, and infrastructure. This study aimed to map flood hazards, estimate flood damages, and assess the impacts of flooding on human settlements, agriculture, and national infrastructure. The research utilized spatial-temporal analysis, employing high-resolution satellite imagery and Geographic Information Systems (GIS). By applying multi-temporal satellite imagery and GIS analysis tools, the authors created Flood Hazard maps and estimated flood damages within the study area to help mitigate risks to human life, property, and infrastructure, as well as to evaluate the effects of flooding on land cover.To define flood extents during the rainy months, two sets of remote sensing data were obtained: images captured before and after the floods. High-resolution optical Sentinel-2 imagery, with a spatial resolution of 10 meters and advanced classification techniques, was used to produce land cover classes. Flood damage was then assessed across various land cover types.Hydrological modeling techniques, combined with land cover data, were employed to generate Flash Flood Hazard maps, which were later merged with River Flood Hazard maps to create a comprehensive Flood Hazard Map. Furthermore, multi-seasonal Sentinel-2 images from before and after the floods were utilized to calculate the Normalized Difference Water Index (NDWI) for the years 2018, 2019, 2020, and 2021. The results of the 2020 flood extent were compared with Sentinel-1 SAR data.The findings from this analysis are highly valuable for flood risk assessment. The identified flood-prone areas and their severity are based on previous flood mapping and flood magnitude. The results of this study also support future modeling and forecasting of natural flooding disasters, as well as the development of the Hydrological Geospatial Information System in Sudan.

Keywords: LULC, NDWI, ESA, SAR, SRTM, SNAP software

1. INTRODUCTION

Sudan has had a series of high floods on the Nile and its tributaries, as well as flash floods in the Wadi system, over the years. The consequent recorded floods of high magnitude significantly affect human lives, animals, agriculture, buildings, and other infrastructure, disrupt personal, economic, and social activities, and threaten the country's security, infrastructure, growth, and development in the agricultural industry andreal estate developments. For example, the 1988 floods in Sudan were one of the most remembered, with more than 90 people killed and 1.5 million people displaced.

Unusually heavy rains and subsequent floods affected tens of thousands of families across Sudan in August and September 2013. The occurrence of such floods caused by heavy rain in the years 2013 and 2014 in Sudan was considered a national catastrophe. Khartoum city was hit by rain exceeding 100 mm in a few hours, which led to heavy floods in east Khartoum and west of Omdurman. The rains caused extensive damage, destroying thousands of houses. In 2019, According to Tarig A. et al 2022, heavy rains that started on 13 August caused flash floods an estimated of 179,000 people in 15 different states in Sudan including Khartoum have been affected, and over 22,800 homes have been destroyed and 11,702 damaged, at least 54 people have died as a result of the flooding, the floods also damaged an unknown number of public facilities including mosques, schools, health centers and government institutions. In September 2020, according to UN agencies, profuse and continuous rainfall in Sudan caused a devastating flood across 17 out of the 18 Sudanese states, with the Blue Nile reaching water levels not seen for nearly a century. It ranks among the most severe floods recorded in the region (Tarig A. et al 2022). A state of emergency was declared, and teams have worked to prevent damage to threatened archaeological sites. The flood affected more than 3,000,000 people, destroyed more than 100,000 homes, and left more than 100 people dead. In recent years,the climatic variability through intensified rainfall,together with urban development without considering the flood effects,has made the city of Khartoum increasingly exposed and vulnerable to extreme both River & flash flooding events (Abdo, G. 2012).

Floods were described in a variety of ways, but commonly refer to the temporary covering of land with water as a result of surface waters escaping from their normal confines or as a result of heavy precipitation (Kron, 2003). Floods can be classified by major differences between flood categories, taking into account the size of the affected area and the duration of the triggering precipitation event. The flood size and duration elements were used to define the spatial and temporal scale of flood outbreaks, which resulted in two basic types of floods: widespread long-lasting floods and localized rapid floods (Bronstert, 2003). Floods have also been classified into three main types, namely: river floodand flash flood (Jonkman, 2005; Younis, Ramos, & Thielen, 2008),and storm surge (Coastal Floods) (Kron, 2003; Jonkman, 2005). This study isonly concerned with the river and flash floods.

The flood type knowledge is essential for proper flood planning, monitoring, management(Uddin et al, 2013), and development,as well as the development of flood early warning systems.

The objective of this study is to create flood hazard maps and estimate flood damage in the study area, thereby reducing risks to human life, properties, and infrastructure. Multi-temporal satellite images and Geographic Information Systems (GIS) spatial analysis techniques were employed to assess the impact of floods on land cover by performing supervised classification. The study alsoaimed to map flood hazards, estimate flood damages, and evaluate the impact of floods on human settlements, agriculture, and national infrastructure. By employing multi-temporal satellite imagery and GIS spatial analysis tools and methodologies, the authors developed flood hazard maps and estimated flood damages in the study area to mitigate risks to human life, property, and infrastructure, as well as to evaluate the impact of flooding on land cover.

This study integrated remote sensing as a data source and GIS as a processing tool to create flood maps using high-resolution, multi-temporal Sentinel-1 and Sentinel-2 imagery. Hydrological modeling techniques, combined with land cover data, were used to generate Flash Flood Hazard maps, which were then merged with River Flood Hazard maps to develop a comprehensive Flood Hazard Mapas given in Townsend et al (1998). Multi-seasonal Sentinel-2 images from before and after the floods were used to generate the Normalized Difference Water Index (NDWI) for the years 2018, 2019, 2020, and 2021. The findings identify and prioritize flood-prone locations based on previous flood mapping and flood magnitudes. The results of this study also support future modeling, forecasting natural flooding disasters, and flood management in Sudan.

2. STUDY AREA AND FLOODS IN KHARTOUM

The study area lies in Khartoum State, illustrated by the Location Rectangle bounded by latitudes from 15.2529˚ N to 15.6280˚N and longitudes from 32.3764˚E to 32.5713˚ E.Khartoum is one of Sudan's 18 states, comprising 3 main cities (Khartoum, the national capital of Sudan; Khartoum North; and Omdurman), with an area of 22,122 square kilometers and administratively divided into 7 localities. The population of Khartoum State in 2014 was 5,061,792, increasing at an average annual rate of 7.3% since 2000. The urban extent of Khartoum in 2014 was 74,297 hectares, increasing at an average annual rate of 7.2% since 2000.

The 1988 floods in Khartoum were frequently described as “unprecedented”. However, an examination of evidence on Nile flooding and rainstorms during the 19th and 20th centuries indicates that neither the Nile flood nor rainstorms, nor their coincidence in one season, was unprecedented, and similar situations are expected to recur. The authors confirmed that most flooding problems arose from complacency, lack of planning, and mismanagement. Greater Khartoum lies on both sides of the confluence of the Blue and White Nile and includes the cities of Khartoum, Omdurman, and Khartoum North.Three of the seven Khartoum State localities fall within the study region, namely:

Omdurman, Jebel Awlia, and the capital city of Khartoum (Figure 1). Figure 2 shows the topography of the study area, with elevations ranging from 378.259 meters to 436.054 meters (above MSL).

Omdurman is situated on elevated ground beneath the Nubian sandstone formations. The lower reaches of the Blue Nile are incised, contrasting sharply with the broader, seasonally flooded regions and the extremely low gradient of the White Nile. This low-lying area of West Khartoum, at an average sea level height of 337.5 meters, is particularly vulnerable to flooding from the Nile River. The rainfall data for the study area, averaged monthly from 1985 to 2020, was presented in Fatima Ali and Kamal A. A. Sami (2024). Omdurman experiences a hot, arid climate, with noticeable precipitation occurring only during the summer months. In January and February, while daytime temperatures are typically very warm, nights can be relatively cool, with average low temperatures just above 15 °C (59 °F).

The Jebel Awlia area primarily comprises urban settlements and agricultural lands. Along the White Nile River, there are five villages in the Jebel Awlia locality, which are closely situated to one another,with a total estimated population of 45,750. Approximately 10,350 people in this area have been affected by flooding.

Table 1 presents the damage estimates caused by floods in the five assessed villages: Al Assal, Um Rabah, Gamar, Wed Mukhtar, and Um Gargeer. In South Omdurman, seven locations were impacted by floods in 2019 and 2020, mainly Salha and Al Qaia'a, along withUm Owaina, Al Zurga, Barkat Al Shati, Al Shigaila, and Al Salamaniya. According to Esther Menduina (2020), approximately 10,000 people were affected by the flood in this area. A total of 416 households were completely damaged, while 755 households suffered partial damage. One of the main causes of the flooding is the overflow of the White Nile River and the lack of adequate flood protection measures along the riverbanks.

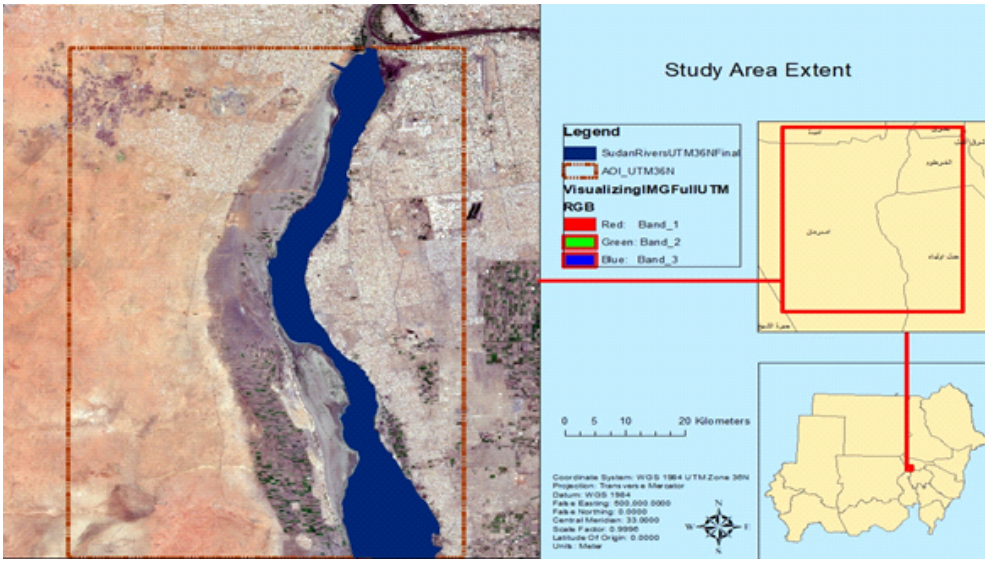

Figure 1: A map of the extent of the study area at the State and localities Level.

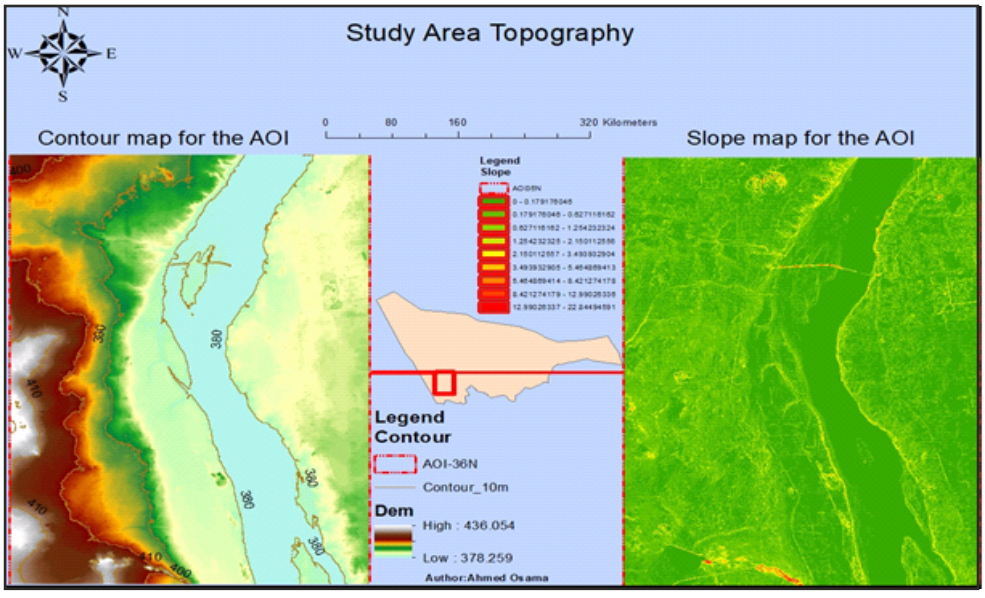

Figure 2: Study area topography Map (contour lines & Slope Layer)

Table 1: Shows the estimated damages at the five villages in Jebel Awlia locality

Village	Population	Destroyed Homes	Damaged Homes	Affected Household	Affected Individuals	Damaged Latrines
Al Assal	25,000	1,100	50	1,150	5,750	1,150
Um Rabah	4,500	10	60	70	350	60
Gamar	1,250	40	10	50	250	50
Wed Mukhtar	10,000	200	350	550	2,750	550
Um Garageer	5,000	150	100	250	1,750	250
Total	45,750	1,500	570	2070	10,350	2,070

3. METHODOLOGY, DATA ACQUISITION, AND PROCESSING

3.1 General

The study is conducted in Khartoum State, specifically in the localities of Khartoum, Jebel Awlia, and Southern Omdurman. It utilizes Geographic Information Systems (GIS) and Remote Sensing tools to accurately map the flooding extent of the White Nile River in the area under consideration and to monitor hazards to urban infrastructure.Satellite imagery plays a crucial role in mapping and monitoring flood behavior, as well as in detecting changes over several years. Data from the European Space Agency (ESA) Sentinel Hub was used for this purpose. The methodology integrates data from different satellite sensors, specifically Sentinel-1 (Synthetic Aperture Radar) and Sentinel-2 (optical multispectral), with the aid of SNAP software for processing the satellite imagery(Sentinel-2 Hub, 2020). ARCGIS software is employed to process the images, map flood extent and inundation, assess the flood's impact on land cover, and produce a flood risk map that can support decision-making.

Additionally, satellite imagery is utilized for river flood analysis. A Digital Elevation Model (DEM) has been employed for hydrological modeling to identify areas susceptible to flash floods and to create a Flash Flood Hazard Map. The results from the river flood analysis and the flash flooding analysis have been combined to produce the final Ranked Flood Hazard Map. An evaluation of Sentinel-1 SAR imagery was also conducted to detect flood inundation during the specified flood season. These data have been made available under ESA Sentinel Hub's (2020) open-source data policies.

3.2 Data Acquisition

Sentinel-1 (SAR) Data: Sentinel-1 Ground Range Detected (GRD) images were acquired based on rainfall data, specifically focusing on maximum precipitation and the observed water index for each rainy month, as analyzed on the Sentinel Playground platform. The study recorded the dates for pre-flood (May 2, 2020) and post-flood (September 23, 2020) conditions. A total of 44 dual-polarization Sentinel-1 level-1 GRD products were used for inundation mapping during the pre-flood (May) and post-flood (September) periods.

The focused synthetic aperture radar (SAR) data were detected, multi-looked, and projected to the ground range using the WGS-84 Earth ellipsoid model.

The terrain height indicated in the product's general annotation was employed to rectify the ellipsoidal projection of the GRD products. In this investigation, data were obtained as Level-1 GRD products from both like-polarized (vertical transmit and vertical receive, denoted as VV) and cross-polarized (vertical transmit and horizontal receive, denoted as VH) channels. The Sentinel-1 SAR images were advantageous as the data were publicly available within 3 hours of acquisition for near real-time (NRT) emergency response and within 24 hours for real-time (RT) emergency response (Uddin, Matin, & Meyer, 2019).
Sentinel-2 (Multi-spectral) Data: The peak flood periods in the rainy season occurred in September 2018, August 2019, September 2020, and September 2021.

The water indicators for these dates were visualized on the Sentinel Playground platform. Sentinel-2 images were collected on September 15, 2018; August 31, 2019; September 19, 2020; and September 14, 2021 (all during flooding seasons), as well as on May 27, 2020 (during the dry season).

These images were used to calculate the Normalized Difference Water Index (NDWI) for each year's floods. By subtracting the NDWI values from the dry season imagery from those of the flood season imagery, the resulting images indicated the NDWI of flooded lands, thus showing the exact extent of floodwaters during each season. Table 2 outlines all the remotely sensed data utilized in the study.

Table 2: Description of all the remotely sensed data acquired for the study.

Sensing Date	Platform	Sensor	No. of Bands	Spectral Range	Spatial Resolution (m)
23 Sept 2020	Sentinel-1B	SAR-C Band	2	VV, VH	30
2 May 2020	Sentinel-1B	SAR-C Band	2	VV, VH	30
27 May 2020	Sentinel-2B	MSI	13	(0.443-2.190 μm)	10, 20 &60
15 Sept 2018	Sentinel-2B	MSI	13	(0.443-2.190 μm)	10, 20 &60
31 Aug 2019	Sentinel-2B	MSI	13	(0.443-2.190 μm)	10, 20 &60
19 Sept 2020	Sentinel-2B	MSI	13	(0.443-2.190 μm)	10, 20 &60
14 Sept 2021	Sentinel-2B	MSI	13	(0.443-2.190 μm)	10, 20 &60

Digital Elevation Model (DEM): A digital elevation model with a spatial resolution of 10 meters has been acquired from the Federal Ministry of Infrastructure, covering a larger area than the study area's rectangle (as shown in Table 2), which contains the DEM coordinates.

This broader coverage allows for better delineation of drainage lines (streams) by providing a more accurate perspective of elevation, thereby improving flash flooding hazard mapping. The vertical accuracy of the heights in the provided DEM is ±30 cm, significantly better than the global SRTM 30m DEM, which has a vertical accuracy of 9.73 m RMSE. The tools utilized in this study include: ESRI Desktop ArcGIS with the Arc-Hydro extension, SNAP ESA (Sentinel Application Platform of the European Space Agency, an open-source application), QGIS (an open-source GIS software), Microsoft Office Professional Plus, and Google Earth Pro. The processing was conducted using SNAP ESA software, specifically employing the Graph Processing Tool (GPT) and Batch Processing Tool (BPT) to apply the processing graph to multiple images simultaneously.

The sequence of pre-processing techniques applied using the GPT tool includes the following steps: Read, Resample, Reproject, Subset, and Write (Kiran et al., 2019).The pre-processing techniques were also

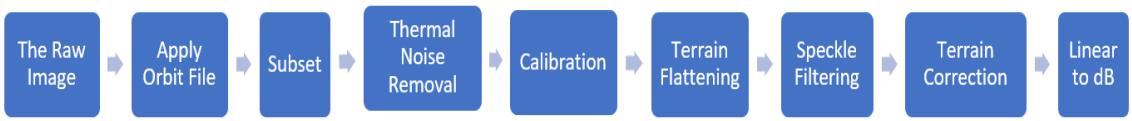

Figure 3: Flow chart of Sentinel-1 SAR data Pre-processing (Kiran et al., 2019)

applied to Sentinel-1 SAR imagery, following a specific sequence of methods. Figure 3 illustrates the flow chart for Sentinel-1, which includes the following steps: Apply Orbit File, Subset, Thermal Noise Removal, Calibration, Terrain Flattening, Speckle Filtering, Terrain Correction, and Linear to Decibel Conversion (Linear to dB).

The use of GIS and Remote Sensing (RS) technologies in flood management encompasses various applications throughout the entire flood cycle. These applications include:

a. Before the Flood: Flood simulations and predictions, as well as flood prevention efforts.

2. During Floods: Locating flooded areas, mapping evacuation plans, and implementing emergency response applications.

3. After Floods: Conducting flood damage assessments.

GIS and remote sensing play critical roles in flood prediction, hazard assessment, vulnerability analysis, risk mapping, as well as flood prevention and mitigation efforts. In the study area, the primary seasonal water streams that flow into the Blue Nile in a regional parallel pattern include Wadi Soba, Green Valley, and Wadi El Sileit. According to the findings of Fatima A. and Kamal A. Sami (2024), a flood hazard map was created to categorize the area into three risk zones: low, moderate, and high.

3.3 Techniques Used for Flood Mapping

Flood mapping requires two sets of remotely sensed data: images captured before the flood event and images taken after the flood event. The pre-flood images serve as a reference, while the images obtained during the flood season are often referred to as "crisis imagery." To assess flood hazards, multi-spectral satellite data, such as that from Sentinel-2, are collected and utilized for the following purposes:

(a) Flood Mapping Using SAR Imagery: To identify flooded areas in Synthetic Aperture Radar (SAR) images, two images are obtained—one during the flood season and another during a dry period. Karin et al. (2019) developed a comprehensive workflow (shown in Figure 4) for processing SAR data for flood detection, taking into account several important factors. One significant consideration is whether to use the multi-looking tool; utilizing the tool can result in smoother imagery but may reduce overall accuracy.

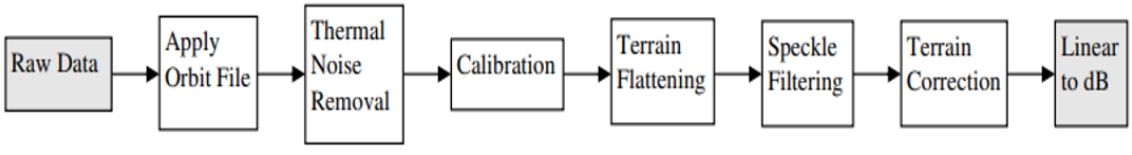

Figure 4: Flow chart for SAR Data Preparation for flood detection. (Kiran et al., 2019)

(b) Normalized Difference Water Index (NDWI): The NDWI (Sentinel-2 Hub, 2020) is used to distinguish open water features and enhance their visibility in remote sensing images. Its primary purpose is to differentiate between water and non-water features. Various definitions of NDWI utilize different combinations of spectral bands, including Green and Near Infrared (NIR), NIR and Short-Wave Infrared (SWIR), and Red and Middle Infrared (MIR). Multiple studies have employed these band combinations to delineate flood-prone areas (Sivanpillai et al., 2021). The NDWI is calculated using the following formula:

NDWI =(Green-NIR) /(Green+NIR)
For Sentinel-2 images, the green band corresponds to Band 3, and the Near Infrared band corresponds to Band 8. Thus, the NDWI formula becomes:
NDWI = (Band 3 – Band 8) / (Band 3 + Band 8)

(c) Hydrological Modeling:Hydrological modeling refers to the characterization of real hydrologic features and systems by utilizing conceptual and physical models, mathematical models, and computer simulations. The objective of hydrological models is to account for water distribution, flow over land, underground water movement, and the water stored in soil and natural bodies such as lakes and rivers. These models also examine the interactions between these various elements. Due to the variability and complexity of climatic, hydrological, soil, and land use data, which may be limited or unavailable, hydrological models have been developed and increasingly used in recent decades (Tariq A. et al. 2022). Watershed numerical models can be categorized into five key components: model geometry, input data, governing equations, initial and boundary conditions, and output results. A central aspect of hydrological models is to derive hydrological and topographic parameters from Digital Elevation Models (DEMs), which reflect the watershed characteristics.
(d) Supervised Imagery Classification Using the Random Forest Algorithm: Random Forest (RF) is a classification and regression tree technique that produces outputs representing the average of all regression trees grown in parallel without pruning. RF has several advantages, including internal error estimates, the capacity to assess variable importance, and the ability to handle weak explanatory variables. The United Nations Food and Agriculture Organization has developed a hierarchical land cover catalog suitable for remote sensing, particularly for the emerging regions of North Africa and the African continent as a whole. This method was implemented in the AFRI cover project to differentiate among 90 distinct land cover classifications in East African countries. Additionally, the German Surveys and Mapping Administration has created an object-oriented land cover catalog featuring multiple major categories.

3.4 Data Processing

3.4.1 Supervised Classification using RF

After processing the optical data from Sentinel-2 multispectral imagery to prepare it for analysis, the first step was to perform a supervised classification using the Random Forest algorithm. This approach classified the area of interest into eight pre-determined land cover classes: Settlements, Water, Agricultural, Cultivated, Bare Land, Sand, Vegetation, and River Shore. The classification was conducted using the SNAP-ESA software.A total of 98 samples were collected, covering an area of 1.8471 km². The resulting Random Forest supervised classification (Table 3) yielded two raster images (Land Cover Classes raster Evaluation). In total, there were 18,471 pixels across all training samples, with 8,918 samples (48.8% of the total sample pixels) used for accuracy testing. The Root Mean Square Error (RMSE) was calculated to be 0.02236.

Table 3: Samples used for RF Supervised Classification.

Sample class	Number sample	Total Area (Km²)	Sample class	Number sample	Total Area (Km²)
Cultivated	16	0.2735	Water	7	0.1996
Sand	12	0.2915	Bare-Land	5	0.0674
Settlements	19	0.5890	Agricultural Land	16	0.1552
vegetation	9	0.0727	River-Shore	14	0.1982
Total				98	1.8471

4.3.2 Hydrological Modelling

The Digital Elevation Model (DEM) serves as the primary data input for hydrological analysis and is crucial for any study related to terrain surface and elevation. This DEM was obtained from the Federal Ministry of Infrastructure, featuring a spatial resolution of 10 meters and a vertical accuracy of ±30 centimeters. After pre-processing the DEM through various subset processes, contour lines were generated at 10-meter intervals to define the topography of the study area. A hydrological analysis was conducted to highlight the hydrological characteristics, including flow direction, flow accumulation, drainage network, and ordered streams for the water drainage system.

To develop hydrological modeling using the DEM of the region (Tariq A. et al. 2022), the "Arc Hydro Tools" module in ArcMap was utilized. An automated model for the hydrological modeling process was created using the ArcGIS Model Builder (Figure 5).

4.3.3 Flash Flood Hazard Map

In this stage, the land cover layer, produced from the Random Forest (RF) supervised classification, and the buffered streams feature layer were both utilized. First, the buffered streams feature class was converted to raster format using the feature-to-raster tool. The Clip Raster tool was then employed to clip the land cover layer to the extent of the buffered streams layer, identifying the flash flood vulnerable area. The resulting raster was subsequently reclassified into four hazard classes:

- Class 1: Very high hazard (settlement class)
- Class 2: High hazard (cultivated class)
- Class 3:Moderate hazard (agricultural land)
- Class 4:Low hazard (inclusive of all other land cover classes)

This process resulted in the creation of the Flash Flood Hazard Map.

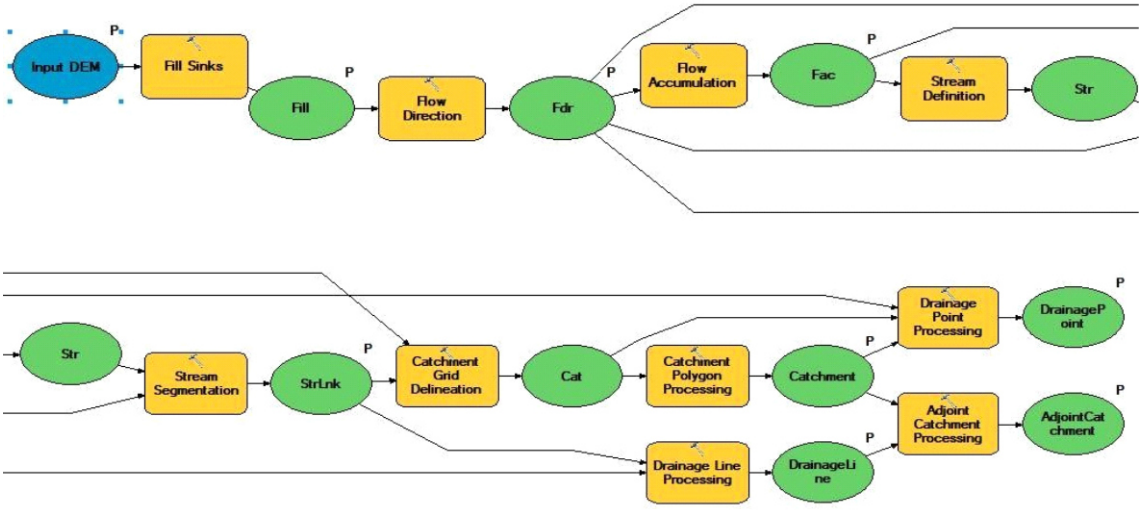

Figure 5: The model used for the Hydrological Modelling process to extract the streams

4.3.4 River Flood Hazard Map

The two pre-processed Sentinel-1 images (one from the dry season and one from the crisis period) were stacked as layers, and an RGB composite was created. In this composite, the dry season imagery was used for the red channel, while the crisis imagery was utilized for both the green and blue channels to highlight the flooded areas, identified as regions with the lowest backscatter.

To differentiate land from water in the flood season imagery, the histograms of the two images were analyzed to determine a stable threshold value, which was then applied using the reclassify tool. After identifying the flooded area in 2020, the elevation of this same area was extracted from the Digital Elevation Model (DEM). The result was the elevation of the flooded area, a crucial indicator for identifying regions with the highest hazard potential.

The river flood hazard map was classified into four hazard categories. The grid raster was reclassified into the following classes: 1 (very high hazard, ranging from 377 to 379), 2 (high hazard, ranging from 379 to 381), 3 (moderate hazard, ranging from 381 to 382), and 4 (low hazard, ranging from 382 to 383.722).

4.3.5 Combined Hazard Map

The combined hazard map integrates the hazards of both flash floods and river floods. This was achieved by merging the results from the flash flood hazard map analysis with those from the river flood hazard map using the merge tool. The outcome illustrates the combination of similar values from both hazard maps. For instance, pixels with a value of 1 in the flash flood hazard map represent urban areas (very high hazard) and are merged with pixels of the same value in the river flood hazard map, which indicate areas with the lowest elevation (also very high hazard).

This workflow illustrates the sequence of processes applied to the inputs in this study to create the final combined (Flash Flood & River Flood) map for the year 2020. The hydrological modeling techniques used, alongside the DEM, Sentinel-1 SAR imagery, and a land cover layer derived from Random Forest supervised classification (Figure 6).

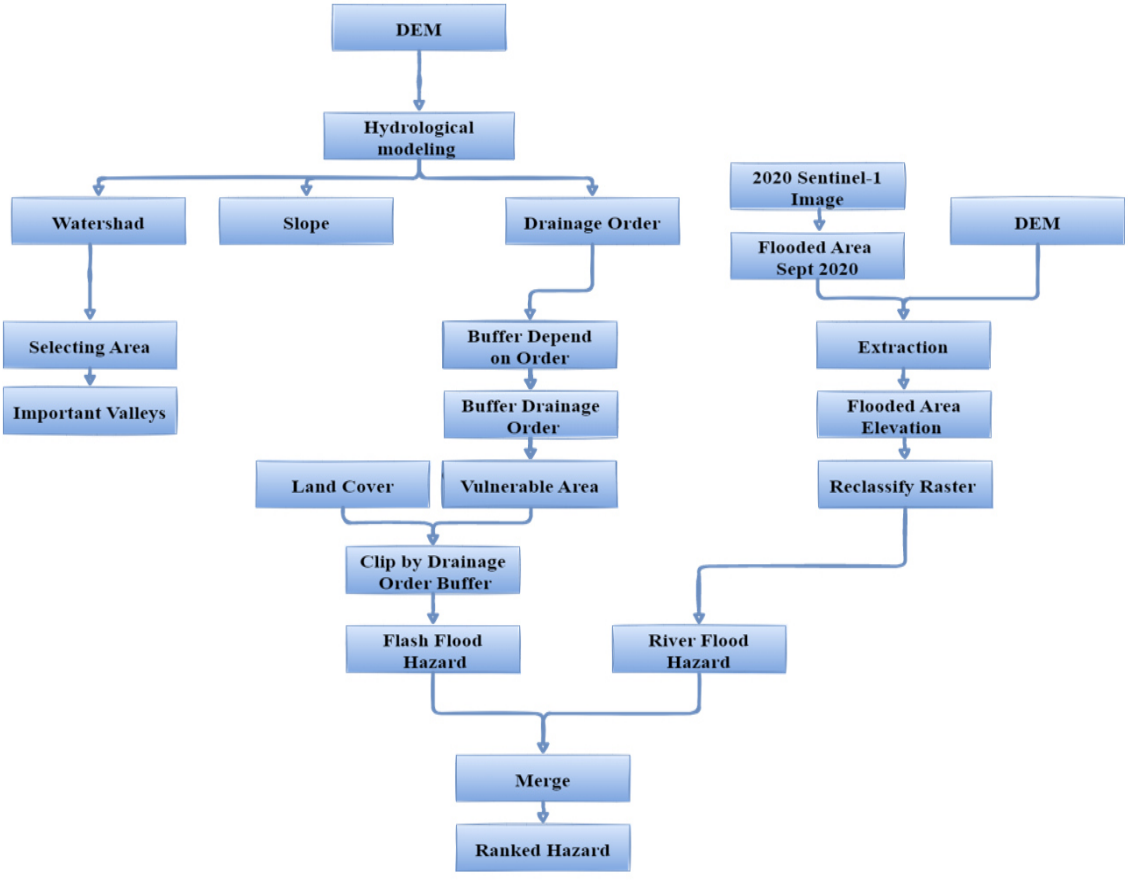

Figure 6: Shows the Sequence of processes to derive the Combined Ranked Hazard Map.

4.3.6 Flood Damage Assessment

To assess flood damage and identify the affected land cover classes from the 2020 floods (23 September 2020), the workflow shown in Figure 6 was applied using Sentinel 1 imagery and land cover data obtained from supervised classification, as illustrated in Figure 7.

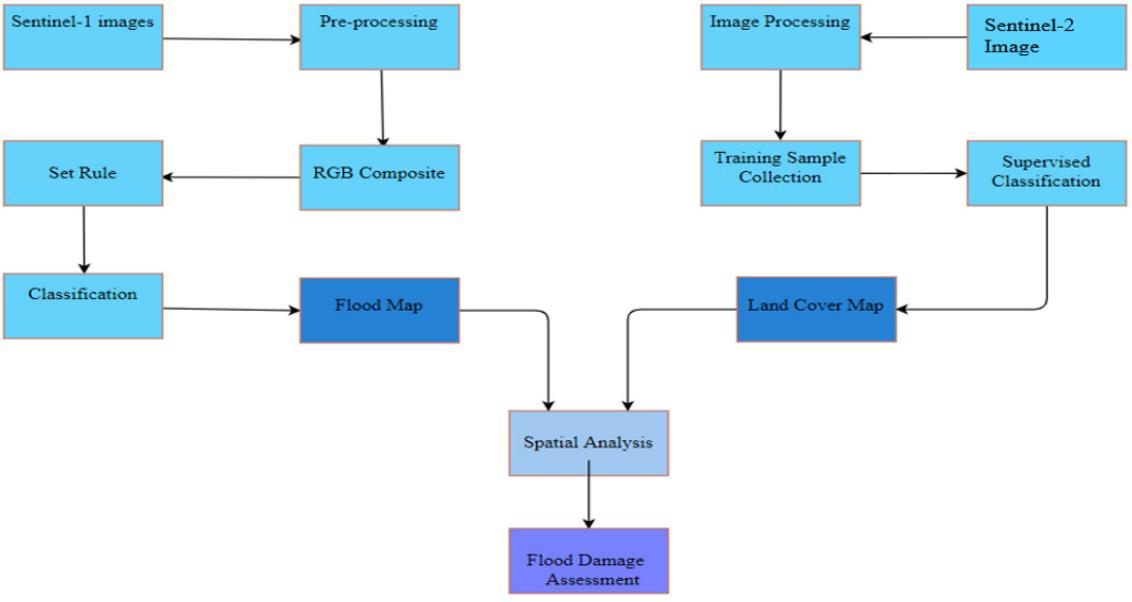

Figure 7: Flood Damage Assessment derived from supervised Classification

4.3.7 Flood Extent Detection Using NDWI

Sentinel-2 multi-spectral imagery has been utilized after pre-processing and layer stacking (Band Composite) to derive the Normalized Difference Water Index (NDWI) for all images. The imagery captured on May 27, 2020, has been selected as a reference image (dry season) to establish the standard waterbody extent of the White Nile River.

The NDWI has been calculated for each image using the following equation:
NDWI =(Green-NIR) /(Green +NIR)
In the case of Sentinel-2 multi-spectral images, "Green" refers to Band 3 and "Near Infrared (NIR)" refers to Band 8, thus the NDWI equation can also be expressed as:
NDWI = (Band 3 – Band 8) / (Band 3 + Band 8)
The Raster Calculator tool in the ArcGIS (Spatial Analyst - Map Algebra) toolbox has been employed to compute the NDWI layer. To classify the NDWI results, a stable threshold has been established using various techniques to differentiate water pixels from land pixels.

The NDWI layer has been reclassified into two values: 0 (Land) and 1 (Water). This reclassified NDWI layer of the reference imagery has been subtracted from each of the other crisis images. The outcome reveals the flood water extent for each crisis image using NDWI. The following flowchart illustrates the workflow used in this process (Figure 8).

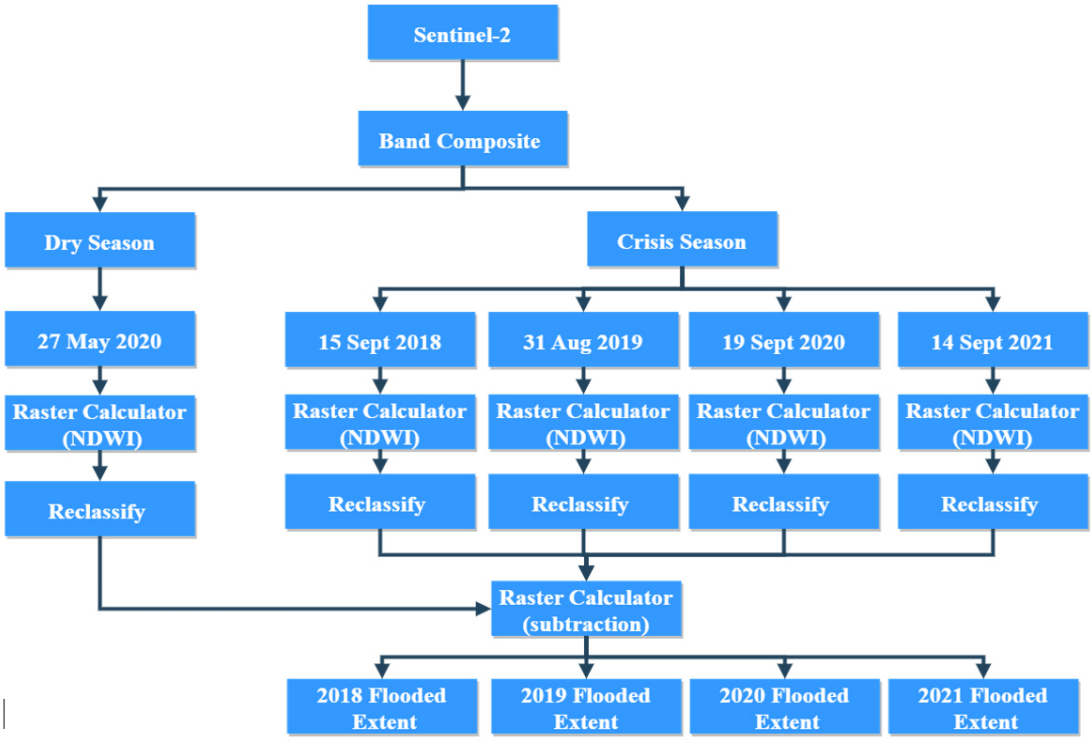

Figure 8: Steps of the formation of Flood Extent maps using the NDWI technique

5. FLOOD MAPPING ANALYSIS

5.1 Land Cover Map Using Supervised Classification

Sentinel-2 multi-spectral imagery, acquired during the dry season on May 27, 2020, was analyzed using supervised classification with the Random Forest (RF) algorithm. Samples were collected for each land cover class within the image, resulting in a classification into eight categories: Settlements, Water, Agricultural, Cultivated, Bare Land, Sand, Vegetation, and River Shore, totaling 98 samples. The combined number of pixels in all training samples was 18,471. Given that Sentinel-2 imagery has a spatial resolution of 10 meters, the pixel area measures 10m x 10m, leading to a total training sample area of 1.8471 km². The Root Mean Square Error (RMSE) of the classification was calculated to be 0.02236.Initially, the number of classes was predetermined to be seven. However, during the classification process (Tariq A. et al. 2022), an issue arose when some river shore areas were incorrectly classified as Settlements. Upon reviewing the spectral graph, it was found that the reflectance of urban areas closely resembled that of river shore soil. As a result, a River Shore class was added. The area for each land cover class was calculated and presented in Table 4. The output map layout displays the eight land cover classes along with the evaluation raster derived from the supervised classification of Sentinel-2 imagery using the Random Forest algorithm, as illustrated in Figure 9.

Table 4: The area of each land cover resulting in sq km

Class	Area (Km ²)	Class	Area (Km ²)
Agricultural Land	95.232	Settlements	103.4385
Bare-Land	135.7933	Vegetation	17.9759
Cultivated	16.3523	Water	62.0776
Sand	293.7358	River-Shore	70.2366

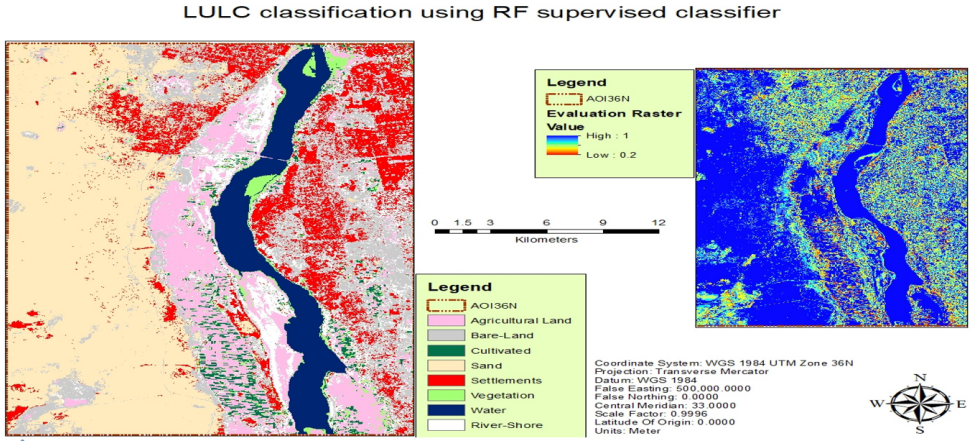

Figure 9: Land Cover Classes & Evaluation Matrix – SupervisedClassification using RF Algorithm

5.2 Streams and Catchment Area

Hydrological modeling was conducted using ArcGIS and the Arc-Hydro toolbox on a 10m DEM to derive several outputs, including Stream Orders, Buffered Streams, and Catchment Area. The results are presented in Figures 10, 11, and 12.

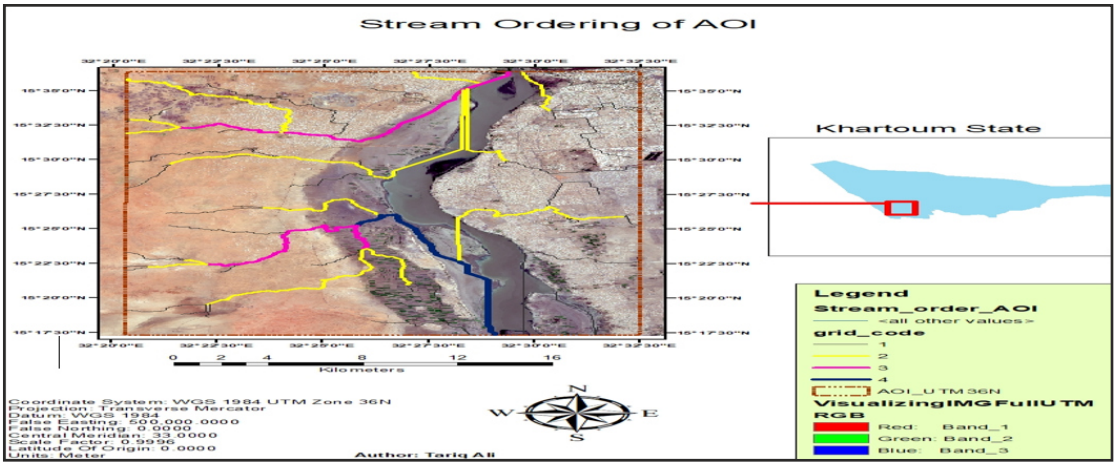

Figure 10: Ordered Streams map using the Strahler technique & Hydrologic Modelling

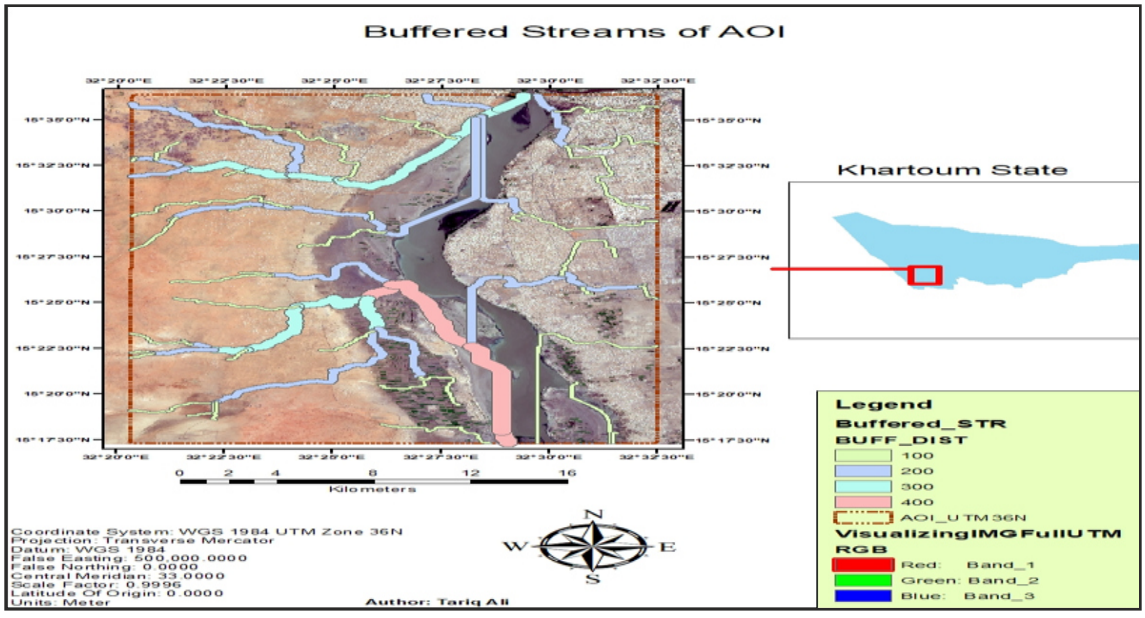

Figure 11: A map of the buffered streams based on stream order (100,200,300,400)

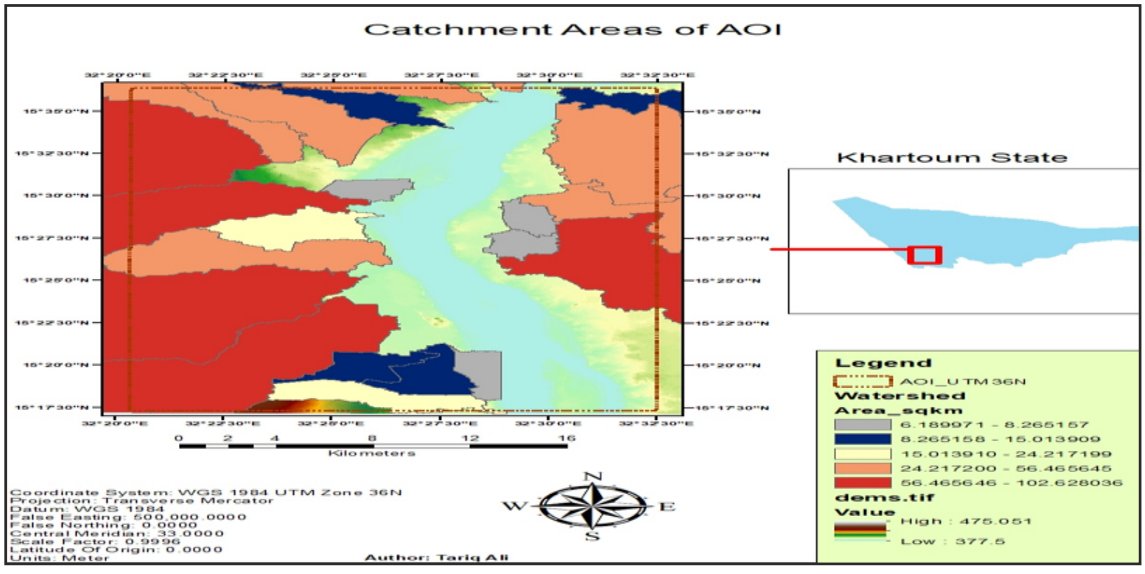

Figure 12: The RGB Composite comprised of 2020 dry season imagery in the red channel & crisis imagery in both the green & blue channels

5.3 Flash Flood Hazard Map

The output of the hydrological modelling phase, namely (buffered streams), has been used along with the derived Land Cover to derive the Flash Flood Hazard Map.An extraction analysis has been performed to clip the Land Cover layer to the exact extent of the buffered streams layer,forderiving the land classes at risk of flash flood. Then, the output raster has been reclassified into four classes: class 1 as very high hazard (Settlements), class 2 as high hazard (Cultivated), class 3 as moderate hazard (Agricultural land), and class 4 as low hazard (Combines the rest of the Land Cover classes). The area of each land cover class susceptible to flash flood meaning that area of each one of the hazard zones (Table 5) has been calculated in square kilometers. The result of this analysis is: Flash Flood Hazard Map (Figure 13).

Class	Pixel Count	Area in (Km²)
Settlements	98132	9.8132
Cultivated	25629	2.5629
Agricultural Land	230992	23.0992
All other classes	772010	77.201

Table 5: The area of each one of the hazard zones of the flash flood hazard map in sq km

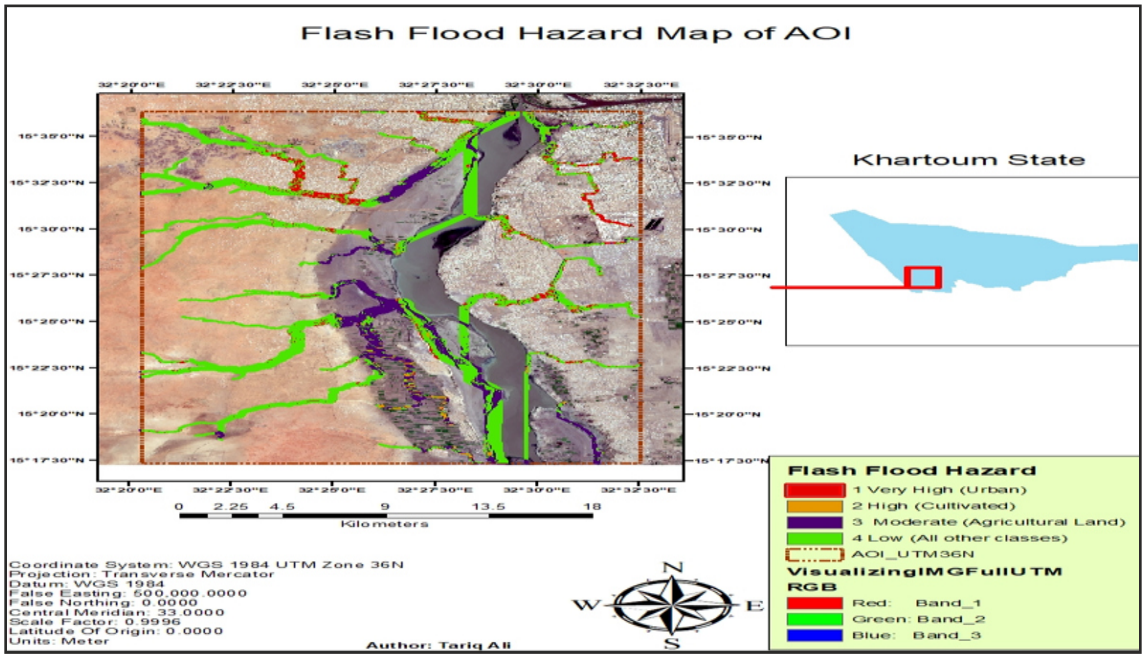

Figure 13: A map showing the Flash Flood Hazard Map with ranked hazards (1,2,3,4)

5.4 River Flood Hazard Map

To create the Flood Hazard map, the initial step involved delineating the flood extent using Sentinel-1 SAR imagery. After preprocessing the Sentinel-1 images, two specific images, acquired during the dry season and the flooding season, were selected. Then,a layer stacking process was performed to overlay these two images in the same view, which allowed us to create an RGB composite.Creating an RGB composite is an effective technique for distinguishing between flooded areas and permanent water bodies. In this process, the dry season image was assigned to the red band, while the flooding season image was used for both the green and blue bands. This choice was made because the flooded areas reflect a high radar response in the red channel (indicative of land in the dry season imagery) and a low radar response in the flooded areas for the crisis images.

As a result, flooded areas appear red on the composite due to a high response in the red channel, while showing low responses in the green and blue channels. In contrast, areas unaffected by flooding will show a shade of grey, representing similar backscatter responses across all three channels. Permanent water bodies, on the other hand, will exhibit a dark return with low backscatter in the red, green, and blue channels (Figure 14).

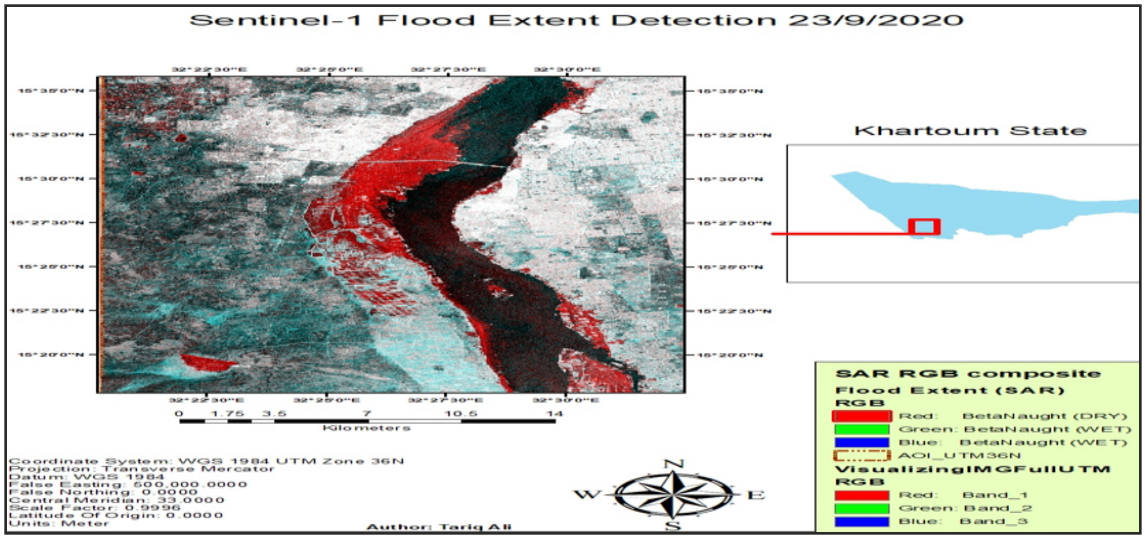

Figure 14: The RGB Composite comprised of 2020 dry season imagery in the red channel & crisis imagery in both the green & blue channels

The RGB composite was exported as a KML file to validate the flood extent using the Google Earth platform, which provides high-resolution imagery with a spatial resolution of 15 cm. The time scale tool was set for September 2020. By utilizing the RGB composite, along with Google Earth validation, and examining the histogram (Figure 15) of Sentinel-1 SAR crisis imagery, the value difference between the two peaks representing land and water was observed. This analysis helped determine the threshold value necessary to differentiatebetween land pixels andwater pixels.

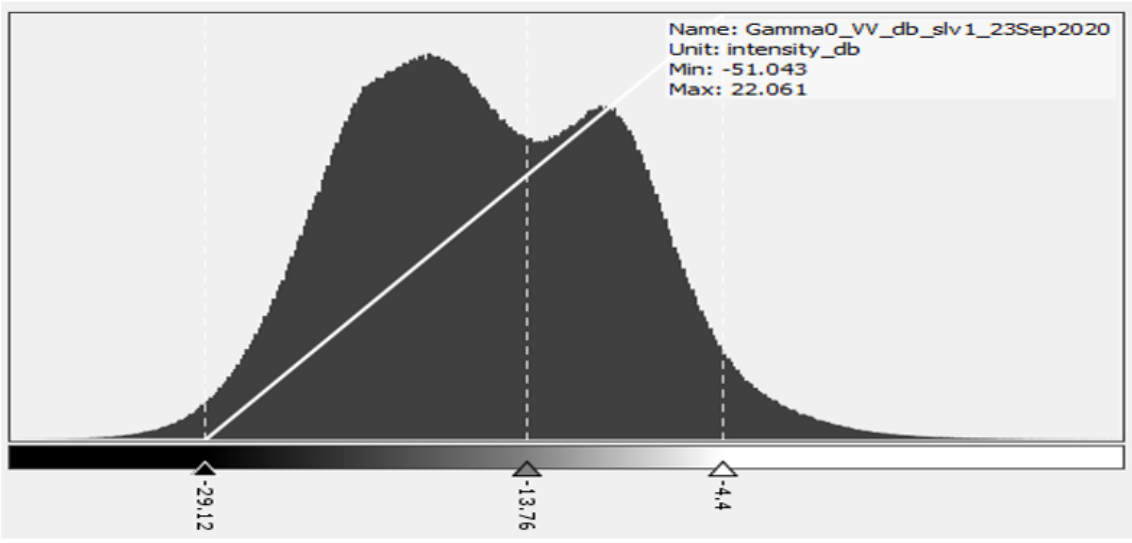

Figure 15: Sentinel -1 SAR crisis season pre-processed imagery histogram

One of the challenges encountered involved the Synthetic Aperture Radar (SAR) images, which typically return low backscatter for both smooth surfaces (water) and rough terrain due to the effects of terrain shadowing (Figures 11 and 12).

In this case, the aim was to determine the river flood extent, which required distinguishing the low backscatter of water from that of the terrain. To address this issue, we developed an equation that successfully reclassified the image using two additional layers: the Digital Elevation Model (DEM), which helped establish a threshold height to exclude low backscatter from terrain, and the Land Cover Layer, which included the water class value in the equation as an exclusion to ensure that normal water extent did not appear in the results.

Through a trial-and-error approach, the most stable threshold found was 13.7 decibels, while the elevation threshold was set at 383 meters after further evaluation and testing of the resultant extent. Thus, the equation was formulated as follows:

Gamma0_VV < 13.7 && landcover = 7 && elevation < 383

It is important to note that the value 7 corresponds to the water class in the Land Cover Layer. The equation was executed using the Raster Calculator tool in the Map Algebra toolbox (Figure 15). The resulting layer represents the final 2020 River Flood Extent Map generated using Sentinel-1 SAR imagery (Figure 16). After determining and defining the thresholds, the final river flood extent was successfully derived.

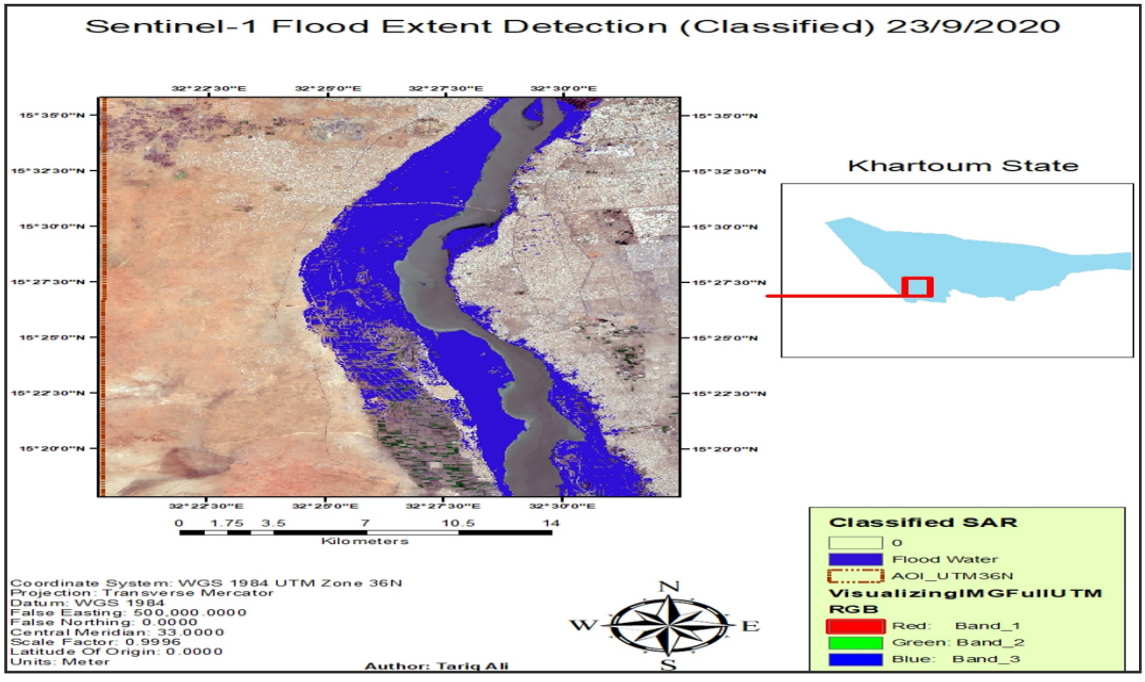

Figure 16: The final map of the river flood extent detection using Sentinel-1+ SAR data after defining all the thresholds

For the 2020 flood map, the elevation (in meters) of the flooded area was extracted from the Digital Elevation Model (DEM). The resulting elevation is a crucial indicator for determining which location poses the most risk. The river flood hazard map has been classified into 4 hazard categories, from 1 (very high) (377-379), 2 (high) (379-381), 3 (moderate) (381-382), to 4 (low) (382-383.722). These values were selected after observing the graph of flooded areas' elevations (Figure 15).

5.5 Combined Hazard Map

The Combined Hazard Map integrates the risks associated with both Flash Floods and River Floods. This final output is generated by merging the results from the Flash Flood Hazard analysis with the River Flood Hazard Map. The results demonstrate the consolidation of similar values from both the Flash Flood hazard layer and the River Flood hazard layer (Figure 17). For instance, pixels with a value of 1 in the Flash Flood hazard map, which indicate settlements at very high risk, are combined with pixels of the same value in the River Flood Hazard layer, representing areas at very low elevation, categorized as very high risk.

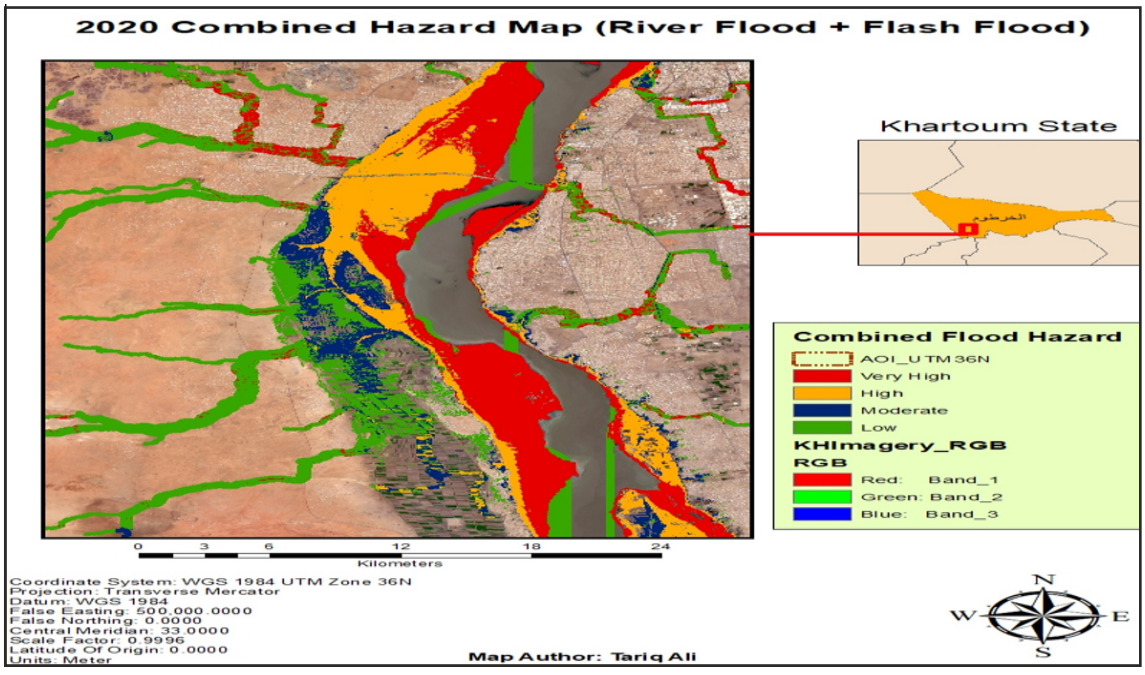

Figure 17: The final 2020 Combined Hazard Map (Flash Flood+ River Flood)

5.6 Flood Damage Assessment using 2020 Inundation Map

To assess flood damage and to identify the land cover classes affected by the floods of September 23, 2020, two raster images were multiplied using the raster calculator in the map algebra toolbox. The first raster represents the 2020River Flood Extent, created using Synthetic Aperture Radar (SAR) data. The second raster is the Land Cover layer obtained from Supervised Classification using the Random Forest (RF) algorithm. The analysis produced pixel values for each inundated land cover class along with their corresponding counts. Further measurements were conducted to extract the inundated area for each land cover class, as detailed in Table 6.

Table 6: Flooded area in squarekilometers per land cover class

Type	Flooded Pixel Count	Flooded Area (Km²)
Bare-Land	149416	14.9416
Sand	23032	2.3032
Agricultural Land	549409	54.409
Vegetation	103796	10.3796
River Shore	293829	29.3829
Cultivated	45837	4.5837
Settlements	33112	3.3112

5.7 River Flood Maps Using NDWI for the years (2018, 2019, 2020, 2021)

After pre-processing and stacking the layers (Band Composite), Sentinel-2 multispectral images were used to calculate the Normalized Difference Water Index (NDWI) for all images. The imagery from May 2020 was selected as the reference image, which will be used to determine the regular extent of the White Nile River's water body.

We encountered similar issues with thresholding when distinguishing land from water in both the Sentinel-1 SAR data and the NDWI analysis. The methods employed to establish a fixed threshold for all crisis imagery included:

1. Creating a histogram of NDWI images to identify the two peaks representing land and water.
2. Utilizing Otsu's thresholding technique, which involves iterating through possible threshold values to find the optimal result.
3. Assessing the accuracy of each result by exporting the image as a KML file and testing the extent in the Google Earth Platform using the time-scale tool.

Table 7: flooded area in square kilometers (2018, 2019, 2020, 2021)

Year	Flooded Pixel Count	Flooded Area (Km²)
2020 SAR	1198431	119.8431
2018	849658	84.9658
2019	1154230	115.4230
2020	1273985	127.3985
2021	1069362	106.9362

The fixed threshold value determined for all crisis imagery was 0.014, which was then applied to reclassify all NDWI images to extract water. The NDWI reclassified layer from the reference imagery (May 2020) was subtracted from each of the other crisis images (September 2018, August 2019, September 2020, and September 2021).

This process produced the floodwater extent for each crisis imagery using NDWI.
The study involved a comparison of the river flood extent extracted by NDWI during the crisis years (2018 vs. 2019 and 2020 vs. 2021).

Additionally, it compared the river flooded areas derived from Sentinel-1 SAR processing with those extracted from NDWI for September 2020, as well as the flooded areas for the years 2018, 2019, 2020, and 2021 (Table 7) obtained from NDWI in relation to the river flood area derived from SAR analysis for 2020.

6. CONCLUSIONS

The study emphasized the significance of flood mapping for effective decision-making, planning, and the implementation of flood control systems. It utilized methods commonly found in recent research on Rapid Flood Mapping through modern techniques. The findings illustrated that combining remote sensing data with spatial analysis can yield valuable insights for managing flood disasters and associated risks. This integration is particularly beneficial for determining evacuation routes and formulating emergency response plans, thereby supportingCivil Defence and Humanitarian Aid Organizations.

Geographic Information Systems (GIS) can enhance the interpretation and analysis of remote sensing data by creating satellite-based maps that show the extent of flooded areas. This method simplifies data processing for the subsequent stages of disaster damage assessment, especially when it comes to reconstructing damaged facilities and infrastructure. The high-resolution imagery from the Sentinel-2 Multispectral satellites has been particularly useful for visualizing damage and classifying land cover.

Sentinel-2 satellite images have revealed significant variations in flood inundations. Flood extent mapping using satellite imagery is extremely valuable for planners, enabling more effective city planning, damage estimation, and disaster response. Sentinel-1 satellites are particularly advantageous for rapid responses to flooding, as they can provide high-resolution imagery of the Earth's surface at any time, regardless of weather conditions.Sentinel-1 Synthetic Aperture Radar (SAR) earth observation data holds great potential for accurately mapping floods with high spatial resolution. By overlaying land cover classifications developed from Sentinel-2 images with flood maps produced from Sentinel-1 SAR images, a better understanding of flood damage through land cover layers will be gained. Additionally, hydrological modelling analysis, in conjunction with land cover maps, has led to the development of Flash Flood Hazard maps. These maps were combined with River Flood Hazard maps created from Sentinel-1 river flood extent data and Digital Elevation Models (DEMs) to produce a final, comprehensive Flood Hazard Map.

Considering the study's findings and the limited availability of accurate geospatial information necessary for hydrological investigations, modelling, and flood risk mapping, the Ministry of Irrigation and Water Resources, water institutions, and research centres in Sudan must act to unify the height systems in Sudan and initiate the development of a Hydrological Geospatial Information System. Such a system would serve the water community, facilitate hydrological investigations and modelling, support flood risk mapping, and contribute to climate change assessments and flood mitigation efforts.

7. REFERENCES

Abdo, G. (2012). An Improved Flood Forecasting Model of the Blue Nile River in Sudan. https://doi.org/10.21427/D77K7W
Ali, E., Zeinelabdein, K. A. E., & Rahamtallah, K. A. (2017). Flash Floods Risk Assessment of Sharg Alneel area, Khartoum State, Sudan Using Remote Sensing, GIS and Geophysical Techniques. 8.
Bronstert, A. (2003). Floods and Climate Change: Interactions and Impacts. Risk Analysis, 23(3), 545–557. https://doi.org/10.1111/1539-6924.00335
Fatima Ali A. Ali Nawai and Kamal Abdellatif A. Sami (2024). "Towards Enterprise Geospatial Web for Sudan Water Harvesting," International Journal of Multidisciplinary Research and Publications (IJMRAP), Volume 7, Issue 1, pp. 216-229, 2024.
Ganaie, H. A., Hashia, H., & Kalota, D. (2013). Delineation of Flood Prone Area using Normalized Difference Water Index (NDWI)&Transect Method: A Case Study of Kashmir Valley. 3(2), 6.
Jonkman, S. N. (2005). Global Perspectives on Loss of Human Life Caused by Floods. Natural Hazards, 34(2), 151–175. https://doi.org/10.1007/s11069-004-8891-3
Kiran, K. S., Manjusree, P., & Viswanadham, M. (2019). Sentinel-1 SAR Data Preparation for Extraction of Flood Footprints- A Case Study. Disaster Advances, 12, 11.
Kron, W. (2003). Flood Risk=Hazard×Exposure×Vulnerability. Journal of Lake Sciences, 15(Z1), 190–204. https://doi.org/10.18307/2003.sup23
Li, Z. (2014). Watershed modeling using Arc Hydro based on DEMs: A case study in Jackpine watershed. Environmental Systems Research, 3(1), https://doi.org/10.1186/2193-2697-3-11.
Tariq Abu Obeida Ahmed Ali, Ahmed Osama Jabr'Allah Mohammed (2022). Flood Analysis Study in South Omdurman, Khartoum & Jebel Awlia Localities Using RS & GIS Techniques. A thesis submitted in partial fulfillment of the requirements of the B.Sc. degree in Surveying Engineering, University of Khartoum.
Townsend, P. A., & Walsh, S. J. (1998). Modeling floodplain inundation using an integrated GIS with radar and optical remote sensing. Geomorphology, 21(3–4), 295–312. https://doi.org/10.1016/S0169-555X(97)00069-X.
Sentinel Hub. (2020). NDWI of Italy, Sentinel-2 imagery. Custom Script: NDWI. [Image]. Retrieved from Copernicus Sentinel-2 dataset via Sentinel Hub.
Sivanpillai, R., Jacobs, K. M., Mattilio, C. M., & Piskorski, E. V. (2021). Rapid flood inundation mapping by differencing water indices from pre- and post-flood Landsat images. Frontiers of Earth Science, 15(1), 1–11. https://doi.org/10.1007/s11707-020-0818-0
Uddin, K., Raj Gurung, D., Giriraj, A., & Shrestha, B. (2013). Application of RS and GIS for Flood Hazard Management: A Case Study from Sindh Province, Pakistan. American Journal of GIS, 2(1), 1–5. https://doi.org/10.5923/j.ajgis.20130201.01.

Uddin, Matin, & Meyer. (2019). Operational Flood Mapping Using Multi-Temporal Sentinel-1 SAR Images: A Case Study from Bangladesh. Remote Sensing, 11(13), 1581. https://doi.org/10.3390/rs11131581.
Younis, J., Ramos, M.-H., & Thielen, J. (2008). EFAS forecasts for the March–April 2006 flood in the Czech part of the Elbe River Basin—A case study. Atmospheric Science Letters, 9(2), 88–94. https://doi.org/10.1002/asl.179

List of Tables

Table 1: Shows the estimated damages at the five villages in Jebel Awlia locality
Table 2: Description of all the remotely sensed data acquired for the study.
Table 3: Samples used for RF Supervised Classification.
Table 4: The area of each land cover resulting in sq km:
Table 5: The area of each one of the hazard zones of the flash flood hazard map in sq km:
Table 6: Flooded area in square kilometers per land cover class
Table 7: flooded area in square kilometers (2018, 2019, 2020, 2021)

List of Figures

Figure 1: A map of the extent of the study area at the State and localities Level
Figure 2: Study area topography Map (contour lines & Slope Layer)
Figure 3: Flow chart of Sentinel-1 SAR data Pre-processing (Kiran et al., 2019)
Figure 4: Flow chart for SAR Data Preparation for flood detection. (Kiran et al., 2019)
Figure 5: The model used for the Hydrological Modelling process to extract the streams
Figure 6: Shows the Sequence of processes to derive the Combined Ranked Hazard Map.
Figure 7: Flood Damage Assessment derived from supervised Classification
Figure 8: Steps of the formation of Flood Extent maps using the NDWI technique
Figure 9: Land Cover Classes & Evaluation Matrix – SupervisedClassification using RF Algorithm
Figure 10: Ordered Streams map using the Strahler technique & Hydrologic Modelling
Figure 11: A map of the buffered streams based on stream order (100,200,300,400)
Figure 12: The RGB Composite comprised of 2020 dry season imagery in the red channel & crisis imagery in both the green & blue channels
Figure 13: A map showing the Flash Flood Hazard Map with ranked hazards (1,2,3,4)
Figure 14: The RGB Composite comprised of 2020 dry season imagery in the red channel
& crisis imagery in both the green & blue channels
Figure 15: Sentinel -1 SAR crisis season pre-processed imagery histogram
Figure 16: The final map of the river flood extent detection using Sentinel-1+ SAR data after defining all the thresholds
Figure 17: The final 2020 Combined Hazard Map (Flash Flood+ River Flood)

وأبرز ما يرصـــده الزائر لكهوف جبال أكاكوس هو أن الرســـومات متباينة التفاصـــيل لجماعات بشـــرية مرتبطة بتاريخ المنطقة القديم جدا، ويفســـر ذلك ان هذه التجمعات البشرية تجسد مظاهر الصيد والزراعة وطقوس الزواج بجانب استعدادات الحرب بين سكان المناطق الذين نزلوا عند جبال أكاكوس. ويوجد في سلسلة جبال أكاكوس مجموعة مختلفة من المناظر الطبيعية، من الرياح الرملية الملونة إلى الأقواس الصخرية والأحجار الضـخمة إلى الوديان. من أهم المواقع في المنطقة قوس "افازاجار" وقوس "تن خلجة" ورغم أن المنطقة من أشد المناطق القاحلة في الصـــحراء الكبرى إلا أنه يوجد بها بعض النباتات مثل نبات "الكالوتروبيس". وتعتبر سلســـــــــلة جبال أكاكوس من المعالم الجيولوجية الهامة في ليبيا ولها أهمية كبيرة في مجال السياحة الجيولوجية.

بقلم: أ. د. نوري محمد فلّو
منسق مشروع الحدائق الجيولوجية – دولة ليبيا

ونود الإشـــارة الي الدور الذي تقوم به اللجنة الوطنية الليبية للتربية والثقافة والعلوم في ليبيا ويهدف لتعزيز الوعي بالمشروع واستقطاب الخبراء للاستفادة من التجارب الدولية ونود الإشارة الي دور المركز الجهوي للاستشغار عن بعد لدول شمال افريقيا لدعم مشاريع الحدائق الجيولوجية للدول القاطنة بحوض البحر المتوسط وشمال افريقيا.

جبال اكاكوس ومقترح لمشروع الحدائق الجيولوجية – جنوب ليبيا

تقع سلســـلة جبال أكاكوس أو (تدرارت أكاكوس) تقع بالجنوب الليبي بحوض مرزق، فيما كان يعرف "أقليم فزان" وضمن الصـــــحراء الكبرى، والمرتبطة مع بلدة العوينات ومدينة غات، على بعد 1400 كم جنوب العاصمة طرابلس، وتمتد سلسلة جبال أكاكوس من الجزائر غربا إلى شمال النيجر شرقا. وصنفتها منظمة التربية والعلوم والثقافة (اليونســـكو) عام 1985 ضمن قائمة مواقع التراث العالمي الخمســـــة في ليبيا (صبراتة ـ شحات ـ غدامس ـ لبدة). ويعود تاريخ هذا المرتفعات الصـــــخرية، التي تتكون غالبيتها من صخور بركانية صماء شديدة الصــلابة تتخلّلها كثبان رملية، إلى ما قبل العصــر الجرماني، أي بنح 12 ألف سنة قبل الميلاد.

القوس الصخري "تن خلجة" في سلسلة جبال أكاكوس ـ ليبيا

وتشـــتهر سلســـلة جبال أكاكوس بكهوفها القديمة، كما أنها غنية بمجموعة المنحوتات واللوحات المرسومة على الصخر ولقد تم الاعلان من قبل اليونسكو كموقع للتراث العالمي في العام 1985 بســبب أهمية هذه اللوحات والمنحوتات والتي يعود تاريخ بعضـــها إلى 21,000 عام والتي تعكس ثقافة وطبيعة التغيرات في المنطقة.كما تضــم سلســـلة جبال أكاكوس في تشكيلها الصخري آلاف الرسومات على جدرانها والتي تنقل للإنسان المعاصر شـــــكل التعديلات العميقة التي طرأت على الثروة الحيوانية والنباتية بجانب توثيق الأنماط المتنوعة لحياة الشعوب التي توالت على هذا الجزء من الصحراء الكبرى.

حدائق جبل مكون الجيولوجية بدولة المغرب

خلال سنة 2025 اليونسكو تمنح ثماني عشر حديقة جيولوجية جديدة تسمية "حدائق جيولوجية عالمية"

أعلنت اليونسكو عن إضافة 18 حديقة جيولوجية جديدة، ليصبح العدد الإجمالي 229حديقة في 50 دولة خلال سنة 2025. ولقد أقرّ المجلس التنفيذي لليونسكو منح ثمانية عشر حديقة جيولوجية جديدة تسمية "حدائق جيولوجية عالمية لليونسكو"، ليصبح عدد مواقع الشبكة العالمية للحدائق الجيولوجي 229 موقعاً موزعاً في 50 بلداً.تعتبر الحدائق الجيولوجية مناطق جغرافية موحدة تعمل على حماية التراث الجيولوجي وتعزيزه من خلال السياحة المستدامة والتعليم والتنمية الاقتصادية المحلية، مع التركيز على المشاركة المجتمعية.

دولة ليبيا ومشروع الحدائق الجيولوجية المستقبلية

ليبيا ليست لديها حدائق جيولوجية معتمدة من اليونسكو بعد، لكنها تعمل حاليًا على إطلاق مشروع وطني للحدائق الجيولوجية للتعاون مع الشبكة العالمية التابعة لليونسكو. يهدف المشروع إلى تحديد مواقع جيولوجية فريدة مثل جبال أكاكوس والجبل الأخضر والعمل على الحفاظ عليها وتنميتها سياحيًا وتعليميًا. والمواقع المحتملة هي تشمل المواقع ذات الأهمية الجيولوجية في ليبيا جبال أكاكوس والجبل الأخضر، بالإضافة إلى مواقع أخرى في الشرق والجنوب .يهدف المشروع إلى استخدام هذه المواقع الجيولوجية كرافد للتنمية المستدامة، حيث تُستخدم في السياحة البيئية، والتعليم، والبحث العلمي . ولقد عُقدت اجتماعات وورش عملمحليه وبالإضافة للمشاركة في ورشة العمل الدولية وذلك بمشاركة المنسق العام للمشروع في ليبيا (الأستاذ الدكتور: نوري محمد فلّو) والتي انعقدت في الفترة (20-24 أكتوبر 2025) في جزيرة ماديرا بالمحيط الأطلسي والتابعة لدولة البرتغال وذلك بمشاركة 30 شخصية عالمية من 25 دولة لغرض مناقشة خطة العمل وتقديم التوجيهات الداعمة لمشاريع المنتزهات والحدائق الجيولوجية اقلميا وعالميا.

وفي الوطن العربي توجد حديقتان جيولوجيتان عالميتان في المنطقة العربية، وهما حديقة شمال الرياض في المملكة العربية السعودية، وحديقة جبال طويق في السعودية أيضًا، والتي مُنحت صفة الحديقة الجيولوجية العالمية في أبريل 2025. وتُعد هاتان الحديقتان، إلى جانب "مكون" في المغرب، من المواقع القليلة في المنطقة العربية التي تم الاعتراف بها ضمن شبكة الحدائق الجيولوجية العالمية لليونسكو. وتوجد في تونس حديقة جيولوجية واحدة هي حديقة "الظاهر" وهي مشروع قيد التصنيف ضمن الشبكة العالمية للحدائق الجيولوجية التابعة لليونسكو. تمتد هذه الحديقة على مساحة 6000 كلم مربع في الجنوب الشرقي التونسي، وتغطي مناطق في ولايات قابس ومدنين وتطاوين. تتميز المنطقة بأهميتها الجيولوجية الاستثنائية، وباحتوائها على آثار ديناصورات، مما جعلها مشروعًا نموذجيًا في تونس لتعزيز السياحة المستدامة والحفاظ على التراث .فيما تبقى عشرات العجائب الجيولوجية العربية خارج القائمة حتى الآن، مثلما هو الحال بالنسبة لوادي الحيتان في مصر، ومغارة جعيتا في لبنان، ووادي رم في الأردن، ومنطقة اللجاة في سوريا، وجبال اكوكوس في ليبيا،وغيرها.

حديقة جيولوجية بدولة الصين

حديقةجبل مكون الجيولوجية بدولة المغرب:

تقع حديقة جبل مكّون الجيولوجية على بعد 100 كم من مدينة مراكش في وسط سلسلة جبال الأطلس المركزية. وتبلغ مساحة الحديقة أكثر من 5700 كيلومتر مربع تضم 15 مجتمعاً محلياً. يرتفع الجبل إلى أكثر من أربعة آلاف متر فوق سطح البحر، وتكلل الثلوج مرتفعاته بين (نوفمبر) و(مايو) من كل عام. وهو مقصد سياحي لهواة الترحال نظراً لبناه الجيولوجية التي تشكلت قبل 250 مليون سنة، وما يحتويه من طبعات مذهلة لأقدام ديناصورات الصوروبودا والثيروبودا.

مقدمة حول الحدائق الجيولوجية

يمكن تحديد مفهوم الحدائق الجيولوجية في منظور اليونسكو في النقاط التالية:

أولا: الحدائق الجيولوجية العالمية هي مواقع للتراث الجيولوجي في مناطق جغرافية محددة، ويتم فحصها ودراستها من قبل المتخصصين، وتحضى بالحماية ويستفاد منها في التعليم والتنمية المستدامة.

ثانيا: الحدائق الجيولوجية العالمية لليونسكو هي مناطق معروفة واضحة المعالم ذات هيكل اداري معترف به على المستوى الوطني، وتتمتع أي حديقة جيولوجية عالمية بالشخصية الاعتبارية والوضع القانوني. وينظم عملها التشريعات المحلية والوطنية التي ينبغي أن تنسجم مع الوضع الإقليمي والدولي المتعلق بالحدائق الجيولوجية العالمية.

ثالثا: تتولى ادارات ومؤسسات الحدائق الجيولوجية العالمية لليونسكو القيام بالأنشطة والمهام ذات العلاقة بالحدائق الجيولوجية من حيث الرعاية والمحافظة والاستخدام الأمثل لصالح المجتمعات المحلية بالشراكة مع مؤسسات المجتمع المدني. وينبغي أن تشتمل هذه الحدائق الجيولوجية على خطة مرسومة تلبي الاحتياجات الاقتصادية للسكان المحليين مع حماية المناظر الطبيعية التي يعيشون فيها.

رابعا: تعمل الحدائق الجيولوجية العالمية لليونسكو على تبادل المشورة والخبرات فيما بينها. كما ينبغي أن تشجع للقيام بمشاريع مشتركة مع الشبكات الإقليمية للحدائق الجيولوجية، وعلى اليونسكو أن تواصل دعمها لأنشطة الشبكة الدولية للحدائق الجيولوجية.

الحدائق الجيولوجية العالمية في المنطقة العربية

تسعى الدول من خلال إدراج مواقعها على قائمة اليونسكو العالمية إلى زيادة الوعي حول القضايا الأساسية التي تواجه المجتمعات مثل استخدام موارد الأرض على نحو مستدام، والتخفيف من آثار تغير المناخ، والحد من المخاطر المرتبطة بالكوارث الطبيعية. كما أن هذا التصنيف يمنح السكان المحليين شعوراً بالفخر تجاه منطقتهم، ويعزز هويتهم المحلية، ويدفع باتجاه إنشاء شراكات مبتكرة.

مقاله علمية
" المنتزهات والحدائق الجيولوجية والمستقبل القادم "

ما الغرض من تسمية الحدائق الجيولوجية؟

أن فكرة الحدائق الجيولوجية العالمية لليونسكو هي استجابة للاهتمام المتزايد من قبل العديد من الدول الأعضاء في المنظمة لنجاح الحدائق الجيولوجية العالمية كأداة لتحقيق التنمية المستدامة. لقد لوحظ الاهتمام بمفهوم الحدائق الجيولوجية في الدورة 36 لمؤتمر عام اليونسكو وفي اجتماعات الدورتين 191,190 للمجلس التنفيذي. كما لوحظ في شهر يونيو 2013 وجود 90 حديقة جيولوجية عالمية في 27 دولة من الدول الأعضاء في المنظمة، وتدعم اليونسكو هذه الحدائق الجيولوجية العالمية. ووفقا لليونسكو، فإن الهدف من تسمية "الحدائق الجيولوجية العالمية لليونسكو" في تقدير التراث الجيولوجي يكتسي أهمية دولية كبيرة .وكانت الدول الأعضاء قد صدّقت بالإجماع على إنشاء هذه التسمية في عام2015.

توزيع لبعض الحدائق الجيولوجيا بدولة اليابان

ويقول بيان منظمة الأمم المتحدة التي تعنى بالتربية والعلم والثقافة إن مواقع تلك الشبكة "تكتنز تنوعاً جيولوجياً استثنائياً يعزّز التنوع البيولوجيّ والثقافيّ في مختلف المناطق كما أن "هذه الحدائق الجيولوجية تعود بالفائدة على المجتمعات المحليّة من خلال الموازنة بين صون تراثها الجيولوجي الفريد وبين التوعية العامة والتنمية المستدامة".

كلمة العـــدد

بسم الله الرحمن الرحيم،

يسـرّ المركز الجهوي للاستشـعار عن بُعد لدول شمال إفريقيا، بالشـراكة مع اتحاد مجالس البحث العلمي العربية، أن يقدّم إلى القرّاء والباحثين الكرام العدد الحادي عشـر من المجلة الإقليمية للعلوم والتقنيات الفضـائية، التي تمثّل منصـة علمية رصينة تُعنى بتعزيز البحث العلمي وتطوير المعارف في مجالات علوم الفضاء وتطبيقاتها المختلفة

تصدر هذه المجلة تحت إشراف هيئة علمية محكّمة تضم نخبة من الأساتذة والباحثين من الدول الأعضاء، بما يضمن جودة الأبحاث المنشورة وموثوقيتها العلمية، ويكرّس الالتزام بالمعايير الأكاديمية الدولية وأخلاقيات البحث العلمي.

ويضـــم هذا العدد مجموعة من الأبحاث والدراسات العلمية المتخصـــصـــة التي أنجزها باحثون ومختصـــــون من دول شمال إفريقيا، وتتناول موضوعات حديثة ومتنوعة في مجالات الاستشـعار عن بُعد، ونظم المعلومات الجغرافية، والعلوم والتقنيات الفضـائية، وتطبيقاتها في مجالات التنمية المســـــتدامة، وإدارة الموارد الطبيعية، وحماية البيئة، والحد من المخاطر، ودعم السياسات وصنع القرار.

إن مواصـــلة إصـــدار هذه المجلة تعكس حرص المركز وشـــركائه على دعم البحث العلمي العربي، وتعزيز التعاون الإقليمي وتبادل الخبرات، وإتاحة منبر علمي متخصص يُسهم في إبراز الكفاءات البحثية في المنطقة وربط البحث العلمي بقضـــايا التنمية والتقدم العلمي والتكنولوجي.

وإذ أتقدّم بجزيل الشكر والتقدير إلى أعضاء الهيئة العلمية المحكمة، وإلى جميع الباحثين الذين أسهموا بأعمالهم العلمية القيّمة في هذا العدد، فإنني أتطلع إلى أن يشـــــــكّل هذا الإصدار إضافة نوعية للمكتبة العلمية العربية، وأن يسـاهم في تشـجيع المزيد من البحث والابتكار في مجالات العلوم والتقنيات الفضائية.

وتفضلوا بقبول فائق عبارات التقدير والاحترام.

أ.د. الهادي امحمد قشوط
المدير العام للمركز الجهوي
ورئيس تحرير المجله

المناقشة – الاستنتاج – الاعتراف بجهود من ساعد في انجاز البحث ان وجد – المصادر (المراجـع) – وخلاصة باللغـة الإنكليزية او الفرنسية في حدود [200] كلمة إذا كان البحث باللغة العربية وخلاصة باللغة العربية في حدود [300] كلمة إذا كان البحث مكتوب باللغة الإنكليزية .

- على الباحث أتباع القواعد المتفق عليها عالمياً ، في مجال الاختصارات والاصطلاحات.
- ترسم الاشكال والخطوط البيانية بواسطة طابعة الليزر أو ما يماثلها أو باستخدام أدوات الرسم بحيث تكون واضحة ولا تتجاوز أبعادها 12 x 18 سم ويلحظ عدم الكتابة باليد عليها .
- يجب ترقيم الأشكال وكتابة مفاتيح المصطلحات مع الإشار ة إلى أماكنهـا وترقيم جميع الصفحـات تسلسليا بما في ذلك الجداول والأشكال التي تلحق بالبحث.
- تذكر جميع المراجع التي وردت في متن البحث، على أن تكتب في القائمة وفقاً للحروف الهجائية بالنسبة لأسمـاء المؤلفين وحسب اسم الكنية للمؤلف ويرتب كل مرجع كما يلي:-

اسم المؤلف – سنة النشر – عنوان المؤلف – دار النشر – ترميزه – الصفحات

- تعطى الأ ولوية للأ بحاث المقدمة باللغة العربية.
- يرسل للباحث (الباحثون) [2] نسخ من المجلة بدون مقابل كهدية / وفي حال طلب الباحث نسخ إضافية فبمقابل. ويمكن تسليم الباحث إفادة بأن بحثه مقبول للنشر معتمد من المركز لحين النشر.

إرسال البحوث إلى المجلة :

ترسل البحوث مباشرة بريديا إلى رئيس هيئة تحرير (مجلة) على العنوان التالي:

18، شارع موسى ابن نصير المنز ة الخامس 1004 تونس الجمهورية التونسية

أو

يُفَضَل ويُوصى بإرسال مسودات البحوث على ملف وورد إلكترونياً على البريد الإلكتروني:

dg.crtean@crtean.intl.tn

الاشتراك السنوي بالمجلة:

داخل الدول الاعضاء بالمركز:

- الأ فراد : 20 دولار امريكي بما في ذلك أجور البريد.
- المؤسسات : 40 دولار امريكي بما في ذلك أجور البريد.

خارج الدول الأعضاء بالمركز:

- الأ فراد : 25 دولاراً أمريكياً بما في ذلك أجور البريد .
- المؤسسات: 50 دولاراً أمريكياً بما في ذلك أجور البريد.

شروط النشر بالمجلة :

1. أن لا يكون البحث المقدم للنشر قد نشر أو قبل للنشر في مكان آخر.
2. تقبل البحوث بالعربية وباللغات الانجليزية او الفرنسية.
3. تقديم ملخص العربية للبحث المطلوب نشره في المجلة.
4. تخضع البحوث للتقويم العلمي ولا ينشر البحث الغير متكامل لشروط النشر.
5. توضع المصادر في نهاية البحث كاملة وتأ خذ أرقاما متسلسلة ويشار إليها في متن البحث بأرقام مع ذكر الصفحة.
6. تنشر المجلة الأوراق البحثية للطلاب المسجلين لدرجتي الماجستير والدكتوراه.
7. تعبر كافة الدراسات والبحوث والمقالات عن رأى مؤلفيها ويأ تي ترتيبها بالمجلة وفقاً لاعتبارات فنية لاعلاقة لها بالقيمة العلمية لاي منها.
8. تنشر المجلة التقارير والبحوث والدراسات الملقاه في مؤتمرات ومنتديات علمية والنشاطات الأكاديمية في مجال تخصصها دونما تحكيم في أعداد خاصة من المجلة.
9. تنشر المقالات غير المحكمة (أوراق العمل) فى زاوية خاصة في المجلة.

قواعد نشر البحوث فى المجلة:

1) تقبل المجلة كافة البحوث والدراسات التطبيقية والأكاديمية في مجال العلوم المساحية والفضائية .
2) يجب أن يلتزم الباحث بعدم إرسال بحثه إلى جهة أخرى حتى يأ تيه رد المجلة.
3) يجب أن يلتزم الباحث بإتباع الأسس العلمية السليمة في بحثه.
4) يجب أن يرسل بحثه إلى المجلة من نسختين مطبوعة، ملخص باللغة الإنجليزية أو العربية أو الفرنسية فى حدود 8-12 سطر، ويجب أن تكون الرسوم البيانية والإيضاحية مطبوعة وواضحة، بالإضافة إلى نسخة Soft Copy، ونوع الخط Times New Romanes 14 للعربى، و12 للانجليزي والفرنسية .
5) يجب كتابة عنوان البحث وأسماء المشاركين وعناوينهم كاملة في الملخص العربي للبحث المقدم باللغة الإنكليزية او الفرنسية.
6) ترسل البحوث إلى محكمين متخصصين وتحكم بسرية تامة.
7) في حالة قبول البحث للنشر، يلتزم الباحث بتعديله ليتناسب مع مقترحات المحكمين، وأسلوب النشر بالمجلة.
8) يتحمل الباحث او المؤسسة التي يتبعها كلفة نشر البحث والتي تعادل 100 دولار امريكي وقيمة 50 دولار للطلبه.
9) ينظم البحث كالآتي:

- عنوان البحث – اسم الباحث (الباحثين) – عنوانه (عناوينهم) – خلاصة – مقدمة – المواد والطرق – النتائج –

مجلة العلوم والتقانة الفضائية

FASRC

C.R.T.E.A.N
المركز الجهوي للاستشعار عن بعد لدول شمال إفريقيا

مجلة العلوم و التقانات الفضائية

عدد 11
ديسمبر 2025

مجلة علمية إقليمية محكمة تصدر عن المركز الجهوي للاستشعار عن بعد لدول شمال إفريقيا بالتعاون مع إتحاد مجالس البحث العلمي العربية

خريطة الارتفاعات لوادي مجردة السفلي - تونس

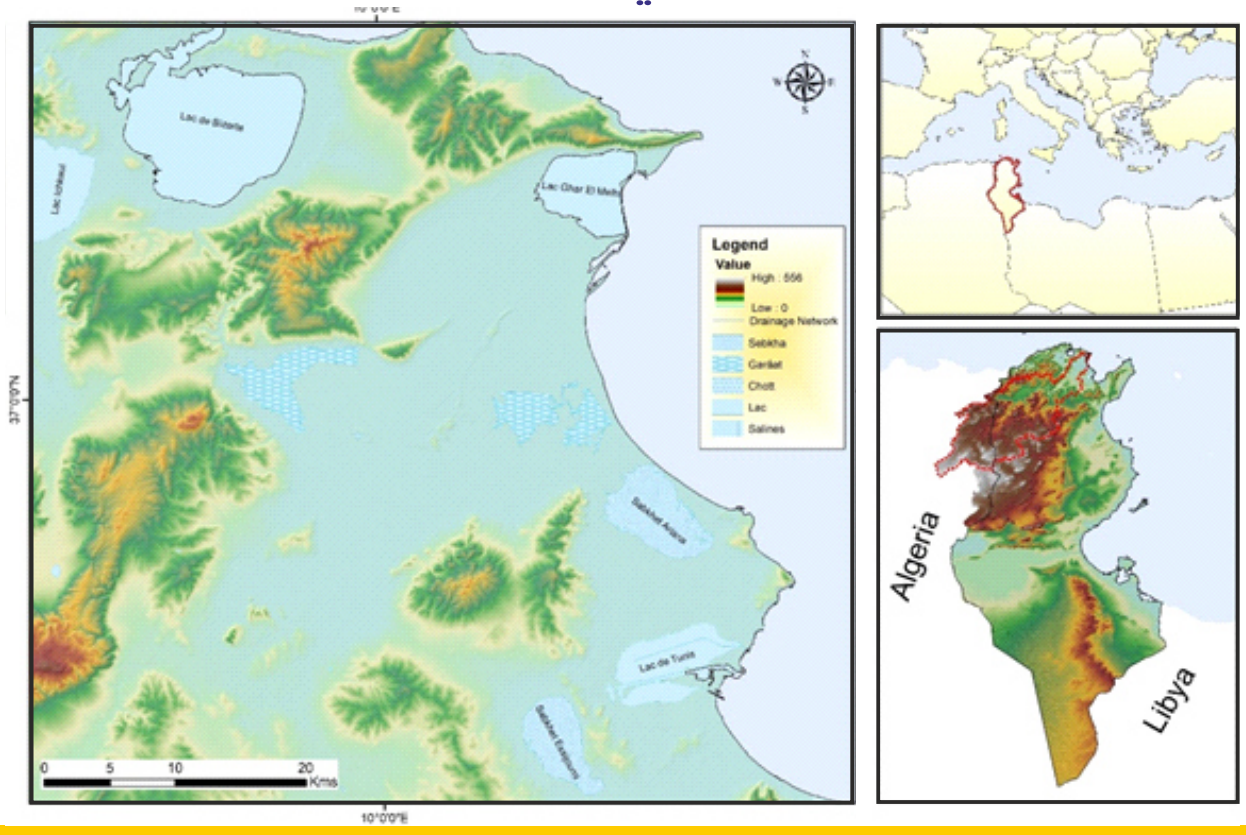

ISSN : 2490 - 4244

www.crtean.org.tn